The Dissertation Committee for Christian John Schrandt Certifies that this is the approved version of the following dissertation:

Chronic Monitoring of Cortical Hemodynamics after Ischemic Stroke using Functional Optical Imaging Techniques

Committee:

Andrew K. Dunn, Supervisor

Theresa Jones

Timothy Schallert

James Tunnell

Hsin-Chih Yeh

Chronic Monitoring of Cortical Hemodynamics after Ischemic Stroke using Functional Optical Imaging Techniques

by

Christian John Schrandt, B.S. Biomed. E.

Dissertation

Presented to the Faculty of the Graduate School of

The University of Texas at Austin

in Partial Fulfillment

of the Requirements

for the Degree of

Doctor of Philosophy

The University of Texas at Austin

May, 2015

Dedication

To my wife, parents, and children

Acknowledgements

I would like to thank my advisor Dr. Andrew Dunn for all the help and guidance through graduate school and this research effort. Thanks also to all of the members of my dissertation committee for taking the time to provide your insights helping to advance this research effort. To my lab-mates I am grateful for all of the research and classwork discussions and in particular to Shams Kazmi, who helped me to focus my research and guide me through the dissertation process. I would also like to thank my wife, Rachel, my parents, and my children for their love and support over the past 5 years.

Chronic Monitoring of Cortical Hemodynamics after Ischemic Stroke using Functional Optical Imaging Techniques

Christian John Schrandt, Ph.D.

The University of Texas at Austin, 2015

Supervisor: Andrew K. Dunn

The roles of the vascular architecture and blood flow in response to neurovascular diseases are important in predicting physiological outcomes. Observing these parameters chronically with optical imaging techniques provides insight into the neurovascular recovery process. We develop and deploy optical imaging systems for monitoring the progression of vascular structure, perfusion, and functional blood response after ischemic stroke in a chronic rodent model to observe vascular dynamics of the cortex under normal and diseased pathologies.

Specifically, we monitor the progression of the vascular structure and cerebral blood flow (CBF) over a chronic period in the rodent cortex after photo-thrombotic occlusion. Multi-Exposure Speckle Imaging (MESI) provides surface measurements of microvascular flow dynamics while Two-Photon Fluorescence Microscopy offers direct visualization of the microvascular structure. We observe the occurrence of vascular reorientation in the sub-surface microvascular structure over a 35 day post-occlusion period. We also correlate MESI flow estimates in the parenchyma with sub-surface microvascular volume fractions from two-photon microscopy to assess how vascular density influences the surface-integrated MESI measurements.

Next, we develop and validate a MESI technique for measuring absolute changes of the functional blood flow response to forepaw stimulation in rodents, termed FA MESI. The optimal camera exposures for capturing the CBF response to forepaw stimulation are extracted from a training set of animal data and the feasibility of the technique is demonstrated in a testing animal set by comparing functional response results between new and existing techniques. We then deploy this system in a chronic study monitoring the progression of hemodynamic parameters after ischemic stroke within the functionally responding area of the cortex. The progression of the regional CBF perfusion and absolute changes in the magnitude of the functional blood flow response are monitored chronically after photo-thrombotic occlusion. We compare the differences between absolute and relative measurements of the functional blood flow responses, and validate FA MESI by comparing baseline measurements to 15-exposure MESI over the sampled flow distributions. We demonstrate the differences measured between the functional outcomes and the regional CBF perfusion over a three week post-occlusion time period.

Table of Contents

List of Tables

List of Figures

List of Illustrations

Chapter 1: Background and Significance

Neurovascular disease encompasses any abnormality of blood vessels in or supplying the brain or spine. The most prevalent form of neurovascular disease is stroke, which is the third leading cause of death and the leading cause of chronic disability in the United States.[1] Strokes are classified into three types, ischemic, hemorrhagic, and transient ischemic strokes. In ischemic strokes, which account for ~80% of strokes, the most frequent causes are blood clots that lodge in an artery and blocks blood flow to part of the brain. Hemorrhagic strokes occur when a blood vessel ruptures in the brain, and transient ischemic strokes are the result of a blood clot blocking an artery for a period of time and then cleared. Each stroke has different effects on the brain, but the focus of this research will be on ischemic strokes. Focal ischemia is characterized by reduced blood flow in a localized region of the brain, with the size of the region depending on where the stroke occurs. As the supply of blood is reduced, a cascade of cellular and molecular events occurs which leads to neuronal injury and tissue damage.[2] The most severe damage is found in the area called the ischemic core, where flow ranges are generally <20% of baseline. The area surrounding this is known as the penumbra, where there is still a flow decrement but no immediate cell death.[3,4] Current clinical treatments for ischemic stroke rely on an acute administration of a thrombolytic pharmaceutical, recombinant tissue plasminogen activator (tPA), within a therapeutic window of only three hours after stroke onset.[5] While this short window limits the impact of tPA to five percent of stroke victims, clinical trials are looking into the extension of this therapeutic window in order to treat

more patients.[6] After this window ends, blood thinners and statins are often prescribed on a chronic basis to patients for disease management.[7–9] Post-stroke rehabilitation is often prescribed in order to help patients relearn skills lost when the brain was damaged, often taking advantage of neuro-plasticity within the brain.[9–11] The goal of current research in this area is to develop new therapeutic interventions that work through pharmacological, behavioral, or surgical means.[13] This creates a need for testing platforms that can evaluate the efficacy of these interventions with measurements of hemodynamic parameters over long periods.

Many studies focus on restricting the expansion of the ischemic core and reduce tissue damage by targeting the penumbra with neuro-protective agents.[4] The degree of the injury is highly dependent on the area and duration of the ischemia, as it affects the temporal and spatial duration of oxygen deprivation, making the recovery process reliant on re-vascularizing these areas to bring in new oxygen. Vascular remodeling occurs through formation of new blood vessels, termed angiogenesis, and flow changes, which have been observed in these injured areas, though the mechanisms driving the recovery are not well known. This lack of information stems from limitations of existing techniques including invasiveness, shallow imaging depths, and animal models poorly suited for this type of study. In order to elucidate the remodeling processes in the brain, we require imaging techniques that can non-invasively investigate the cortical hemodynamics and vascular anatomy of the brain in a chronic setting.

Small scale occlusions are another form of stroke implicated in several neurovascular diseases, where prolonged hypoperfusion and atherosclerosis within the

microvasculature have been observed in regions of the brain associated with the memory circuitry in Alzheimer's disease patients.[14] These type of occlusions are prevalent with ischemic strokes after the main thrombus has broken up and begins to flow down-stream and block smaller diameter vessels. The role of microvasculature and capillary beds in clearing cellular waste has recently been posed as a contributing factor to Alzheimer's disease.[15] The cerebrovascular architecture seems to be unique in that it doesn't follow the nutrient and waste exchange found in other circulatory systems of the body. Regional supply routes in the brain are dominated by specific arterial braches of the carotid artery. Branches of the middle cerebral artery (MCA) and anterior cerebral arteries (ACA) supply large segments of the gray matter, while supply routes from the meninges feed the cerebral cortex. Occlusions found in these regional supply arteries, specifically the MCA, account for the majority of persistent global ischemia. Downstream of these arteries are arterioles critical to supplying the cortical microvasculature, beginning as pial vessels and penetrating down into the cortex.[16] These penetrating arterioles are predominately responsible for oxygenating the cortical layers, and recent studies measuring blood flow and cell death suggest that a clot in one of these arterioles results in a greater focal ischemia than clots in large pial arterioles or micro-vasculature in the rodent brain.[17] Clinically, occlusions within the penetrating arteries and arterioles, known as lacunar infarcts, account for nearly 25% of all ischemic strokes.[18] Part of our study will examine the rebuilding of the vascular architecture after strokes in pial arterioles and penetrating arterioles both at the surface and below the surface of the cortex. By characterizing the vascular progression

in and around the occlusion site using optical imaging techniques, we will have the platform to understand and further develop neurorestorative therapies.

1.1 IMAGING OF HEMODYNAMICS IN THE BRAIN

Many imaging modalities have been developed to better understand the hemodynamics and functions of the brain. Optical techniques have played a critical role in understanding the neurovascular dynamics of normal[19] and diseased pathologies, such as stroke[20], epilepsy[21], Alzheimer's[22], and Parkinson's.[23] Despite these advances, optical techniques are limited in the clinical setting the inability of light to be delivered through the skull without significant scattering. For animal models in the research setting, effects of scattering from the skull can be eliminated by a surgical procedure to replace the skull with an optically clear cranial window. This window allows direct access to the brain, allowing for hemodynamic changes during pathophysiological events to be measured. Understanding of human hemodynamics relies on well-established techniques such as magnetic resonance imaging and positron emission tomography to probe the function and metabolism of the human brain.

1.1a Non-Optical Hemodynamic Imaging

The main clinical technique used for studies of hemodynamic changes in the brain is Magnetic Resonance Imaging (MRI).[24,25] With the ability to observe structural anatomy and localize functional changes without the need for contrast agents, MRI has become a standard tool in the clinical setting for studying neurovascular function. Functional studies with MRI largely depend on observing changes in the blood oxygen level (BOLD) signal

due to the paramagnetic deoxyhemoglobin species. As the brain is functionally stimulated, the BOLD signal within the responding region can be observed by the recruitment of oxygen, giving MRI the ability to measure the cerebral metabolic rate of oxygen consumption, or CMRO2, within this region. This gives an indirect measure of the cerebral blood flow (CBF) of the area, as the metabolic rate is dependent on CBF. One of the main drawbacks of MRI is the low temporal resolution for these fMRI studies. Though the CMRO2 can be presented from regions of the brain, studies lack the resolution to specifically probe the microvasculature.

Other clinical techniques have shown the ability to measure functional changes in the brain with high sensitivity, such as positron emission tomography (PET). This technique relies on an exogenously delivered contrast agent, one of which is fluorodeoxyglucose (FDG), which has been used for tracking glucose consumption.[24, 25] Transcranial ultrasound measurements in the human brain have shown the ability to measure changes in the CBF associated with vascular pathologies affecting large supply arteries.[28] Both of these techniques provide insight into the neurophysiology and anatomy of the human brain, but lack the resolution to specifically probe the CBF dynamics of the microvasculature.

1.1b Optical Imaging of Hemodynamics

Optical imaging modalities offer techniques that are able to offer a good combination of spatial and temporal resolution for imaging in the brain, so long as optical access can be achieved. Increased resolution is important for studying physiological events

in the brain that generally contain complex temporal and spatial dynamics. These techniques also directly benefit from constantly improving camera and detector technologies. Improvements in the optical imaging field have also resulted from increased camera sensor sensitivity and decreased readout and dark current noises. As a result of the commercial interests in this area, optical imaging systems generally have lower costs than other modalities due to less expensive components and reduced amount of required infrastructure to house and operate equipment, making them more accessible to a larger range of experimenters.

In the clinical field, the most prevalent form of optical imaging of hemodynamic parameters comes in measuring arterial oxygen saturation. This technique requires no contrast agent, as it is based off absorption differences between oxygenated and de-oxygenated hemoglobin. Measurements are able to be taken from vessels near the surface of the skin, allowing for pulse oximetry to remain a non-invasive technique. Other optical techniques have been sparingly used in clinical settings, such as transcranial near-infrared spectroscopy (NIRS), used for visualized functional and damaged cerebral hemodynamics.[22, 23]

The use of hemoglobin to establish a contrast agent can also be used for functional blood flow information, such as with Imaging of Optical Intrinsic Signals (OIS), which uses a camera to measure changes in the reflectance of tissue to a particular wavelength.[31] These changes can originate from a number of physiological variables such as blood volume, oxygenation, and metabolic activity.[32] Due to high spatial and temporal resolution without the need for exogenous dyes, imaging of OIS can obtain information about

functional stimulation, and has provided insights into the functional organization of the cortex.[33–35] This technique can be used to image the changes in cortical reflectance arising from the hemodynamic changes accompanying functional activation. In a research setting for cerebral hemodynamics, multi-spectral absorption of hemoglobin has been used in combination with relative CBF information from Laser Doppler or Speckle Contrast imaging to obtain estimates of the relative metabolic activity or the cortex.

By either tracking or labeling the erythrocytes, or red blood cells, optical imaging techniques can directly measure flow velocities in vessels where the lumen is thin enough to image through. In small animals, such as rodents, the technique is viable for imaging vasculature at the cortical surface through cranial windows provided the sampling criteria are met. For intrinsic measurements of the surface vessel velocities, a high speed camera can be used to follow erythrocytes in space and time. In the case of laser scanning microscopy, fluorescent contrast agents can be used to label the blood plasma and track erythrocytes over a spatial span, called a line scan, by observing the negative contrast they present. These absolute measurements of flow velocities can be used as a gold standard for comparison of flows measured with DLS-based imaging methods.

1.1c Dynamic Light Scattering based Techniques

Monitoring the dynamics of perturbations in the blood flow *in vivo* for normal and diseased pathologies is of critical importance to understanding neurovascular function. Optical techniques based on dynamic light scattering (DLS), such as Laser Doppler Flowmetry (LDF), Laser Speckle Contrast Imaging (LSCI), and photon correlation

spectroscopy, are often utilized to monitor blood flow.[36] Though each of these techniques varies in measurement geometry and analysis, they are all based on intrinsic signals from laser-tissue interactions, with no need for exogenous dyes.

Imaging techniques based on DLS have recently shown the ability to accomplish rapid particle sizing and flow analysis.[37–39] Monitoring of the relative cerebral blood flow *in vivo* at a single spatial location with high temporal resolution has been demonstrated with LDF. The main drawback of this technique is the lack of spatial information, which can be alleviated by introducing a scanning component, though a tradeoff with the temporal resolution must be made. The alternative to LDF is laser speckle contrast imaging, which offers a widefield mesoscopic perspective of blood flow. With this technique, the camera images interference patterns formed by dynamically scattered coherent light[40] traveling slightly different path lengths. LSCI offers a technique with scalable fields of view that typically achieves millisecond temporal resolution with a spatial resolution on the order of tens of microns. This technique is also non-invasive other than the need for optical access, and presents a relatively simple and inexpensive technique for obtaining depth-integrated information on the relative dynamics of the CBF. Over the past decade, LSCI has emerged as a powerful imaging modality for real-time *in vivo* measurements of relative blood flow.

1.2 Specific Aims

The overall aim of this dissertation is to utilize and further develop optical imaging techniques capable of measuring absolute changes in hemodynamic parameters associated

with vascular and functional progression after ischemic stroke. The specific aims of this research are to:

- Utilize Two-Photon Microscopy and Multi-Exposure Speckle Imaging to chronically monitor the vascular progression of the cortex following photo-thrombotic ischemic stroke.
- Develop an optimized Multi-Exposure Speckle Imaging technique capable of sufficient temporal resolution to measure the functional blood flow response to forepaw stimulation and compare results with an existing LSCI technique.
- Monitor the chronic functional blood flow dynamics of the mouse forepaw response after photo-thrombotic ischemic stroke with Functional Activation MESI technique.

Chapter 2: Instrumentation and Methods

Optical imaging systems generally utilize the absorption and scattering properties of either endogenous chromophores or exogenous dyes by exposing a sample to a particular wavelength of light and analyzing the reflected light or induced fluorescence. The first imaging system described in this chapter will be Laser Speckle Contrast Imaging, followed by an extension to this technique termed Multi-Exposure Speckle Imaging. In addition to these imaging techniques will be a depth-resolved technique termed Two-Photon Fluorescence Microscopy. Methods for photo-thrombotic stroke utilized in Chapters 3 and 5 will also be described in this chapter, as well as the progression of optical techniques this research used for imaging functional forepaw response in a mouse model.

2.1 Laser Speckle Contrast Imaging

Laser Speckle Contrast Imaging (LSCI) is a technique that offers a full field, depth-integrated view of relative blood flow. This technique was introduced in 1981 by Fercher and Briers,[41] and has become increasingly popular as camera technology has improved. The physics behind LSCI are very similar to those in Laser Doppler Flowmetry, which uses the Doppler Effect to detect the frequency shift of laser light as it encounters a moving red blood cell, allowing for point measurements of blood velocity. With LSCI, a camera records a speckle image when a specimen is illuminated by a coherent laser light source due to the light reaching each pixel of the image having traveled slightly different pathlengths. The speckle pattern exhibits time varying changes which contain information about the motion of the moving particles encountered in the specimen, such as perfused

tissues. The advantage of LDF is its high temporal resolution, though measuring full-field images would require a scanning source, making the technique very time consuming. By replacing the point detector with a camera to collect laser light after it is scattered off of the tissue surface, LSCI's spatial resolution does not come at the expense of scanning time. Combining this technique with a high speed camera allows LSCI to achieve millisecond temporal resolution with tens of microns spatial resolution. This technique also requires no direct contact with tissue, though optical access is necessary, making LSCI a great technique for obtaining detailed CBF measurements without disturbing the physiology of the brain.

Many groups have used LSCI for imaging CBF dynamics, with studies including stroke,[42–44] functional activation,[45,46] and even human studies during intra-operative neurosurgery.[47,48] LSCI is also finding applications outside the brain in the skin[37] and retina.[49,50]

Laser Speckle Contrast Imaging relies on illuminating the specimen with coherent laser light that produces a speckle pattern at the camera due to the slight difference in pathlengths traveled by the light at each pixel. If the sample contains scattering particles in motion, such as flowing blood cells, they manifest themselves as temporal fluctuations in the imaged speckle pattern. Several techniques utilize coherently scattered light for monitoring of tissue perfusion, including Laser Doppler Flowmetry,[51,52] and diffuse correlation spectroscopy.[53,54] These fluctuations are integrated over the exposure time of the camera, resulting in the appearance of blurring of the speckle pattern. When choosing a camera exposure time for biological samples, LSCI requires an integration period slightly

longer than the motion dynamics of the specimen, approximately 1 millisecond, to result in a visible blurring of the raw speckle image. The degree of blurring is dependent on the camera exposure duration, and can be quantified by taking the ratio of the standard deviation, σ_s, to the mean intensity of pixel values, $\langle I \rangle$, over a small pixel window, producing a value known as the speckle contrast, K.[55,56]

$$K = \frac{\sigma_s}{\langle I \rangle} \qquad \text{(Eqn. 1)}$$

The speckle contrast value is computed at each point in the image from the surrounding 5 x 5 or 7 x 7 region of pixels, producing a spatially resolved map of the speckle contrast over the field of view. Higher regional flows will result in more speckle fluctuations at a given exposure, raising the measured speckle contrast value for those pixels. As the exposure duration is shortened, only the highest flows are able to be captured due to their high speckle fluctuations. In order to capture flow in regions of lower flow, such as small vessels, the exposure duration must be increased to allow the camera capture their slower speckle fluctuations. The spatial analysis of the temporal phenomena assumes equivalence of spatial and temporal (e.g. ergodic) statistics. This assumption breaks down in two particular scenarios, areas with the either absence of flow or significant contributions of static scattering. Both of these scenarios can be accounted for through multiple exposure imaging. Though using a spatial window to compute speckle contrast lowers the spatial resolution of the technique, LSCI simulations using actual neurovascular anatomies have indicated that a large degree of spatial integration already occurs in widefield speckle imaging, [57] suggesting that imaging regions are sensitive to neighboring

and sub-surface flows that likely remove the effects of any added blurring caused by the moving spatial window.

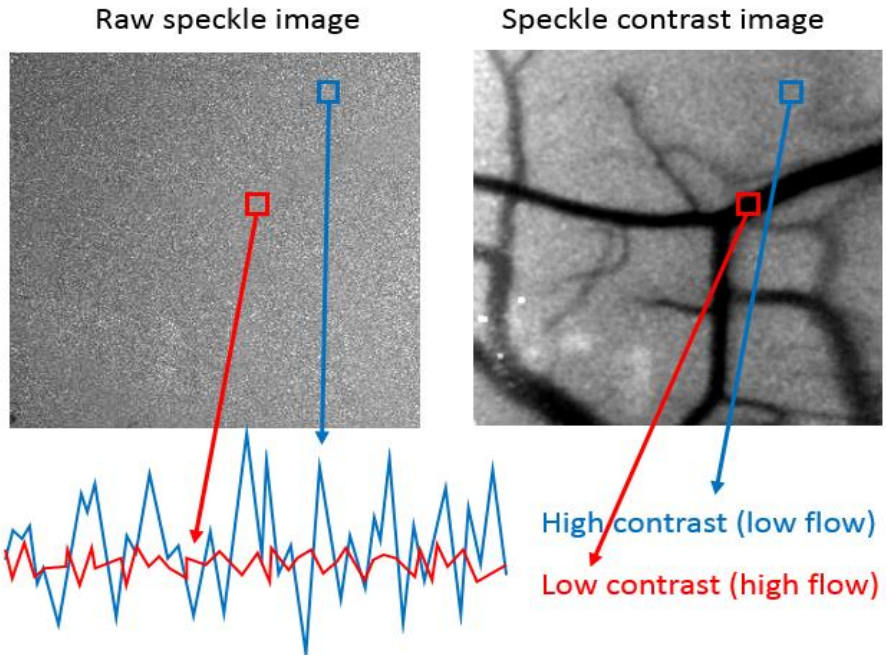

Illustration 1: Laser Speckle Contrast Imaging. Raw speckle image of scattered laser light from tissue imaged onto the CCD (left). Image of speckle contrast values, K, computed from raw speckle image by a moving 5 x 5 window (right). Areas of high flow originate from small fluctuations over the camera exposure duration (red) while areas with low flow result from high fluctuations (blue).

With LSCI, an approximation of the correlation time of the speckles, τ_c, which quantifies the observed rate of dynamic light scattering can be made. This allows an estimate of the inverse correlation time (ICT: $1/\tau_c$), which can be used to determine relative change in the CBF velocity. Stemming from Fercher and Briers,[41] and improved upon by Bandyopadhyay[58] and later Dunn and Parthasarathy,[59] we have arrived at a mathematical model relating our speckle variance to a fixed exposure time, allowing us to decouple flow

contribution from speckle contrast measurements by finding the temporal autocorrelation decay time of the speckles. This speckle autocorrelation time has been posed to be inversely proportional to the speed of the scattering constituents[60] in a single scattering regime, and weighted by the number of dynamic scattering events under multiple scattering.[61] Some studies have shown that the inverse correlation times of specific regions and full-field regions correlate well with CBF in vivo, assuming single dynamic scattering.[43,62] The exact physical relationship between the inverse correlation times and the cerebral blood flow across both resolvable and unresolvable vasculature requires further examination, but is known to be a function of the specimen properties and imaging geometry.[51] The speckle correlation time is typically extracted from the following relation:

$$K(T,\tau_c) = \left(\beta \frac{e^{-2x} - 1 + 2x}{2x^2} \right)^{1/2} \qquad \text{(Eqn. 2)}$$

where $x = T/\tau_c$. This relationship highlights that the observed contrast is a function of the exposure duration of the camera, the autocorrelation time of the field, and is scaled by the instrumentation factor, β. Both this model and its further simplified variant have been used to predict similar $1/\tau_c$ changes[63] in the relative CBF dynamics have been used in a wide range of blood flow imaging applications.[64]

Inverse correlation times from speckle imaging have often been reconciled both theoretically[65] and empirically[63,66] with those measured with laser Doppler flowmetry. The inverse of the correlation time is often interpreted as being proportional to the speed of the moving particles (i.e. blood cells), an assumption retained from Laser Doppler Flowmetry (LDF) of capillary flow.[51] With this assumption, in the limiting case of imaging an isolated

capillary vessel, the inverse correlation times present a measure of the volumetric flux through the vessel. When measuring only relative flow dynamics from the same region, this assumption may scale to larger vessels, which has been shown by a number of calibration studies in single microfluidic flow channels with comparable sizes to large rodent micro-vasculature,[67–71] where the changes in the speckle flow indices have been significantly proportional to the pump flow rate dynamics. This result leads most studies to interpret the ICT measurements as the flow velocities in their vessels. However, this assumption does not account for variations in blood vessel caliber and hematocrit, and is potentially inaccurate. There is also the case when ICT measurements are taken from parenchymal regions, where the speckle flow indices cannot be deterministically decoupled to each contributing micro-vessel. Though ICT may not directly represent flow velocities, strong correlations between speckle based flow measures and alternative perfusion indices[72–75] across single vascular and parenchymal regions suggest that relative changes in flow dynamics within any given region of interest may be accurately captured with LSCI, allowing for the use of ICT measurements to describe a regional perfusion index in arbitrary physical units.

The hardware scheme for basic LSCI consists of a laser and CCD camera, with optics to expand the laser light to illuminate the region of interest as well as collection optics to focus the scattered light onto the CCD. Lasers generally used for hemodynamic imaging in the brain are in the red to near infrared wavelengths where the light is known to have low absorption with high scattering coefficients, allowing for deeper light penetration to sample more tissue. This simple LSCI technique can utilize widely available

diode lasers in these wavelength ranges. The other main component of the basic LSCI setup is the camera. Choices of specific cameras for LSCI vary widely, but inexpensive cameras have demonstrated the ability to provide blood flow information for detailed physiological studies.[76,77] The raw speckle image (Illustration 1) is a result of the scattered light from the cranial window reaching the camera, allowing for computations of speckle contrast.

Criticisms of LSCI have been the inability to measure and quantify an absolute baseline.[78] Although this is may not present a hindrance to groups studying small changes in CBF dynamics in acute settings,[44] the lack of absolute measurements will limit the ability to compare measurements over a chronic setting, as well as large changes (>50%) in an acute setting, as each single exposure used for LSCI has a flow range in which the relative measurements are accurate. For this reason we will use multiple exposure durations to obtain speckle contrast measurements, and subsequent inverse correlation time measurements, with increased quantitative accuracy.

2.2 Multi-Exposure Speckle Imaging

Multi-Exposure Speckle Imaging (MESI) has been shown to provide high quantitative accuracy of chronic blood flow dynamics and reliable spatial perfusion indices that help to characterize the vasculature over periods of several weeks.[79] In addition to this, LSCI has also been shown to underestimate large changes of flow, which will drastically change results in occlusion studies.[59] This critique of LSCI is also solved by using MESI, which is shown to accurately model flow change from an induced stroke.[80]

Multi-Exposure Speckle Imaging for these studies was performed[79,81] by illuminating the cranial window with a laser diode (λ=660 nm, Micro Laser Systems, Garden Grove, CA, USA). An acousto-optic modulator was used to control the exposure and amplitude of the illumination, while a camera (A602f: Basler Vision Technologies, Ahrensburg, Germany) was simultaneously triggered over 15 exposure durations ranging from 0.05 ms to 80 ms. The backscattered light from cranial window was collected by a 10 × objective (Figure 1A) and imaged onto a CCD camera. Each of the chosen 15 exposure durations generated a single exposure speckle contrast value at each pixel, and together are used to generate one MESI computed frame (Figure 1B).

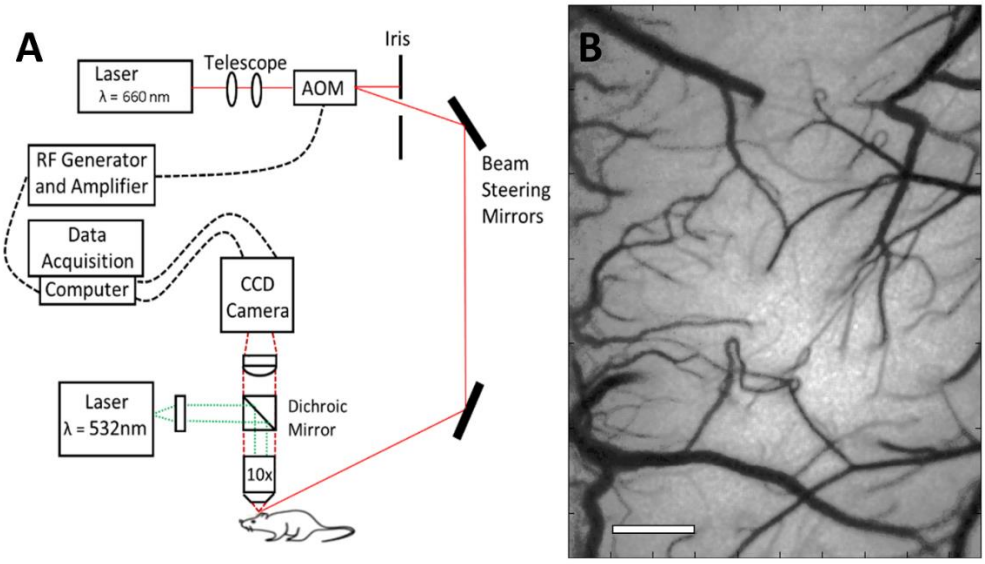

Figure 1: (A) Schematic of Multi-Exposure Speckle Imaging hardware. Dichroic mirror was used to deliver 532nm laser for photo-thrombotic occlusion. AOM, acousto-optic modulator. CCD, charge coupled device. (B) Multi-Exposure Speckle Imaging inverse correlation time (MESI ICT) image of flow computed from 15 exposures. Increased flow is denoted by darker pixels. Scale bar = 500 µm.

With the MESI model, the dependence of the speckle contrast value, K, on the exposure duration of the camera, T, is mapped to obtain a better determined estimate of the correlation time of the speckles, τ_c, at each pixel:

$$K(T,\tau_c) = \beta^{1/2}\left\{\rho^2 \frac{e^{-2x} - 1 + 2x}{2x^2} + 4\rho(1-\rho)\frac{e^{-x} - 1 + x}{x^2} + (1-\rho)^2\right\}^{1/2} + v_{noise} \quad \text{(Eqn. 3)}$$

Where $x = T/\tau_c$, ρ is the fraction of light dynamically scattered, β is a normalization factor to account for speckle sampling, and v_{noise} accounts for instrument noise.[59] By accounting for the exposure dependence, instrument factors can be estimated regardless of speckle sampling, enabling a more absolute estimate of the inverse correlation time. A significant improvement with MESI is the ability to account for the effects of heterodyne mixing,[51] where light is scattered by both moving and stationary particles in the specimen. This process is particularly necessary when examining measurements from parenchymal flows as well as though thinned skull preparations.[82,83]

Both in vitro and in vivo validations of MESI have demonstrated substantial improvements in the quantitative accuracy of the speckle flow measurements.[70,75,82,84,85] Within resolvable surface vessels, ICT measurements have been shown to be proportional to red blood cell speed with MESI.[79] In regions of parenchyma between resolvable vessels, where contributions to speckles result from the integration of scattering over a host of unresolvable microvasculature, the ICT measurements can be treated as a regional perfusion index.[45,76,86]

2.3 TWO-PHOTON FLUORESCENCE MICROSCOPY

Two-photon fluorescence microscopy is an optical imaging modality that provides significant improvements over widefield and single photon confocal microscopy. This technique utilized near-infrared laser excitation for better depth penetration and limits both photo-damage and out of focal plane excitation, allowing for improved depth resolution and sectioning. The combination of two-photon microscopy with the designing of more efficient fluorescent contrast agents has resulted in this optical imaging technique widely expanding the possible uses for *in vitro* and *in vivo* studies. Multiphoton absorption and excitation was theorized in 1931 by Maria Goeppert-Mayer in her doctoral dissertation.[87] Specifically within this multiphoton regime, two-photon absorption takes advantage of nonlinear processes of intense light. Being a nonlinear process, two-photon absorption efficiency is intensity dependent, requiring high spatial and temporal co-localization of the photons. This is achieved by use of a high repetition rate femtosecond laser source in combination with high numerical aperture objectives. Further advances in fields of photochemistry and optical engineering also progress two-photon microscopy further, with recent improvements in resolution breaking the diffraction limit with Two-Photon Excitation - Stimulated Emission Depletion Microscopy.

The process behind multiphoton excitation is that when a sufficiently high photon density is reached, two photons of half the energy difference of an electronic transition can simultaneously absorb. This simultaneous moment can be more appropriately characterized as a temporal transition period of approximately 0.5 fs or less, which is the approximate lifetime for the notion of the intermediate one photon virtual transition step.

Depth localization with two-photon microscopy comes from the fact that the probability of two-photon absorption depends on the squared incident intensity, which spatially confines the generation of fluorescent signal to the focal spot size of the microscope. This depth confinement process was first demonstrated by Denk and Webb in 1991,[88] allowing for three dimensional sectioning of the imaged object by constraining the presence or absence of fluorescent signal to only the focal volume. This ability to observe living cells in three dimensions makes two-photon microscopy an invaluable technique in the progression of *in vivo* imaging.

Two-photon fluorescence microscopy was used in conjunction with LSCI system, which provided a surface view of the animal allowing for targeting of the same regions of interest (Illustration 2). This combination of techniques allowed for depth-resolved and depth-integrated images of the same regions to be co-registered.

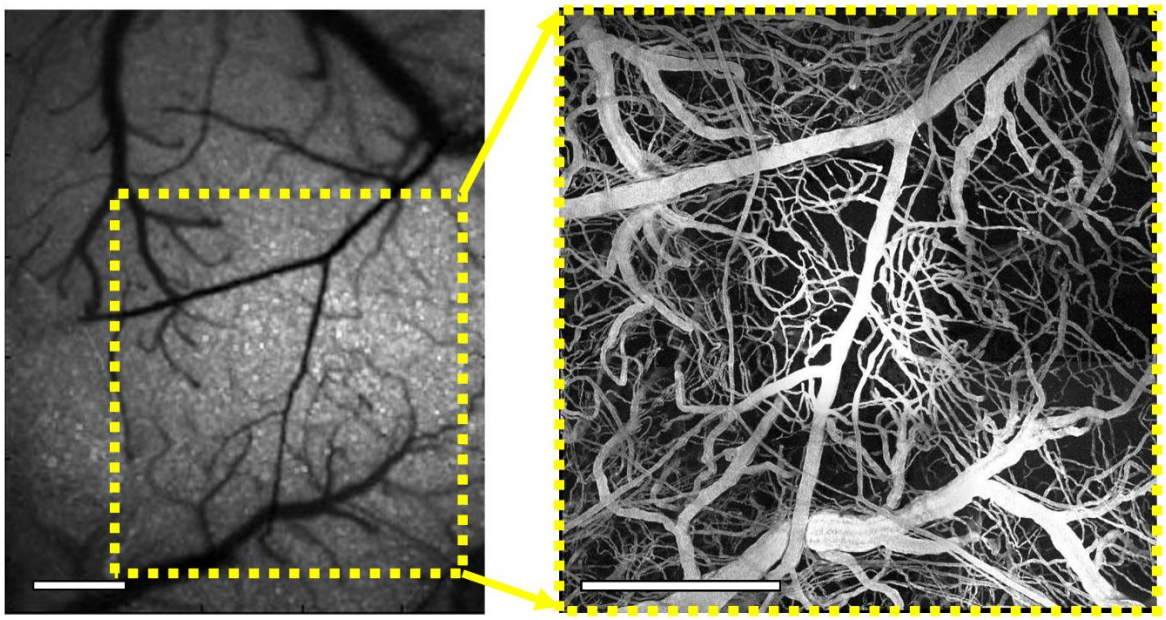

Illustration 2: Speckle contrast image (left) of cortex used for targeting region of interest and corresponding two-photon projection (right) of labeled vasculature to depths of 300 μm. Scale bar = 500 μm.

Two-photon fluorescence microscopy was performed using a custom-built system that also integrates laser speckle contrast imaging (Figure 2). The system uses a large back-aperture objective with a long working distance, two-inch collection optics, and un-cooled, un-housed photon-counting PMTs (H10770PB-40, Hamamatsu Photonics, Japan) to optimize collection efficiency.[89] A Ti:sapphire femtosecond excitation laser (Mira 900f, 140fs, 76MHz, Coherent Inc.) was tuned to optimize acquisition of signal from the fluorescent vascular label. Laser intensity was controlled with an electro-optical modulator, and a dichroic mirror, D1, was to separate excitation and emission light. Laser speckle imaging was used to identify and target vascular regions imaged in previous MESI

sessions (Illustration 2). Collection of LSCI signal used the same objective, with a dichroic mirror, D2, separating LSCI contributions from two-photon emission light. The system allowed for an X-Y resolution of 1.12 µm per pixel.

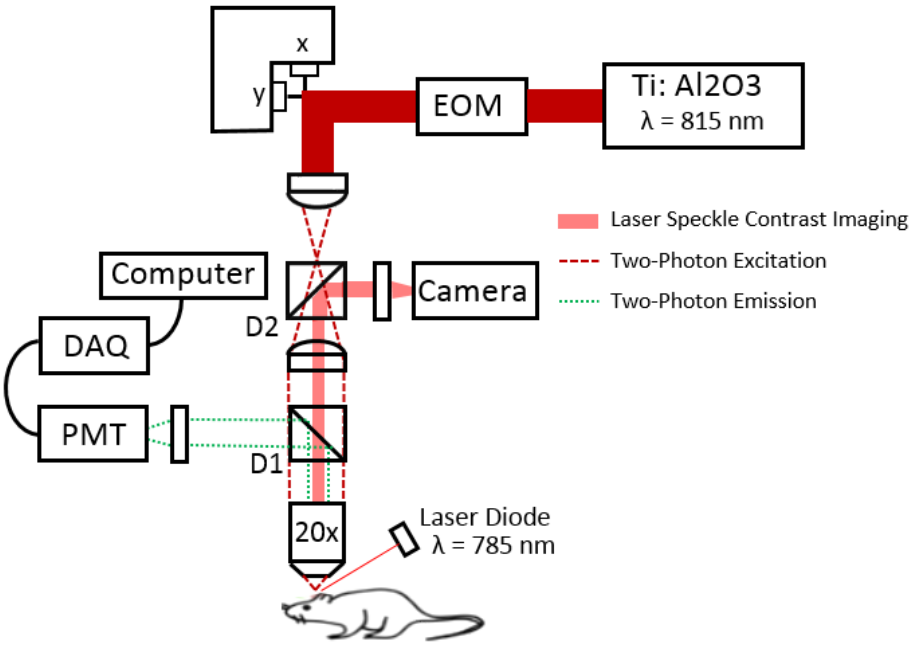

Figure 2: Schematic of custom two-photon microscope with integrated laser speckle contrast imaging. EOM, electro-optic modulator. PMT, photo-multiplier tube. DAQ, data acquisition. D1, dichroic mirror used to separate two-photon excitation and emission. D2, dichroic mirror used to collect laser speckle measurements. X-Y resolution of 1.12 µm per pixel.

2.4 Vascular Occlusion Via Photo-Thrombosis

To induce a focal ischemia in the animal, we use photo-thrombotic mechanisms that utilize photosensitizing agents with triplet states that produce an elevated reactive oxygen species concentration when exposed to a photo-initiator. For these experiments our photosensitizing agent was Rose Bengal administered via injection to the animals

(0.2mL 15mg/mL, intraperitoneal). This agent has been shown to be fast-clearing, which is optimal for these chronic studies.[42,90,91] Our photo-initiator was a 532 nm green laser (Aixiz, USA) fiber coupled into the system to deliver focused illumination. The laser was focused on the targeted descending arterioles (0.6 mm diameter focal spot, 20 mW). The goal of the photo-thrombotic occlusion was to disrupt oxygen delivery to the local area and descending arterioles have been shown to serve as bottlenecks in the cortical oxygen supply (Figure 3).[17]

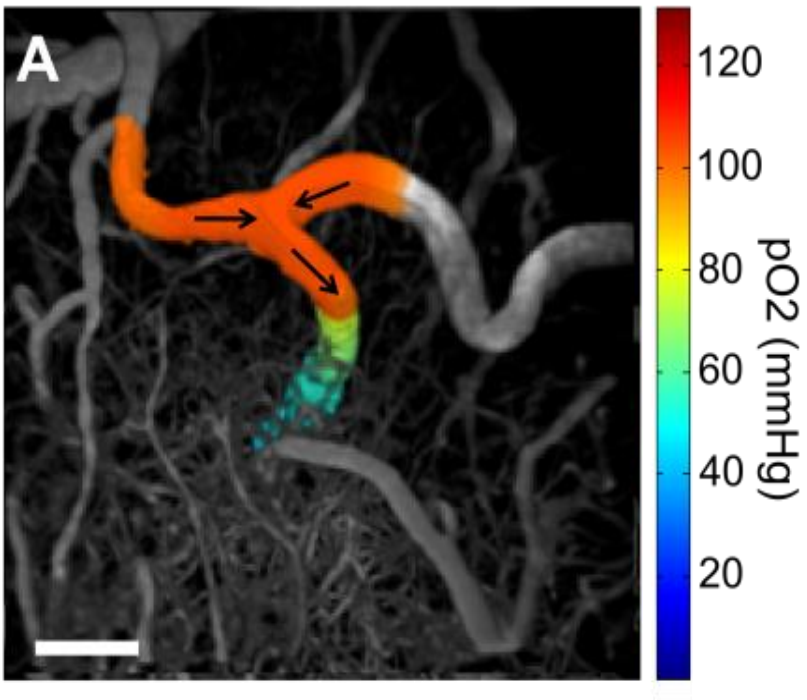

Figure 3: Two-photon microscopy projection of vasculature with partial pressure of oxygen (pO2) measurements along the descending arteriole displaying large drops in pO2 as the arteriole descends. Arrows denoting direction of flow. Scale bar = 100 μm.

As the focused photo-activation occurs at the edges of the vessel lumen, the photosensitizing agent can generate localized concentrations of singlet oxygen. This

causes platelets in the blood to respond by releasing clotting factors and initiating a clotting cascade. The result is a thrombus that can completely occlude the entire lumen cross-section in under a minute. The resulting oxygen supply within these arterioles after these photo-thrombotic occlusions shows large deficits penetrating into the cortex (Figure 4). This causes the brain to begin attempts at recovery of the area and re-oxygenation of the tissue around the occlusion site.

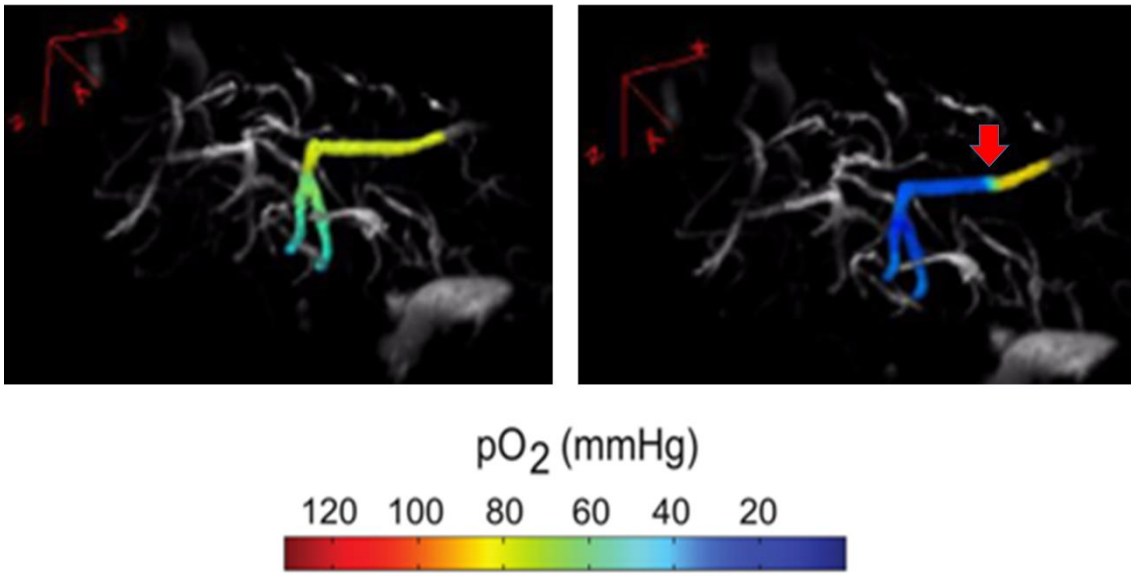

Figure 4: Two-photon microscopy projections of vasculature overlaid with pre- and post-stroke partial pressure of oxygen (pO2) measurements within a descending arteriole that served as a stroke target. Red arrow denoting the site where the photo-activating laser was focused.

We use both LSCI and two-photon microscopy routinely to confirm clot formation and retention. Due to the vessel having no flow, there is no longer any contrast in the speckle image to differentiate the vessel from the surrounding tissue (Illustration 3). This is why it appears that the vessels disappear at the two targeted occlusion areas in Illustration

3. The first post-occlusion imaging session were done approximately 1 hour after clot formation, allowing us to ensure that the thrombus has not been cleared.

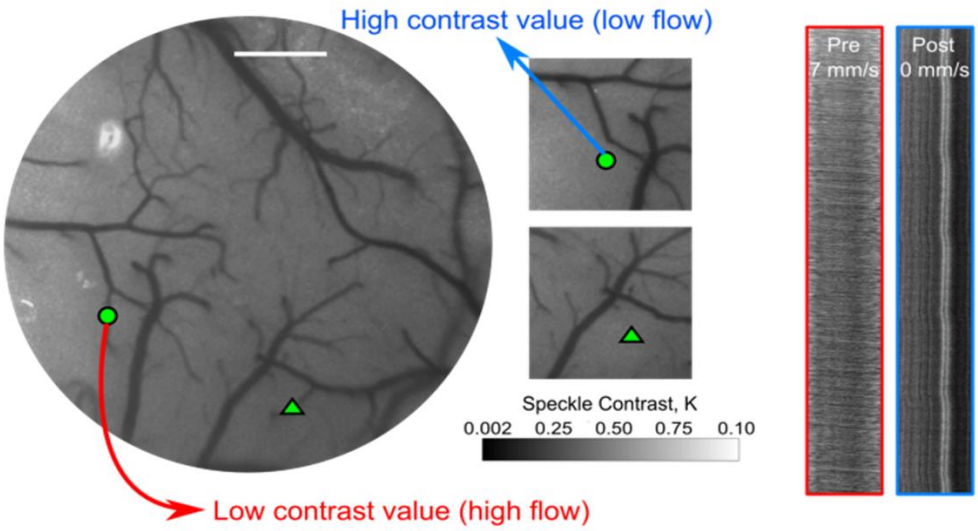

Illustration 3: Laser speckle contrast image of pre-stroke vasculature (left) and corresponding speckle contrast images after two targeted photo-thrombotic strokes delivered at 2 targets (middle) illustrating the lack of flow within the vessels causing loss of contrast in the image. Scale Bar = 400 µm. Line scans taken within arteriole denoted with circle at pre- and post-occlusion time points (right).

2.5 Optical Imaging of Functional Response

Imaging brain function with optical technique relies on measuring changes in the absorption and scattering properties of the tissue. The progression of techniques utilized in this graduate research for measuring functional responses of the rodent cortex to forepaw stimulation include optical imaging of intrinsic signals (OIS), LSCI, and a MESI-based technique. Both OIS and LSCI provide only a map of relative change, leading to a need for quantitative measurements of functional response for a chronic study. The development

of a technique to measure absolute changes in functional blood flow responses using multiple exposures is documented in Chapters 4 and 5.

Optical Imaging of Intrinsic Signals uses a camera to measure changes in the reflectance of tissue to a particular wavelength.[31] These changes can originate from a number of physiological variables at each wavelength such as blood volume, oxygenation, and metabolic activity.[32] Due to high spatial and temporal resolution without the need for exogenous dyes, OIS can obtain information about functional stimulation, and has provided insights into the functional organization of the cortex.[33–35] This technique was initially used in this research for functional mapping of the forepaw response with 580 nm light from a light emitting diode as the chosen wavelength (Figure 5). As 580 nm light corresponds to the highest absorption of oxygenated hemoglobin, a decrease in the reflectance is known to coincide with an increase in oxygenated hemoglobin within the area of interest. This information is then used to tell us that the cortex is being activated, thus drawing more oxygen, in these areas (Figure 5). A drawback of OIS is that even though the absorption coefficient of oxygenated hemoglobin is the main component in the change in reflectance, many other chromophores also contribute to the signal, making it difficult to quantify changes in a particular variable of interest. Measurements are therefore limited to relative changes in the reflectance with OIS.

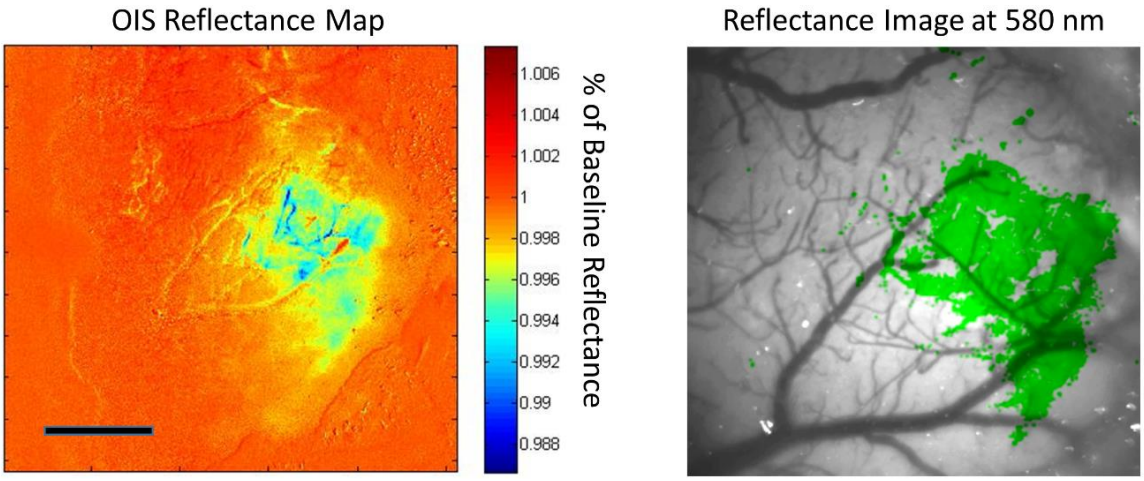

Figure 5: Map (left) of relative change in reflectance of 580 nm light with imaging of optical intrinsic signals during piezo-electric forepaw stimulation. Scale Bar = 500 µm. Reflectance image (right) of vasculature under baseline conditions with responding region overlaid in green.

Laser Speckle Contrast Imaging, as described previously in this chapter, can also be used as an optical technique for measuring functional changes of the blood flow due to forepaw stimulation. This technique, when sampled with sufficient temporal resolution, allows for measurements of the change in blood flow due to the stimulation. This increase in the demand for blood flow in the cortex is associated with higher functional activity of this region, allowing a functional map of the relative response to be produced (Figure 6). Different camera exposures can be used for LSCI to slightly alter the distribution of flows sampled, but 5 ms is generally used for functional activation of the rodent cortex, as it has been shown to display high SNR when capturing the response.[76]

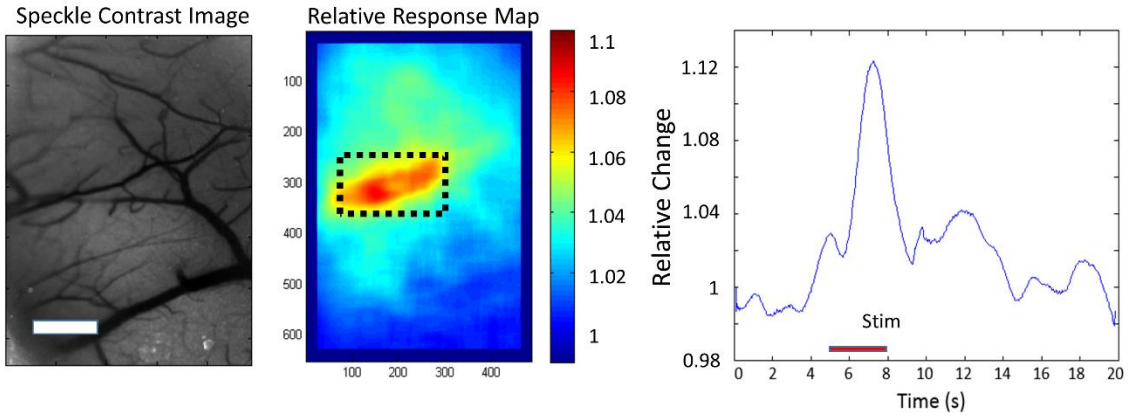

Figure 6: Laser Speckle Contrast Image (left) of vasculature under baseline conditions. Scale Bar = 500 µm. Response map (middle) of relative change in speckle contrast value during piezo-electric forepaw stimulation with time course (right) of region denoted by black box. Stimulus delivered from 5-8 seconds.

Both OIS and LSCI generally require the averaging of functional responses over several time intervals, or stimulation blocks, to reduce effects of signals such as instrument and physiological noise associated with factors other than the forepaw stimulation. Figures 5 and 6 were the result of averaging 25 stimulation blocks, with a piezo-electric transducer stimulating the contralateral forepaw at 100 Hz for a period of 3-5 seconds. Relative maps were produced by dividing images averaged over the stimulation period (5-8 seconds) by images averaged over the baseline period (0-5 seconds).

The choice of the piezo-electric transducer was made for the stimulation of our chronic animal model, as it provides a non-damaging and easily repeatable technique for forepaw stimulation. The relatively long stimulation periods of 3-5 seconds were chosen for better SNR by providing more measurements to average within the stimulated portion of the experiment. The stimulation technique likely activates the forepaw representation of the sensorimotor in these mice. This long stimulus also provides another metric on which

to observe the effects of ischemic stroke post-occlusion functional blood flow response in Chapter 5, as the ability of this region to recruit blood supply over the long stimulation duration is impacted.

Chapter 3: Progression of Vascular Flow and Structure after Stroke

Monitoring the progression of the vascular structure and cerebral blood flow (CBF) after brain injury is vital to understanding the neurovascular recovery process. Multi-Exposure Speckle Imaging (MESI) provides a quantitatively accurate technique for chronically measuring the post-occlusion CBF perfusion of the infarct and peri-infarct regions in rodent stroke models, while multiphoton microscopy offers direct visualization of the microvascular structure. In this paper, we present imaging outcomes extending 35 days after photo-thrombotic occlusion, tracking the progression of the vasculature throughout this period. We compare MESI flow estimates within the un-resolvable parenchyma to sub-surface microvascular volume fractions taken with two-photon microscopy in the same regions to assess how the vascular density influences the surface-integrated MESI flow values. The MESI flow measurements and volume fractions are shown to have high correlations ($r=0.90$) within areas of recovering vasculature in the peri-infarct region. We also observe vascular reorientation occurring within the microvascular structure throughout the 35 day post-occlusion period. With the combination of a chronic mouse model and relatively non-invasive optical imaging techniques, we present an imaging protocol for monitoring long-term vascular progression after photo-thrombotic occlusion with the potential to test the efficacy of rehabilitation and pharmacological therapies.

3.1 INTRODUCTION

Post-occlusion microvascular blood flow has been shown to be an important indicator of overall tissue outcome.[92,93] Many patients experience a partial recovery following stroke onset without treatment during a short period of plasticity occurring within the region of tissue surrounding the occlusion known as the penumbra.[94] This period of neuroplasticity is the beginning of the remodeling process, resulting in neovascularization and reperfusion of the existing vascular structure within the penumbra regions and continuing on into the ischemic core.[95] Residual tissue perfusion and vascular reperfusion play important roles in the remodeling process and overall post-stroke recovery outcomes, giving rise to a need for noninvasive, quantitatively accurate imaging techniques capable of repeatedly measuring tissue perfusion during the stroke recovery process over an experimental period of weeks to months.

Traditional optical techniques used in vascular imaging rely either on the tracking of contrast agents, such as RBCs or exogenous dyes in laser scanning microscopy,[96–99] or on dynamic light scattering, as seen in laser doppler flowmetry[60] and laser speckle contrast imaging (LSCI).[40,43,44,62,100] Recent advances in LSCI termed multi-exposure speckle imaging (MESI) have allowed for the technique to move from primarily acute experiments to chronic studies through improvements in its quantitative accuracy of blood flow measurements.[59] By utilizing multiple camera exposures spanning almost three decades in duration and improved mathematical models, MESI is able to more precisely sample and map the flow distributions prevalent in the rodent vasculature.[79] Studies have shown MESI to accurately estimate a wide range of flows *in vivo*, including complete flow reduction

during middle cerebral artery occlusions,[81] and also shows the ability to determine spatially integrated perfusion measurements from unresolvable microvasculature within the parenchyma.[101] For stroke studies, the technique is able to highlight perfusion boundaries within the peri-infarct region to determine the extent of the damage and chronically track the progression of the vasculature.[79]

Multi-Exposure Speckle Imaging provides high quantitative accuracy of CBF dynamics and provides reliable spatial perfusion indices that help to characterize vascular progression following ischemic stroke, but remains a depth-integrated imaging technique. Two-photon laser scanning microscopy provides a depth-resolved technique with the ability to monitor the degree and time-scale of post-stroke vascular structure in three dimensions. Direct visualization of the vessel organization using two-photon microscopy is necessary for understanding the physiological origin of the MESI measurements within the unresolvable sub-surface microvasculature. By utilizing this combination of techniques, we present a protocol with the ability to chronically track post-occlusion neurovascular outcomes at and below the surface of the mouse cortex.

3.2 METHODS

This study utilized two optical imaging techniques in Multi-Exposure Speckle Imaging and Two-Photon Fluorescence Microscopy, chosen to combine and compare measurements from a global, depth-integrated, field of view with a local, depth-resolved field of view. These methods are discussed in more detail in Chapters 2 of this dissertation. In addition to these imaging techniques, a chronic animal mouse model was used, with the

surgical preparation and upkeep documented in Appendices 1 and 2, as well as the photo-thrombotic stroke model discussed in Chapter 2.4.

3.2a Experimental Protocol

Animals with clear and healthy cranial windows after 4-6 weeks of recovery post-surgery were anesthetized with 70% N_2/O_2 vaporized isoflurane via nose-cone and affixed to a stereotaxic frame. Vitals were recorded via pulse oximetry and temperature was maintained by feedback as described previously. Multi-Exposure Speckle Imaging was performed over a 2.7 × 2.0 mm field of view centered on the region of interest by collecting 300 frames at each exposure. Animals were then carted to a combined two-photon fluorescence and laser speckle contrast imaging system, with FITC-dextran (0.1mL, 5% w-v, Sigma) administered retro-orbitally to label the blood plasma. A vascular image stack was taken by scanning 600 µm × 600 µm images of the vascular structure every 2 µm in depth down to 300 µm. Each animal underwent imaging of a 2 × 2 or 3 × 3 grid of vascular image stacks centered on the infarct area, resulting in 1 x 1 mm to 1.5 x 1.5 mm fields of view, respectively.

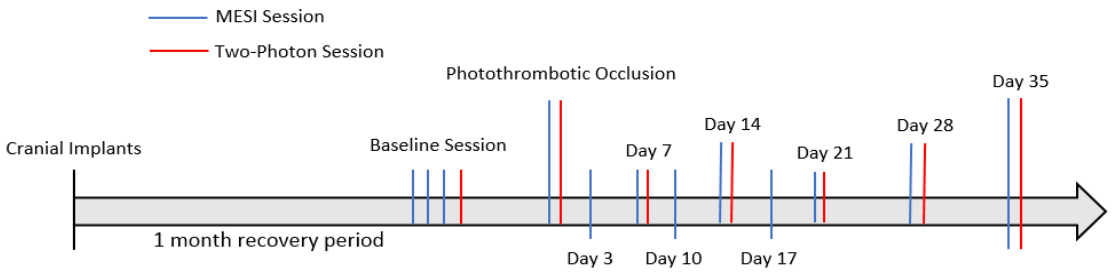

Illustration 4: Experimental time line for Chapter 3 Study.

The experimental time line used for this study is displayed in Illustration 4. Multi-Exposure Speckle Imaging experiments were conducted twice weekly, with 2 weeks of baseline sessions and 5 weeks of post-stroke measurements. Targeted occlusions were delivered immediately after the final baseline imaging session. Post-occlusion imaging sessions were performed twice weekly until 21 days after occlusion, then weekly until an endpoint of 35 days. Two-photon imaging was performed over the same experimental period with 1 baseline session and 7 post-stroke measurements starting at Days 0 and 3, then weekly until the 35 day endpoint. All experiments were approved by the Institutional Animal Care and Use Committee (IACUC) at The University of Texas at Austin under guidelines and regulations consistent with the Guide for the Care and Use of Laboratory Animals, the Public Health Service Policy on Humane Care and Use of Laboratory Animals (PHS Policy) and the Animal Welfare Act and Animal Welfare Regulations.

3.2b Image Processing Techniques for Data Analysis

Images of ICT measurements taken with MESI were processed in MATLAB (Mathworks, Natick, MA). To reduce variability between animals and focus on signal attributed to unresolved microvasculature, an image processing script to remove surface vessels from ICT maps was developed, leaving only ICT measurements taken within the parenchyma (Figure 7). These parenchymal ICT values were used in comparisons with sub-surface measurements of volume fractions from two-photon imaging. Though the contributions from surface vessels are not eliminated, as the speckle contrast measurements

are still laterally sensitive to the high speed surface vasculature, they are at least minimized with this thresholding technique.

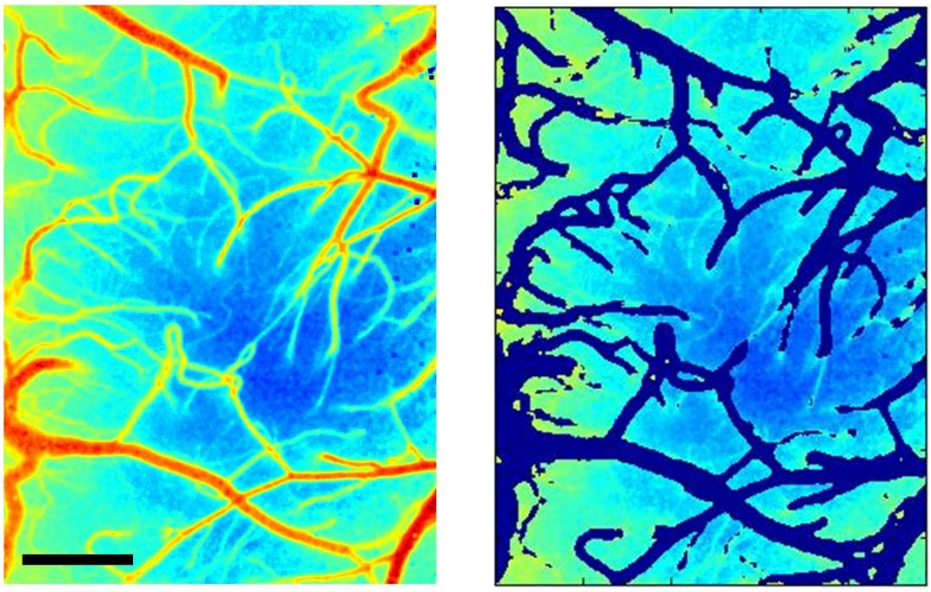

Figure 7: Multi-Exposure Speckle Imaging inverse correlation time (MESI ICT) map of cortex and corresponding map with surface vessels extracted, leaving only parenchyma ICT values. Scale Bar = 250 μm.

To increase the field of view without sacrificing spatial resolution of the two-photon images, vascular stacks were taken around the region of interest and stitched together in post-processing (Figure 8). This process was done in ImageJ with an algorithm developed by Preibisch et al,[102] resulting in a much larger field of view encompassing the infarct area and extending into the surrounding peri-infarct regions. After stitching, ImageJ was then used to filter and binarize the vascular stacks in order to calculate volume fractions seen in each 100 μm layer of vasculature. Li's Minimum Cross Entropy thresholding was used in ImageJ to convert vascular stacks to binary maps.[103]

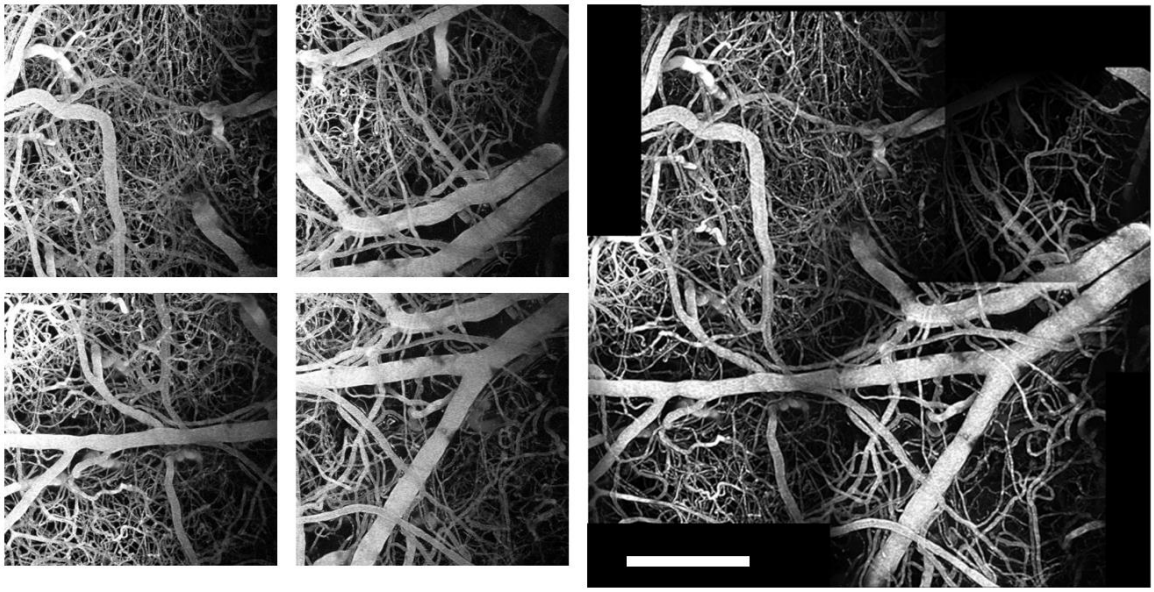

Figure 8: Maximum intensity projections from four individual two-photon vascular stacks (left) of 600 x 600 x 300 μm that were stitched together using ImageJ software. Projection of 2 x 2 stitched maximum intensity projection (right) of all 4 vascular stacks shown. Scale Bar = 500 μm.

Binary images of the sub-surface vascular structure were read into MATLAB to analyze the distribution of orientation angles seen in these vessels. This analysis used the Radon transform,[104,105] which takes line integrals at different tangents along the image. A sinogram (Figure 9) of the Radon transform was generated in order to calculate the variance at each angle, $\sigma^2(\theta)$. This variance measurement describes the distribution of vessels oriented at each angle.[106] By comparing the variances between angles, the distribution of the angular orientations in the binary projection can be measured.

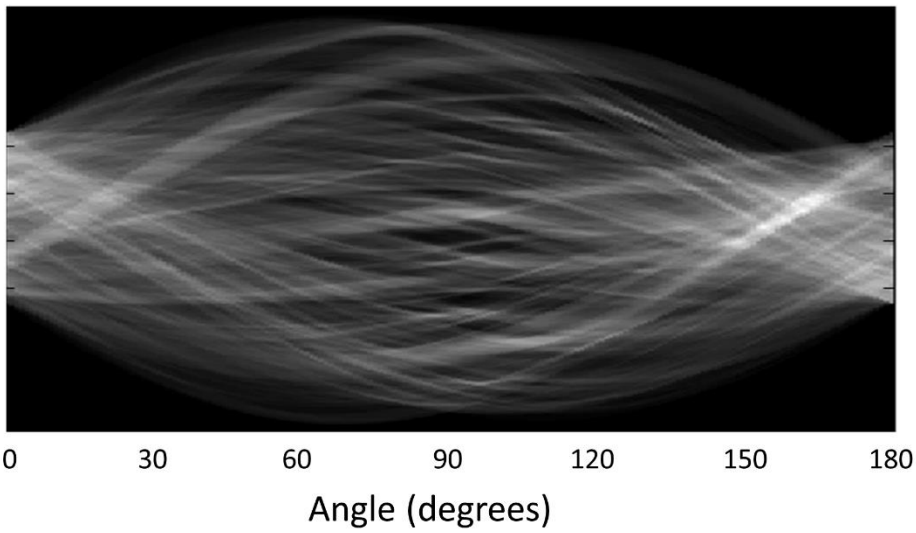

Figure 9: Sinogram displaying the variance from a Radon transform of a two-photon region of post-stroke microvasculature at 90° angle to infarct center. The variance of this sinogram describes the distribution of orientation angles within the imaged vasculature.

3.2c Histology and Statistical Analysis

Following the final imaging sessions at the Day 35 post-occlusion time point, histological assessments of the mouse brain were taken to study the lesion size and location (Figure 10). Nissl staining of a 30 μm coronal section with toluidine blue was used. This stain is selective for Nissl bodies found predominantly in polyribosomal structures in the soma and processes of neurons and glia, and the absence of the stain is indicative of an absence of cells.

Figure 10: Nissl stained coronal section (50 µm thick, 300 µm spacing) with toluidine blue after 35 days post-stroke imaging with infarct area labeled. Scale bar = 1 mm.

In order to determine if baseline pre-stroke MESI ICT values were statistically different from post-occlusion measurements, two-tailed paired t-tests were used. This same analysis was used for comparing pre-stroke and Day 35 post-stroke angular orientation data sets.

3.3 RESULTS

3.3a Cerebral Blood Flow Progression

Measurements of the pre- and post-stroke CBF dynamics of each animal (n=6) were taken with MESI, beginning with 3 pre-stroke measurements taken over a period of two weeks to establish a stable baseline. A baseline parenchymal ICT value was established for each animal by averaging parenchymal ICT values within a 1 × 1 mm region centered on the targeted arteriole over all baseline measurements. This 1 x 1 mm region was chosen for the occlusion site by identifying an area of vasculature containing a descending arteriole

and minimal surrounding surface vasculature to be sure the occlusion impacted the regional blood supply. Due to these two constraints, the baseline parenchymal ICT value established by this area was generally lower than surrounding areas, which can be seen in Figure 11. With this baseline ICT value, relative ICT maps were created (Figure 11) to identify perfusion boundaries created by the occlusion, including regions of at-risk tissue with moderate flow deficits (<75% baseline flow) and severe flow deficits (<25% baseline flow). The ICT measurements taken just after photo-thrombotic occlusion labeled as the 'Day of Stroke' were much lower globally than all other experiments due to animals being on anesthesia for a significantly longer period of time than on other experiment days (Figure 11).

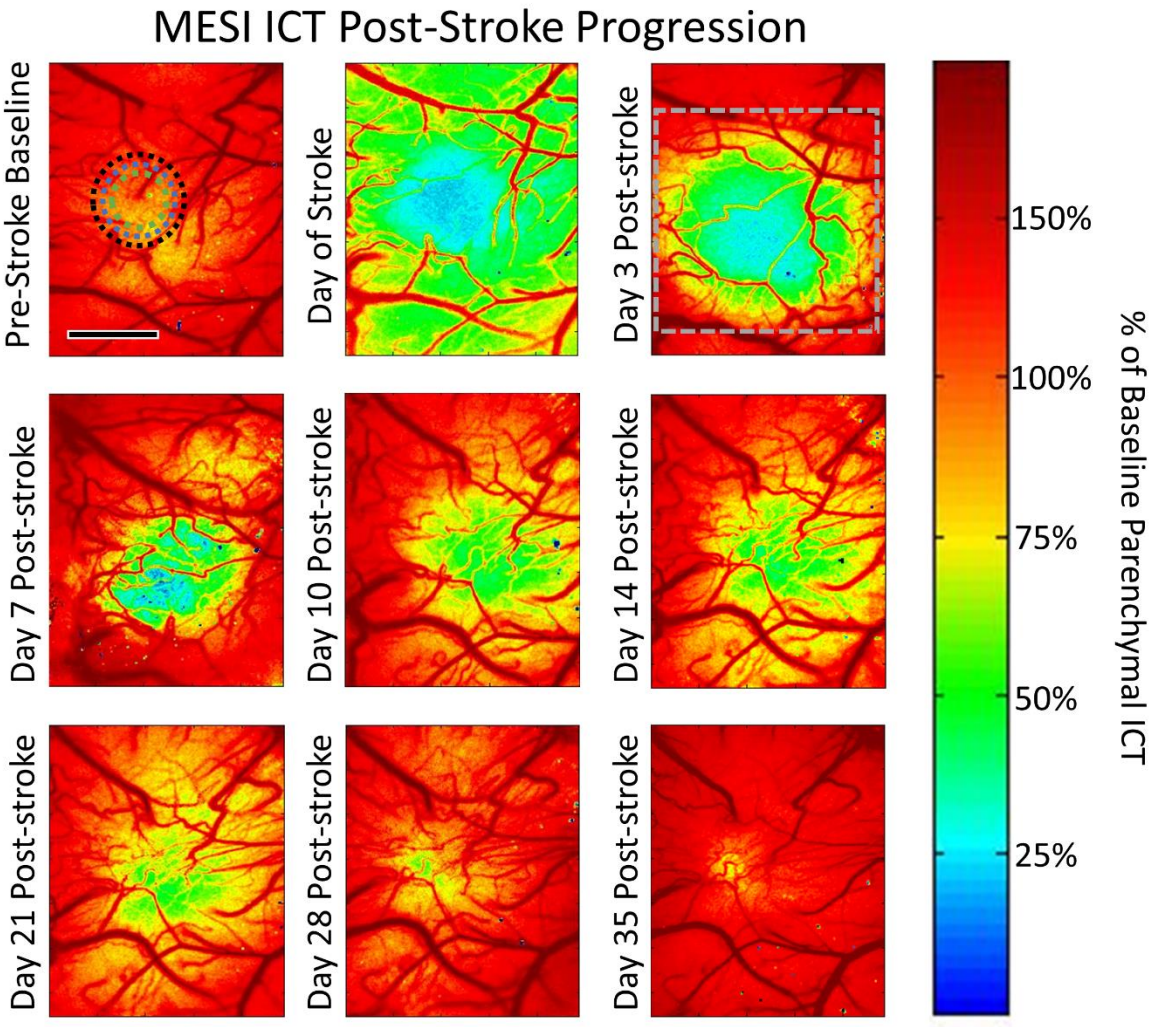

Figure 11: Multi-Exposure Speckle Imaging inverse correlation time (MESI ICT) images of perfusion before and after photo-thrombosis. Color scale established by parenchymal ICT measurements centered on occlusion target. Areas of green to yellow denote areas of moderate flow deficit, while blue to black denote the areas of severe flow deficit. Top right image contains 3 annular rings centered on the infarct denoting Zones 1, 2, and 3 for Figure 12. Day 3 Post-stroke image contains grey box denoting 2 x 2 mm region used for Figure 13. Scale Bar = 1 mm.

After a period of 10-14 days, substantial flow (>50%) returned to the center of the occlusion site (Zone 1), with a severe flow deficit area of <1% of that seen in Day 3

(Figures 11 and 12). This trend of perfusion of the severe flow deficit area by Day 14 was consistently observed over all animals. Though there did not appear to be reperfusion of the vessel targeted during occlusion over the duration of the experiment with MESI, regional perfusion values throughout the peri-infarct region (Zones 2 and 3) were >50% of baseline measurements by Day 21 post-stroke (Figures 11 and 12). As very few surface vessels were observed within areas of severe flow deficit, these ICT measurements suggest that increased flow is occurring within the sub-surface microvasculature. By Day 28, the average area of moderate flow deficit over all animals was reduced to <5% of the area seen in Day 3, suggesting the vasculature had fully perfused the occlusion area within this time frame.

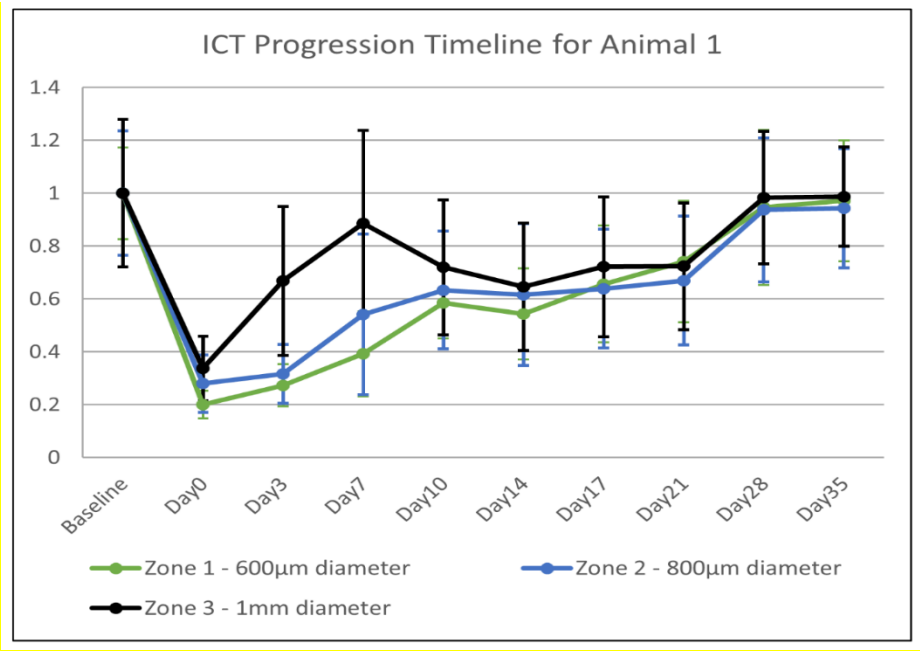

Figure 12: Plot of relative inverse correlation time (M ± SD) for animal 1 shown in Figure 11. Zones 1, 2, and 3 are annular rings centered on the infarct center extending outwards with diameters of 600 µm, 800 µm, and 1 mm, respectively.

Global progression of ICT values averaged over a 2 × 2 mm field of view centered on the occlusion site for all animals (Figure 13) were normalized by the average of the three baseline values. Measurements of ICT across the 2 x 2 mm field of view (Figure 11) showed significant changes in blood flow from the averaged baseline flow were seen for Days 0 and 3 ($p<0.01$, t-test). Progression was seen between Days 3 and 7, with the average severe flow deficit area over all animals shrinking from 0.55 mm^2 to 0.15 mm^2, and the average area of moderate flow deficit shrinking from 1.44 mm^2 to 0.65 mm^2 (Figures 14). Though the areas of moderate and severe flow deficit were still apparent for Animal 1's Day 7 ICT values (Figures 11 and 12), global ICT has returned to an average of 85% of baseline for all animals (Figure 13), largely boosted by an increase in the CBF of the

healthier vasculature surrounding the peri-infarct region beyond the areas measured in Figure 4B. This large increase in the flow of the healthy vasculature surrounding the infarct and peri-infarct regions was observed over the full 35 day post-stroke period.

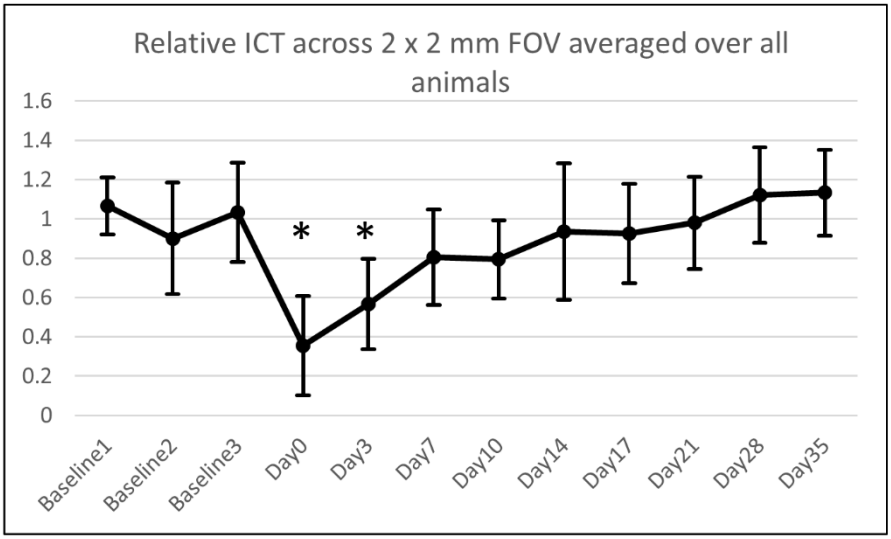

Figure 13: Plot of relative inverse times correlation over the 2 x 2 mm field of view denoted in Figure 4A for all animals (M ± SD, n=6) over the experimental time period. The three baseline measurements were averaged together to normalize the post-stroke relative measurements. Asterisks denoting time points with statistically significant changes in ICT values ($p<0.01$, t-test).

The size of the severe flow deficit area appeared to be reduced to almost zero by Day 14 with an average area of 0.048 mm^2 (Figure 14), suggesting that even the at risk regions with some moderate flow reductions retained enough flow to perfuse the most highly damaged tissue at the infarct center. By Day 21, global ICT returned to 98% of baseline, though an average moderate flow deficit area of 0.26 mm^2 still existed (Figures 13 and 14). As the regions with moderate flow deficits shrank further in Days 28 and 35, the global ICT surpassed the baseline by an average of 12% (Figure 14).

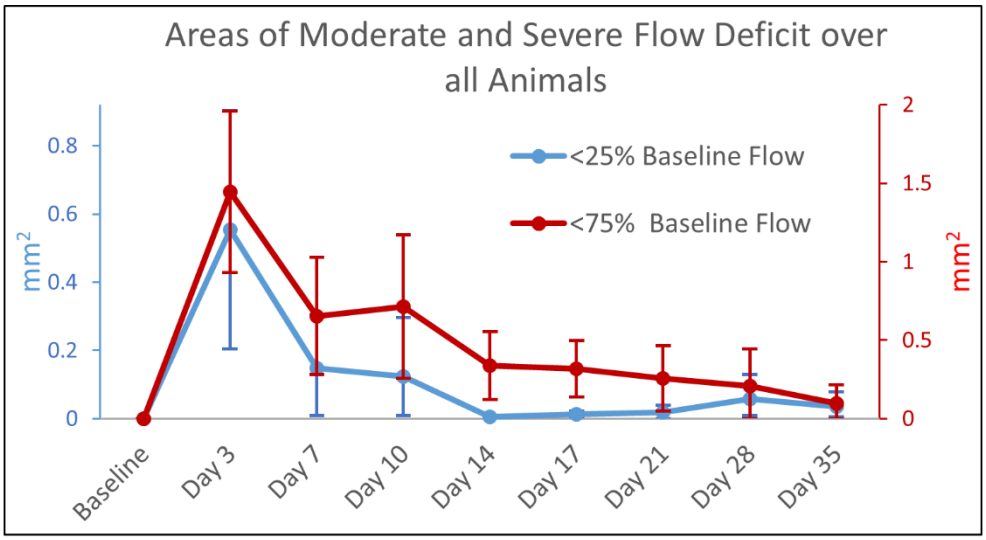

Figure 14: Plot of the Mean ± SD area of moderate (<75% of baseline flow) and severe (<25% of baseline flow) flow deficit for all animals (n=6) over 35 days post-occlusion.

3.3b Structural Progression of Vasculature

Two-photon microscopy projections of vasculature in a 1 × 1 mm field of view at depths from 150-180 µm are presented with damaged infarct areas highlighted to show the progression of the capillary vessel wall recovery over the post-stroke time course (Figure 15). These images correspond to the ICT maps of the animal shown previously (Figure 11). Baseline measurements were taken a minimum of 35 days after placement of cranial windows to ensure recovery from the surgery, with photo-thrombotic occlusion delivery around 50 days post-surgery. Images taken immediately following photo-thrombotic occlusion showed extravasation of the fluorescent dye throughout the vasculature, as well as a darker halo within the center of the image with the same diameter of the 532 nm occlusion laser (Figure 15). By Day 3, no subsurface microvasculature was visible in 4 of the 6 animals, as the combination of cortical damage and dye leakage from the vasculature

at the surface prevented any possible imaging of the sub-surface microvasculature for this time point (Figure 15). This leaked dye was seen before injection of fresh fluorescent dye on Day 3, suggesting it was not cleared from the area between Days 0 and 3, with the same occurrence between Days 3 and 7. Images taken at Day 7 again showed no sub-surface vasculature in the field of view (Figure 15).

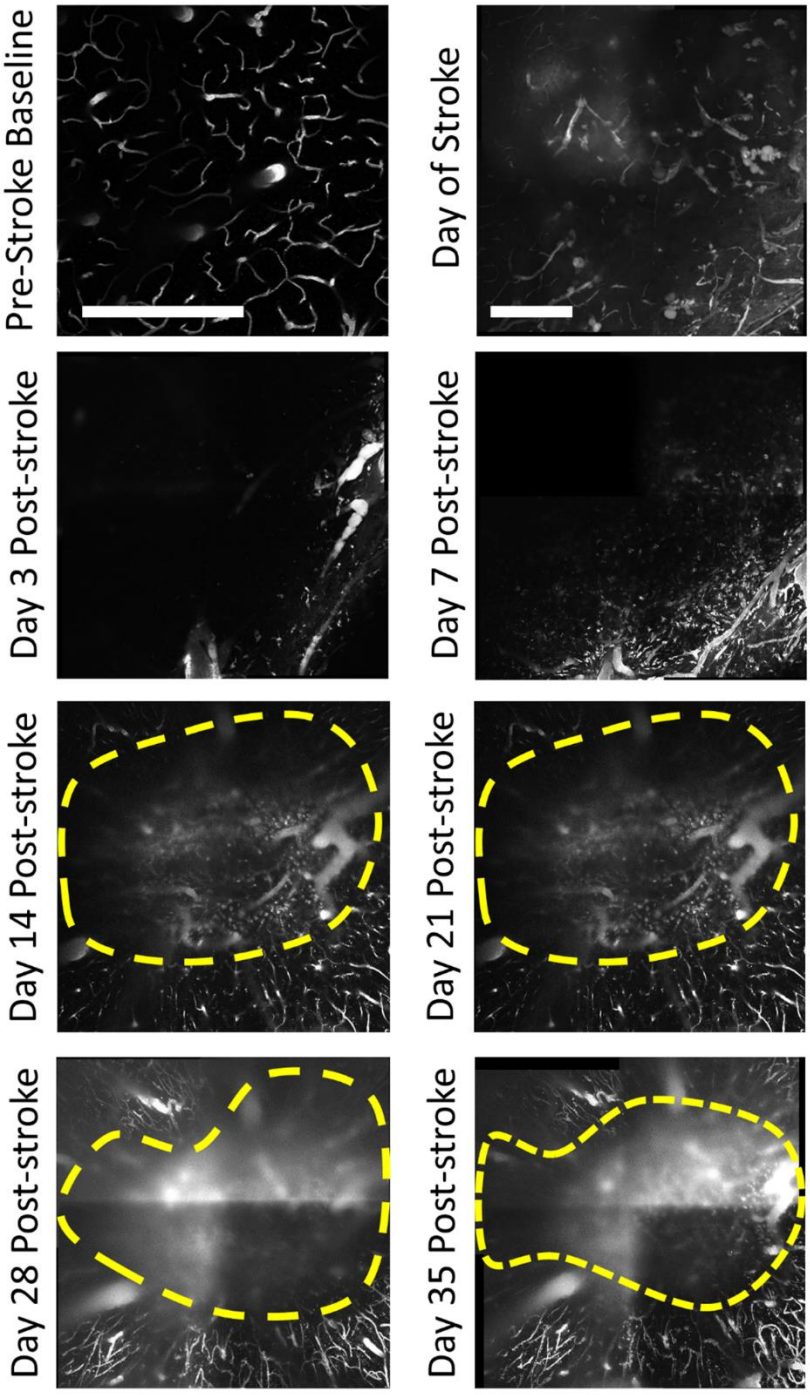

Figure 15: Two-photon microscopy images of vasculature projections from at a depths of 150-170 μm before and after photo-thrombosis. Pre-Stroke Baseline taken at smaller FOV. Scale Bar = 300 μm. Yellow regions denote areas of unresolvable leaky vasculature excluded from volume fraction analyses.

The initial perfusion of the microvasculature into the field of view began on Day 14, allowing for a line to be drawn to denote the damaged area (Figure 15). The marked region was determined by observing the leading edge of the microvascular perfusion within sub-surface depths of 100-300 μm. Blurry areas appearing as vasculature within the marked infarct region originated from shadows of surface vessels as well as signal arising from the leakage of dye within the damaged vessels found in areas of severe flow deficit (Figure 15). The photo-thrombotic occlusion also created a slight cratering affect within the vasculature, causing some of the initial surface vessels to descend in depth within the infarct area (Figure 15). With each step of the progression, the area within the denoted shrinking infarct region had a higher contrast, suggesting that fresh dye was being delivered by blood flow to this area, though it leaked out of the damaged vessels (Figure 15).

Volume fraction analysis was performed by sectioning the stitched vascular stacks into layers of 100 μm in depth, giving volumes of 1 mm × 1 mm × 100 μm. Baseline volume fraction for the surface layer (0 – 100 μm) averaged over all animals was 9.6%, with averages of 4.2% and 4.1% for the following 101-200 and 201-300, respectively (Figure 16). Due to the extent of dye leakage immediately post-stroke, volume fraction for Day 0 could not be measured. A significant drop in volume fraction of >50% was seen in Day 3 measurements for the surface vasculature (Figure 16), though many of these larger vessels remained imageable with largely reduced flows. Volume fractions of the sub-surface microvasculature within the field of view were measured at 0% for Days 3 and 7 of the post-stroke period. As these measurements of zero (n=4) and near-zero (n=2) volume fraction were limited by the methodological approach being unable to sufficiently resolve

deeper vascular depths, the time points for Days 3 and 7 post-stroke are not included in Figure 16. The sub-surface volume fraction from the 101 – 200 µm section for Days 14, saw an increase from no apparent imageable vasculature to a volume fraction of 4.5% (Figure 16). While most of the increase for this layer was due to the cratering effect mentioned earlier causing surface vasculature to descend into this depth section, an accompanying increase in the 201 - 300 µm section to 1.4% volume fraction was also observed, and was solely attributed to capillary perfusion into the field of view around the periphery of the occlusion site (Figure 16).

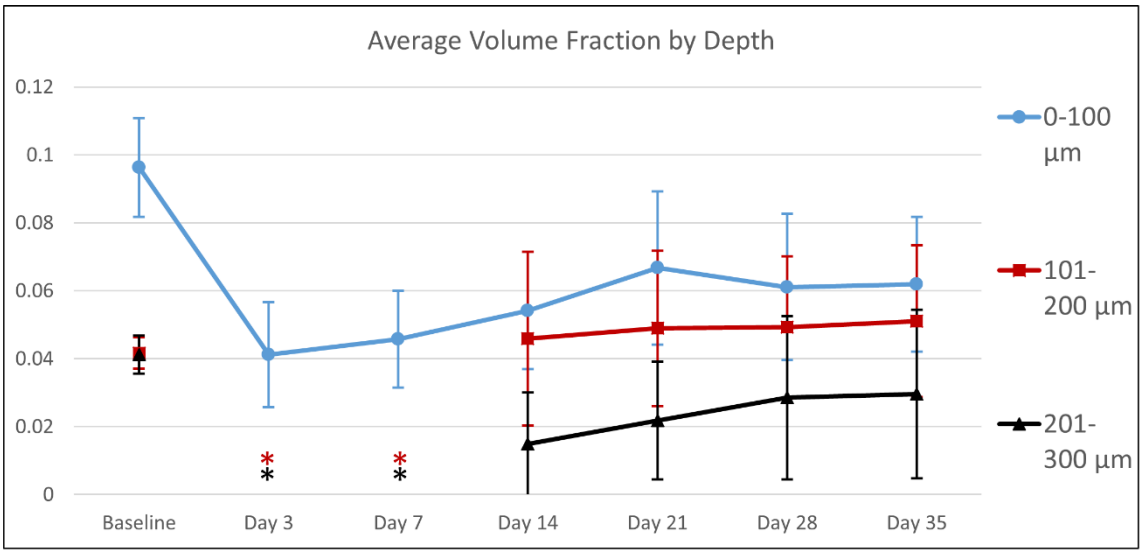

Figure 16: Plot of average volume fractions over different depths for all animals over 35 days of post-occlusion recovery. Asterisks denote time points where Two-Photon Volume Fractions could not be measured for sub-surface vasculature due to the inability to resolve these depths. (M ± SD, n=6).

During the period from Days 14 to 35, the cratering effect of the stroke delivery seemed to lessen and recover, causing the surface vasculature to migrate back up into the 0 – 100 µm section. During this same period, capillaries perfused the peri-infarct area of

the 101 – 200 μm section, serving to balance out the total volume fraction within the section. Due to this lessening of the cortical concavity, a constant volume fraction for the 101 – 200 μm section was measured after Day 14 (Figure 16), though a distinct progression of the microvascular perfusion within images taken within the section was observed (Figure 15).

Histological assessments of the animals after Day 35 imaging sessions showed the lesion still remained below the surface of the cortex. The average lesion size shown with Nissl staining over all animals was 400 μm in lateral diameter and extended from 300 μm in depth to 1.1 μm. This lateral size was fairly close to the focal spot size of the 532 nm laser used for photo-thrombosis.

3.3c Vascular Reorientation

As the sub-surface microvasculature underwent recovery in the integrity of their vessel walls while progressing toward the occlusion site, a significant reorientation was observed in the orientation of the vessels. Sub-surface sections of the baseline vascular stack (Figure 17) were taken every 50 μm in depth and converted into binary projections showing the microvascular distribution for each animal at different depths. This process was repeated for the each of the post-occlusion vascular stacks, and regions of perfusing microvasculature were chosen for analysis, with the angle between the centers of the vascular regions and infarct areas defined as 0° (Figure 17). The Radon Transform analysis described previously was performed for each of the binary projections throughout each point on the time line.

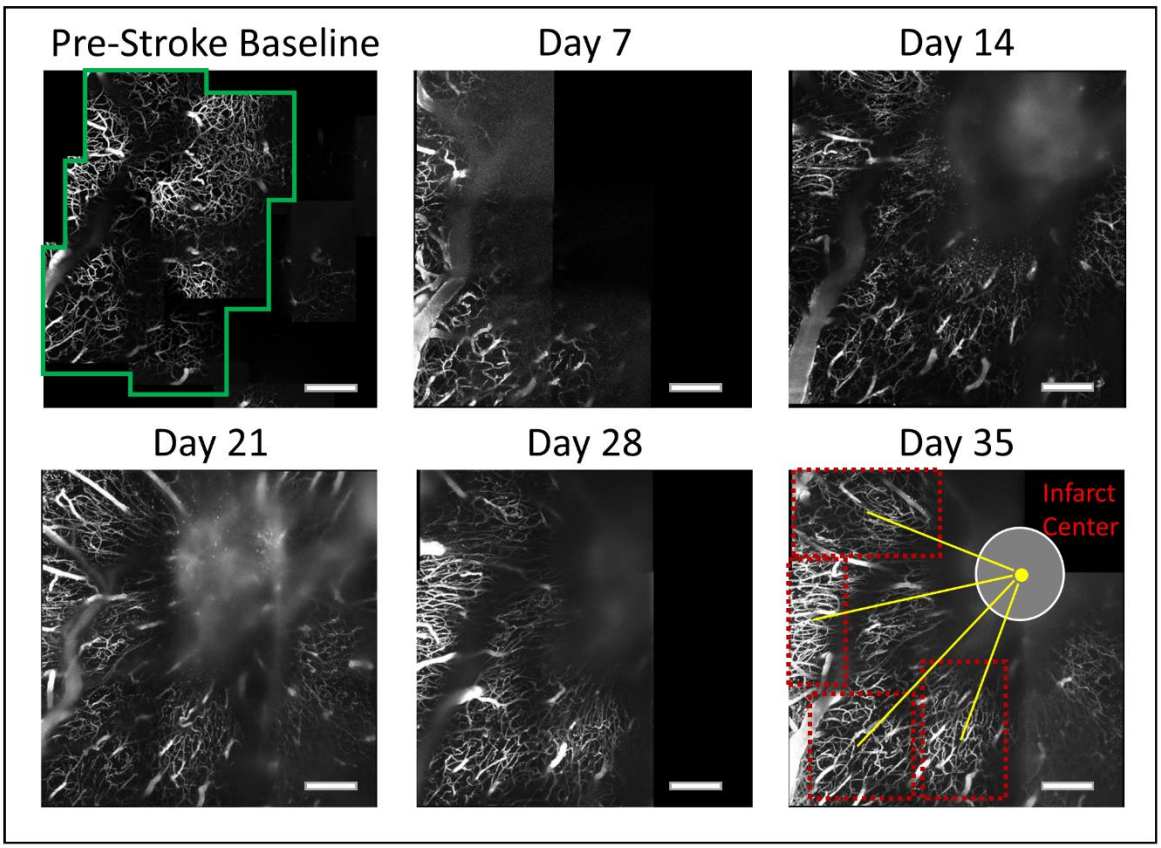

Figure 17: Two-photon microscopy projections from 151 - 200 µm of vascular progression during stroke recovery period. The green box denotes one of the regions included in the orientation analysis of healthy baseline vascular stack. The red boxes on Day 35 highlight 4 regions of interest used for orientation analysis, with the yellow lines denoting the angles between the center of the region and the infarct center. This angle, dependent on the region, is defined 0° in order create a distribution of post-occlusion regions from all animals together based on their position around the infarct center. Scale Bar = 500 µm.

The distribution of angles from regions at each time point were then summed together by lining them up along their 0° angle. The sub-surface regions were from one of four depths including 100-150 µm, 151-200 µm, 201-250 µm, or 251 – 300 µm, with each depth contributing to the overall distribution at each time point. Though projections in Figure 17 only displays projections from the 151-200 µm section, Figure 18 incorporates

distribution measurements from all four depths. The measurement process resulted in a progression of the distribution of orientation angles toward the infarct center from baseline measurements to Day 35 measurements (Figures 17 and 18).

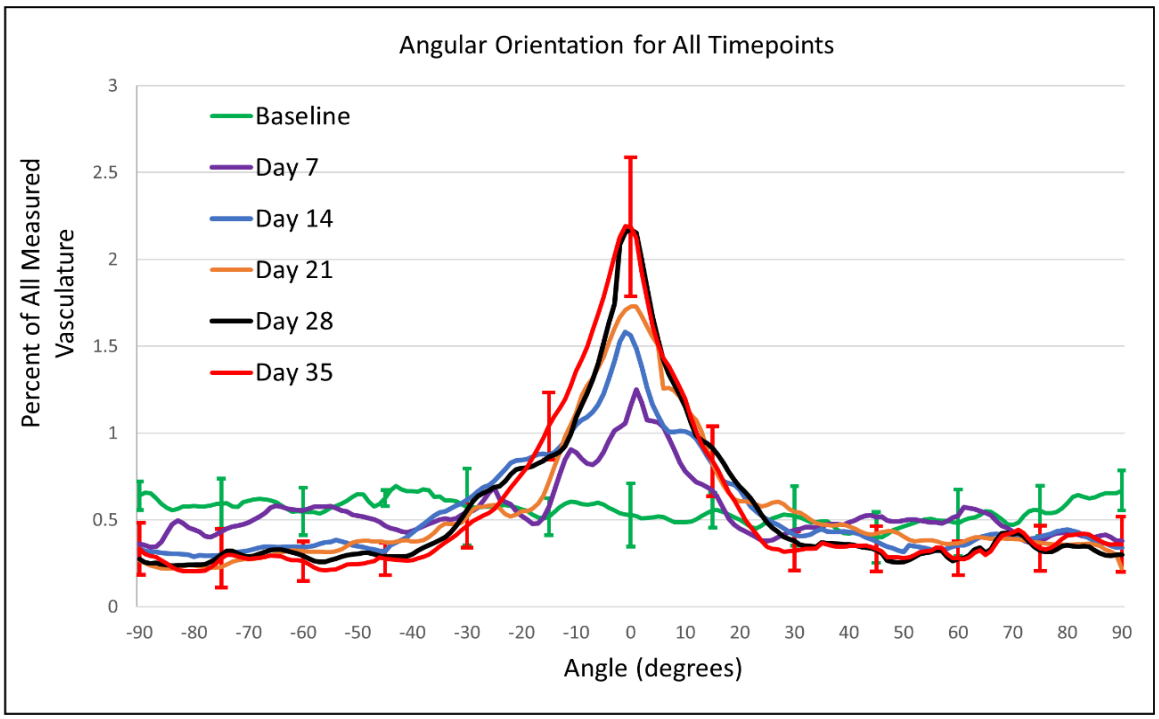

Figure 18: Plot of angular orientations for all sub-surface depth sections (M ± SD) for Baseline (24 regions, n=6), Day 7 (10 regions, n=3), Day 14 (18 regions, n=3), Day 21 (21 regions, n=6), Day 28 (20 regions, n=6), and Day 35 (20 regions, n=6) time points. Error Bars included for Baseline and Day 35 every 15°, with comparable error on remaining angles, excluded for figure clarity. The plot is centered on 0°, as this has been defined as the angle pointing toward the center of the infarct for post-occlusion regions.

While the baseline vasculature showed a fairly uniform distribution of angle orientations, each post occlusion time point shows the vasculature orienting toward the infarct center, with the Day 35 distribution displaying a large peak near 0°, the direction of infarct center (Figure 17). Almost 40% of the vascular distribution for Day 35 falls between

angles of -10° and +10° with respect to the center of the infarct, an increase from 11% measured in the baseline images, demonstrating a significant reorientation process over this post-occlusion period ($p<10^{-12}$, t-test) (Figure 17).

3.3d Quantitative Comparison of Sub-surface Microvasculature

To compare outcomes measured with MESI with those measured by two-photon microscopy, images were centered on the targeted arteriole and three annular rings of interest were overlaid on the infarct and peri-infarct regions (Figure 19A), termed Zone 1, (600 μm diameter circle, matching focal spot of occlusion laser), Zone 2 (800 μm diameter, with inner diameter of 600 μm), and Zone 3 (1000 μm diameter, with inner diameter of 800 μm). These regions were chosen to quantitatively show the perfusion dynamics from the healthy vasculature around the peri-infarct regions (Zones 2 and 3) toward the impacted infarct region (Zone 1). Maps of ICT values from MESI were processed to remove surface to better isolate contributions from the parenchyma (Figure 7), and were compared with sub-surface volume fractions (100 – 300 μm in depth) taken within the corresponding regions of interest.

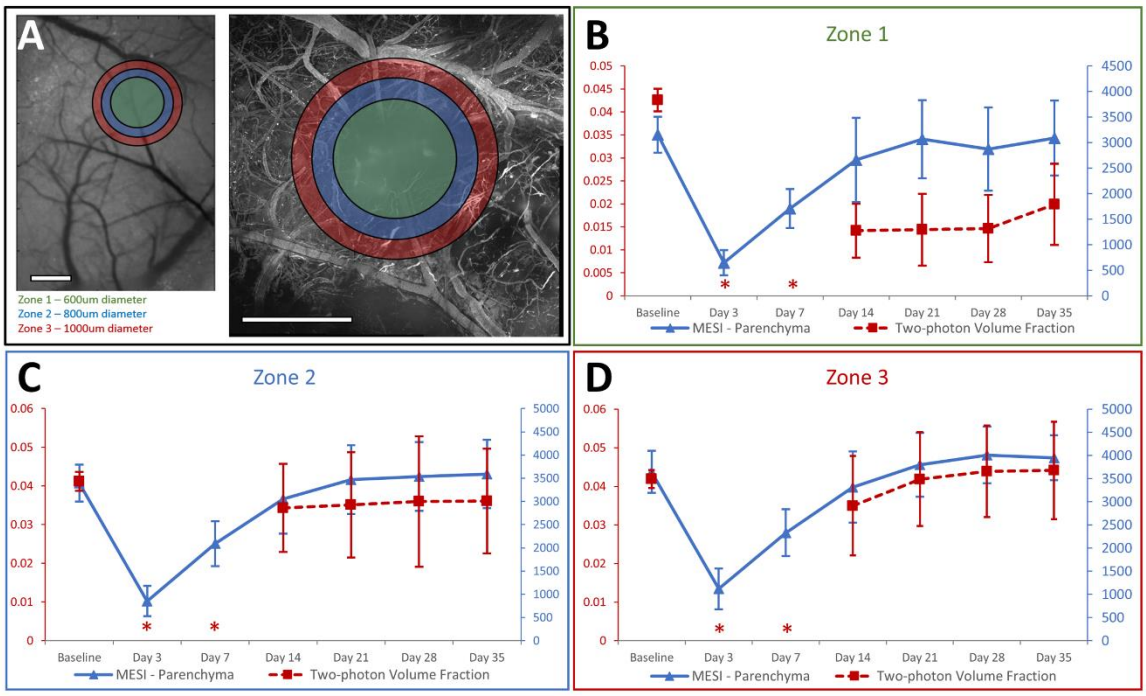

Figure 19: (A) Images from Multi-Exposure Speckle Imaging and Two-Photon Microscopy illustrating the chosen regions for tiered analysis. Zone 1 is defined as a 600 µm diameter circle in green, matching the focal size of the laser used for photo-thrombosis. Zone 2, shown in blue, is defined as an 800 µm diameter annular ring. Zone 3, shown in red, is defined as a 1000 µm diameter annular ring. Scale Bar = 500 µm. (B, C, D) Comparison of Multi-Exposure Speckle Imaging inverse correlation time (MESI ICT) measurements within parenchyma of the titled region with sub-surface (depths of 101-300 µm) two-photon microvasculature volume fractions in the same region over 35 days of post-occlusion recovery. Asterisks denote time points where Two-Photon Volume Fractions could not be measured for sub-surface vasculature due to the inability to resolve these depths. (M ± SD, n=6).

Results of this analysis (Figures 19B, 19C, 19D) showed that while two-photon microscopy volume fractions were not able to be calculated for this first week of post-stroke imaging, MESI ICT values show a distinct period of microvascular progression for this first week. Though we know through MESI analysis that some residual flow remained at the occlusion site immediately after stroke, the leakiness of the damaged surface

vasculature inhibited light penetration to the deeper vascular structures, making the sub-surface vasculature to be unresolvable for Days 3 and 7 post-stroke. This resulted in a methodological volume fraction result of zero for these 2 time points, and was not included for comparisons. By Day 14, when the microvasculature began perfusing into these annular rings of interest (Figures 15 and 17), the volume fractions seen within the peri-infarct regions trended similarly to parenchymal ICT values (Figures 19C and 19D). We did not see the same similarities in measurements taken in Zone 1 (Figure 19B) due to the leakage of dye apparent in the images creating difficulty when taking volume fractions (Figure 15). In Zone 1, parenchymal ICT values showed an increase to 97% of baseline at Day 21, reaching a maximum of 98% of baseline ICT at Day 35 (Figure 19B). Volume fractions within this same region showed a large increase between Days 7 and 14, reaching 47% of their baseline by Day 35 (Figure 19B). Very little progression in the volume fractions of the infarct region was evident between Days 14 and 28 (Figure 19B), as the majority of regional vasculature remained leaky in nature over this period. Within Zone 2 (Figure 19C) and Zone 3 (Figure 19D) regions, parenchymal ICT values reached or surpassed their baseline measurements by Day 35 of the post-stroke period. Day 35 volume fraction measurements within Zone 2 measured 87% of their baseline values (Figure 19C), with an increase to 105% of baseline observed in Zone 3 (Figure 19D). In these regions surrounding the occlusion site, where the vasculature was able to recover from its leaky post-occlusion phase, the results measured by MESI correlated well to two-photon volume fraction outcomes (Figures 19C and 19D). This correlation was not seen in the leaky Zone 1 (Figure 19B).

The comparison between average parenchymal ICT measurements and sub-surface microvascular volume fractions (Figure 19) showed high correlations within Zone 3 (R^2=0.91) and Zone 2 (R^2=0.88). It was within these same peri-infarct regions where vasculature appeared healthy that accurate volume fractions were able to be measured, particularly for Days 14 through 35. Zone 1 had a much lower correlation (R^2=0.36), as the leakage of the dye created difficulty in taking accurate volume fractions for this region.

3.4 DISCUSSION

The data presented shows that a long-term *in vivo* ischemic stroke study can be monitored through the combination of relatively non-invasive imaging techniques with a chronic mouse cranial window model. Animals underwent changes in their vasculature over 35 days of post-occlusion measurements, with the progression captured by MESI and two-photon microscopy. The ability to directly visualize and accurately measure vascular outcomes as they adapt to the post-stroke environment helps us in understanding the perfusion dynamics with this photo-thrombotic occlusion model. A limitation of this occlusion model is the creation of a quickly developing infarct throughout the illuminated region, resulting in a larger ischemic core and smaller penumbra area than would be seen with stroke models selectively targeting vessels.

3.4a Multi-Exposure Speckle Imaging Vascular Outcomes

MESI outcomes from this small scale photo-thrombotic occlusion show that the most at-risk tissue within areas of severe flow deficit saw gains in perfusion past 50% of their baseline on an average of 14 days post-stroke. This suggests that though the available

flow still perfusing the peri-infarct area is reduced from baseline, the first priority of the brain appears to be return flow to the severe flow deficit region. For this stroke model, MESI allows for quickly distinguishing the progression of the vasculature by illustrating the perfusion boundaries separating the healthy and flow deficit regions, as well as marking the extent of flow deficit within the damaged regions. The ICT maps for each animal showed the largest areas of moderate and severe flow deficit at Day 3, with the most significant perfusion of these regions happening in the immediate 4 days thereafter. This small temporal window may be of critical importance to the overall outcome of the animal, and serves as a prime target for future pharmacological stroke studies using a similar small scale photo-thrombotic stroke model.

3.4b Two-Photon Microscopy Vascular Outcomes

The benefits of a depth-resolved imaging technique such as two-photon microscopy are apparent when monitoring the reorientation of the sub-surface vascular structure after occlusion (Figures 17 and 18). The damage caused by the stroke appears to elicit the brain to modify the vascular architecture in response to the new challenges presented. Microvascular reorientation was observed progressing from the healthier outer regions into the peri-infarct area, with vessels angled toward the infarct center (Figures 17 and 18). The lack of increased regional volume fractions in these regions of healthy, perfused vasculature compared to baseline (Figure 19) suggest that these vessels are not angiogenic in nature but rather vasculature with altered orientation that has regained its vessel wall integrity, consistent with results from other groups performing longitudinal two-photon

studies.[107,108] Other studies have noted similar changes in orientation of both vessels as well as dendritic spines.[109] This suggests the mouse cortex to be highly malleable when responding to damage such as stroke, though the driving force in this reorientation process is unknown. One suggested candidate that warrants investigation is the molecular oxygen concentrations in these regions, with particular emphasis on the concentration gradient along these vessels oriented toward the infarct center.[97] The distribution of angular orientations of the resolvable vasculature at each time point after Day 7 progresses toward a larger peak at 0° (Figure 18). In order to document this reorientation phenomena, future studies should include a minimum of 2 imaging sessions (baseline and post-occlusion) with an imaging technique that measures vascular structure, such as two-photon microscopy or OCT. Lengthened future studies can continue to track vascular orientation to observe whether the reoriented distribution remains or progresses back toward a uniform baseline when perfused.

3.4c Correlation between Outcome Measurements

The correlation between parenchymal ICT values and measurable volume fractions demonstrates that although MESI is a surface integrated technique, it can be used as a tool for measuring chronic sub-surface microvascular perfusion. The correlation shown in Zones 2 and 3 suggests that the MESI ICT values within parenchymal regions are partially indicative of the volume fractions of the sub-surface microvasculature. MESI measurements are a convolution of two physiological parameters, the amount scattering occurring within the vasculature and the flow dynamics. The choice of volume fractions

as a metric for describing the vascular structure over large areas limits measurements to only one of the two parameters and only for certain sections of the vasculature which are not leaking dye. The combination of how these parameters affect MESI ICT measurements warrants future study, though results suggest sub-surface volume fraction as an important component. Measuring sub-surface outcomes with MESI presents several advantages for a chronic stroke study, the most significant being the ability to take measurements within the first week of stroke progression, a period that exhibited both substantial increases in ICT value (Figure 13) and decreases in the size of areas with moderate and severe flow deficits (Figure 14). This important portion of the time line was not able to be captured with two-photon microscopy in this study due to the damage inhibiting delivery of the fluorescent dye through the occluded and leaky vasculature. As the vasculature progresses toward the infarct center after the occlusion, the possibility exists that MESI ICT measurements within what appears as parenchymal regions are being affected by nearby surface vasculature, leading to overestimation of the sub-surface flows. Monte Carlo simulations have shown that measurements within parenchymal regions are still highly sensitive to lateral surface vessels.[101] This could be a secondary reason for the poor correlation between MESI ICT and two-photon microscopy volume fraction measurements in Zone 1.

3.4d Relative Benefits of Techniques for Chronic Study

With experimental periods lasting weeks to months, keeping the imaging and anesthesia exposure time as short as possible is of vital importance when considering the

impact on the health of the animal and the progression outcomes. Studies have shown neuroprotective properties of isoflurane[110,111] that must be accounted for by minimizing anesthesia exposure when possible. A balance must be struck between number of experiments, duration of experiments, and duration of the overall study. Though we have the ability to measure the vascular structure of the cortex with high spatial resolution three-dimensionally using two-photon imaging, this modality greatly extends experimental durations, with experimental periods in the presented study averaging 10 minutes for MESI sessions and 90 minutes for two-photon microscopy. Due to the size of the presented photo-thrombotic stroke, it was necessary to take several vascular stacks around the occlusion site to capture the vascular architecture throughout the recovering region with high spatial resolution. With the ability to use surface-weighted measurements of perfusion from MESI to predict sub-surface vascular outcomes, such as vascular perfusion within the parenchyma, experimental times can be greatly reduced.

3.4e Alternate Techniques for Chronic Stroke Progression

The potential exists for eliminating the need for exogenous contrast agents in the presented two-photon microscopy protocol by introducing transgenic mice with endothelial cells expressing fluorescent proteins along their vascular walls and tight junctions,[112] allowing for chronic tracking of vascular structure without exogenous contrast agents. While use of transgenic animals would remove imaging problems associated with the leakiness of the vasculature after stroke, we would be unable to monitor the blood flow, necessitating the development of a metric to differentiate healthy, perfused vasculature

from damaged vessels. Though the structural rebuilding process of the endothelial cells lining the vasculature could be directly monitored with a transgenic model, it remains to be seen whether accurate volume fractions of perfused vasculature could be measured within the damaged infarct region after photo-thrombotic occlusion. Optical coherence tomography offers a potential solution to the problem of measuring both flows and three-dimensional structure within the cortex.[113–116] While MESI measurements do not have the sub-micrometer spatial resolution or detailed renderings of sub-surface microvasculature from two-photon microscopy, they may provide a tolerable spatial-integration of microcirculation for gauging the vascular progression and regional tissue health.

3.5 SUMMARY

A long-term stroke study using a photo-thrombotic occlusion was used to evaluate an optical imaging protocol for monitoring chronic microvascular perfusion on and below the surface of the mouse cortex over experimental time lines extending to five weeks post-occlusion. After photo-thrombotic occlusion, regional perfusion boundaries around the infarct were identified using Multi-Exposure Speckle Imaging, and the areas containing severe flow deficit were shown to be reperfused above 50% of baseline flow within 14 days following stroke while areas of moderate flow deficit showed a 95% reduction in area over a 35 days period. Blood flow in a 2 x 2 mm field of view centered on the infarct measured with MESI was shown to reach baseline values after 3 weeks of post-stroke imaging, overshooting baseline measurements in the 4th and 5th weeks. Vascular reorientation within the sub-surface microvasculature was shown with two-photon

microscopy to occur over a time period of 1-5 weeks after occlusion, with vessels showing a substantial change in their angular orientation by lining up with the most significantly damaged area of the stroke. Chronic two-photon microscopy measurements of volume fraction in peri-infarct regions surrounding the occlusion site containing vasculature with repaired vessel walls showed high correlation with MESI perfusion values in the same regions over the post-stroke period. With a nominally low experimental duration and wide field of view, MESI provides a standalone or complimentary imaging platform for studies requiring characterization of ischemic progression.

Chapter 4: Development of Quantitative Imaging of Functional Hyperemia

A recently developed extension to Laser Speckle Contrast Imaging (LSCI) allowing for the establishment of a quantitative cerebral blood flow baseline, termed Multi-Exposure Speckle Imaging (MESI), presents a quantitatively accurate technique for measuring cerebral blood flow (CBF) dynamics. In this paper, we initially determine the optimal MESI camera exposures for measuring the CBF response to functional forepaw stimulation in the mouse. An optimized subset of 5 exposures was found with the original exposure set, doubling the sampling rate of MESI while maintaining a comparable accuracy of <6% deviation in flow quantification. Next, functional CBF maps of the cortex during forepaw stimulation were obtained with optimized exposure MESI and traditional single exposure LSCI from n=7 activation regions over 5 animals. We demonstrate the feasibility of mapping the functional forepaw response with the optimized subset of 5 exposures, termed FA MESI, allowing for measurements of absolute change in CBF from functional stimulation. The spatial extent of the FA MESI functional maps were shown to be more regionally confined than the single exposure LSCI maps, but responses exhibited similar temporal dynamics and relative CBF magnitudes.

4.1 Introduction

Laser speckle contrast imaging (LSCI) has been shown as a full-field imaging technique with sufficiently high temporal resolution to capture cerebral blood flow (CBF) dynamics associated with functional activation.[45,46,76,77,117] Recent advances in LSCI led to the development of an extension termed Multi-Exposure Speckle Imaging (MESI) which

uses an improved mathematical model and instrumentation to better separate the non-flow related contributions to the speckle contrast.[59,79,81] The use of multiple exposures also enables a wider flow range sensitivity, providing improved characterization of blood flow changes. These factors enable laser speckle flowmetry to move from primarily acute experiments to longer-term chronic studies principally by providing a reliable CBF baseline. The tradeoff for increasing quantitative accuracy when moving from a traditional single exposure (i.e. 5 ms duration) LSCI technique, primarily selected for optical imaging of functional hyperemia, to MESI comes in the form of reduced temporal resolution.

In order to capture functional responses with MESI, a balance must be struck between establishing sufficient temporal resolution while retaining high sensitivity over the range of flow distributions seen in the functionally responding regions. Successfully accomplishing this balance will create an optical technique capable of chronically tracking the region and amplitude of the blood flow response to forepaw stimulation. This technique presents a potential platform for measuring the effects of any neurovascular perturbations, such as disease or damage models, as well as the progression of the functional blood flow response associated with these changes. Long-term tracking of functional progression currently relies on a myriad of techniques, including functional magnetic resonance imaging,[118–123] behavioral tests,[124–131] micro-stimulation and histological analyses,[2,132,133] and imaging of intrinsic optical signals.[134] Measuring functional responses with MESI offers the ability to monitor the blood flow dynamics of activated regions with high spatial resolution while establishing an absolute baseline for chronic monitoring.

This study focuses on the optimization of the camera exposures used in MESI to accurately capture the functional cerebral blood flow response to stimulation of the mouse forepaw. Previous studies have been performed for optimization of LSCI exposures, including MESI exposures over a large range of in-vivo baseline and post-stroke flow distributions[135] and single camera exposures for resting and functional flow dynamics.[136] The optimization process in this study will utilize a training set of animals to identify which exposures best sample the flow distributions observed within regions of the cortex responding to forepaw stimulation, potentially resulting in increases to the temporal resolution of MESI while maintaining high quantitative accuracy.

4.2 METHODS

This study utilized both single exposure Laser Speckle Contrast Imaging and Multi-Exposure Speckle Imaging, which are discussed in more detail in Chapter 2 of this dissertation, to develop and compare against Functional Activation Multi-Exposure Speckle Imaging. This study also used the same chronic animal mouse model from Chapter 3, with the surgical preparation and cranial window upkeep documented in Appendices 1 and 2.

4.2a Experimental Protocol for Training Set

A training set of 5 animals with healthy cranial windows after the recovery period of 3-4 weeks were anesthetized with 70% N_2/O_2 vaporized isoflurane via nose-cone and affixed to a stereotaxic frame. Vitals were recorded via pulse oximetry and temperature was maintained by feedback heating. Multi-Exposure Speckle Imaging was performed

over a 2.7 × 2.0 mm field of view centered on the region of interest by collecting 300 frames at each exposure. This provided ICT maps of the imaged region, giving a global perfusion index of the area. This imaging technique was done at three time points over a period of two weeks for each animal to ensure a stable baseline. In attempts to control for physiologic variability in the cardiac output within each animal, heart rate for each experiment was adjusted to be within 10% of the animal's baseline heart rate by small changes in the animal's depth of anesthesia.

After establishing a repeatable baseline with MESI, functional forepaw stimulation measurements were taken using single exposure LSCI with a sampling rate of 50 Hz. An exposure duration of 5 ms was used for single exposure imaging, as it has been shown to optimally capture functional responses in previous studies.[76] Isoflurane anesthesia was lowered to 1.0 – 1.5% for functional measurements. A piezoelectric stimulator was placed under the forepaw contralateral to the cranial window being imaged (Figure 21). The 35 second stimulation paradigm (Figure 21) consisted of 5 seconds of baseline, 5 seconds of 100 Hz piezoelectric stimulation, and 10 seconds of post-stimulation measurements followed by a 15 second break preceding the start of the next stimulation block. This paradigm was repeated for 25 stimulation blocks. Relative CBF maps of the responding areas were created by dividing inverse correlation time images averaged within the stimulation window (seconds 5 - 10) by images averaged within the baseline window (seconds 0 – 5) shown in the time course of Figure 21.

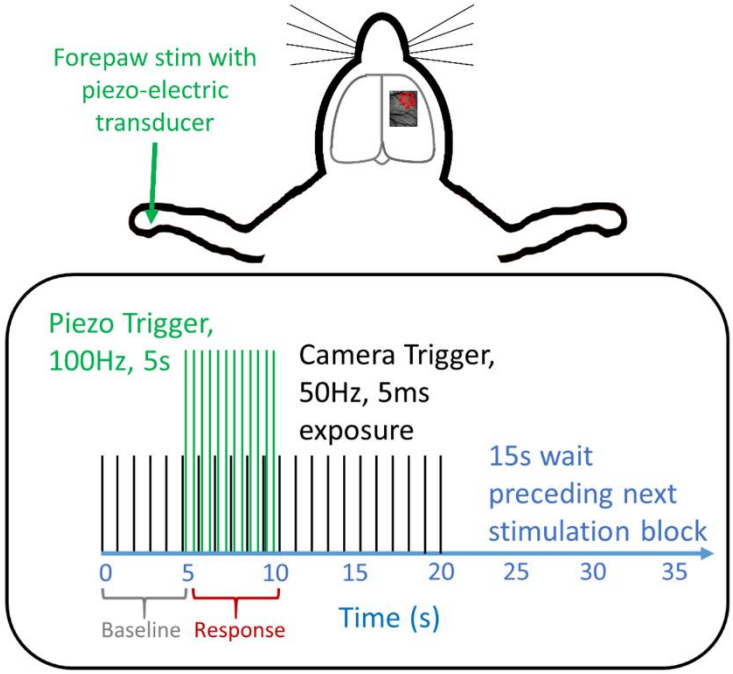

Figure 21: Representation of placement of mouse craniotomy and piezo-electric stimulator under contralateral paw (top). Stimulation paradigm (bottom) denoting 5 seconds of baseline recording followed by 5 seconds of piezo-electric stimulation at 100Hz with 35 seconds between stimuli.

The functional maps from the single exposure LSCI experiments were co-registered with the flow maps from MESI (Figure 22) in order to extract the flow distributions that fell within the functionally responding areas of the cortex. Each animal underwent two functional mapping sessions, and the flow distributions within the responding areas were used to create a training set of data (9 functionally responding experiments over 5 animals) for the optimization algorithm. As the flow distributions were all measured under baseline conditions with MESI, the maximum range for this training data set was extended by 15% to account for increases in the flow from functional stimulation.

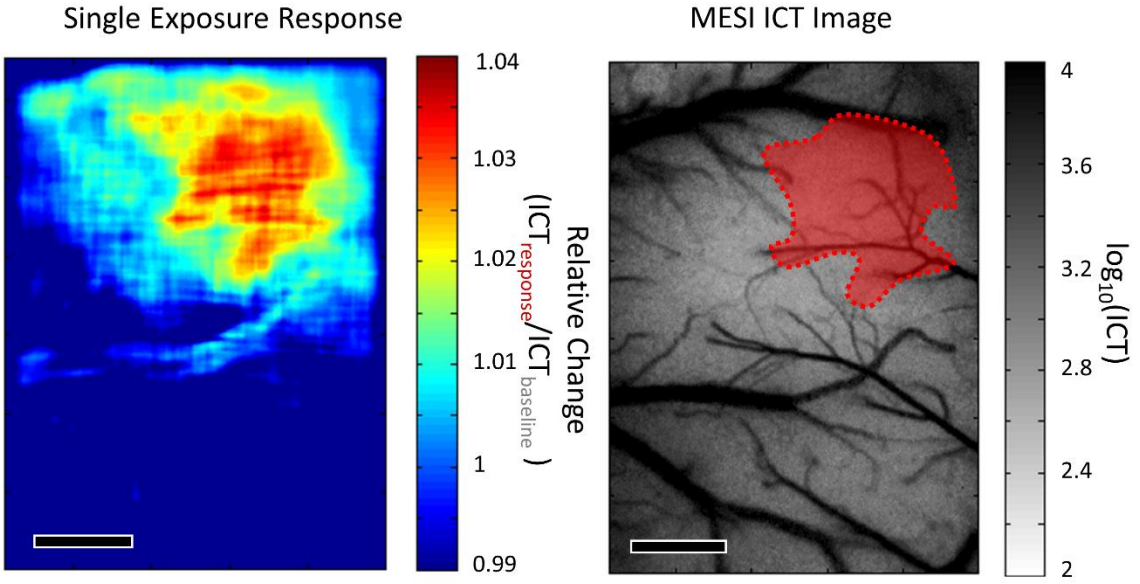

Figure 22: Map of relative change in ICT (left) from single exposure speckle imaging, averaged over 25 stimulation blocks. Multi-Exposure Speckle Imaging inverse correlation time image (MESI ICT) with functionally responding region denoted (right). Scale bar = 500 μm.

4.2b Optimization of Exposures

A Leave-One-Out process described previously[135] was used on the training data set to find the optimal set of exposures for performing Multi-Exposure Speckle Imaging of functional forepaw response. The algorithm found the minimum combination of exposures necessary to provide comparable accuracy to ICT flow estimates from the traditional 15-exposure MESI. The Leave-One-Out process ran sequential iterations in which a single exposure was removed for each subset and MESI ICT flow estimates were re-calculated from the remaining exposure durations and compared to the original ICT estimates, resulting in subsets with 1 fewer exposure for each iteration. The subset of exposures with the lowest percent deviation from the full exposure set was chosen for the next iteration of the algorithm. This new subset of exposures was then recalculated by sequentially leaving

1 exposure out, with accuracy again being compared against results from the original 15 exposure set. Iterations continued until the average percent deviation between the ICT values of the subset of exposures and full set of 15 exposures reached a pre-established deviation of 10%, which is comparable to the reported accuracy of MESI and the tolerable animal heart rate variation.[79,81] The other criteria for ending the algorithm was reaching the theoretical minimum combination of 5 exposures, as 5 variables are required for solving the MESI speckle visibility equation for full determination.

4.2c Experimental Protocol for Testing Set

Testing set animals (n=5) underwent the same anesthesia and vital monitoring as those in the training set described previously. Traditional MESI was performed to provide baseline ICT maps of the cranial window, followed by the optimized 5-exposure functional activation MESI (FA MESI) interleaved with single exposure LSCI (5 ms exposure duration). The same stimulation paradigm (Figure 2A) was repeated five times for FA MESI measurements at a sampling rate of 5.2 Hz, and then single exposure LSCI for five stimulations at a 50 Hz sampling rate. This process was repeated until 25 stimulation blocks were gathered for each imaging technique. Maps of the functional responding areas for single exposure LSCI were calculated in the same way as the training set, while maps for FA MESI used a more determined estimate of ICT value. Each animal underwent two functional mapping sessions, with the functionally responding experiments (7 over 5 animals) used for the testing subset of data.

All experiments were approved by the Institutional Animal Care and Use Committee (IACUC) at The University of Texas at Austin under guidelines and regulations consistent with the Guide for the Care and Use of Laboratory Animals, the Public Health Service Policy on Humane Care and Use of Laboratory Animals (PHS Policy) and the Animal Welfare Act and Animal Welfare Regulations.

4.3 RESULTS

4.3a Exposure Optimization Output

From the Leave-One-Out process on the training data set, we were able to reduce the number of exposures from 15 to 5 while remaining within the pre-established uncertainty level of 10% (Table 1). Each iteration of the algorithm is shown in Table 1, documenting which exposure was removed at each step and the resulting accuracy of the reduced exposure set on the training dataset compared to the original 15 exposure set. The remaining exposures were 0.05, 0.5, 1, 5 and 80 ms. The reduction in number of exposures allows for an increase in the sampling rate of the system from 2.48 Hz for 15 exposures to 5.2 Hz for 5 exposures (Table 1). This sampling rate takes into account the data acquisition delay time of the system (68 ms) and the frame readout time of the camera used in this study (7.5 ms per exposure). In addition to removing some of the longer exposures, the ability to cut frame readout times for 10 of the exposures resulted in a doubling of the sampling rate for FA MESI.

Table 1: Leave-One-Out Analysis for Best Exposure Subsets

# of Exposures	Removed Exposure (ms)	Percent Deviation (%)	Sampling Rate (Hz)
14	10	1.3±0.6	2.59
13	25	1.5±0.8	2.83
12	0.25	2.3±1.6	2.89
11	40	1.6±1.4	3.35
10	0.10	2.5±1.8	3.44
9	7.5	3.0±2.5	3.63
8	2.5	4.4±4.5	3.77
7	0.75	3.9±3.5	3.89
6	50	4.9±4.4	5.00
5	0.075	5.1±4.2	5.20

As the 5.1% deviation at 5 exposures was still well under the 10% cut-off, the algorithm was ended on the criteria that a minimum of 5 exposures are necessary to solve the MESI speckle visibility equation for full determination. The remaining exposures to map the dependence of the speckle contrast on the exposure duration for FA MESI included both the longest and shortest exposures of the original 15 exposures (0.05 and 80 ms), in addition to three exposures sampling a single decade in the middle of the original set (0.5, 1, and 5 ms). With the reduction in exposures, the computational times necessary for performing the nonlinear least squares fitting process to solve the MESI equations were reduced on the order of 25%.

4.3b Functional Response with Optimized Exposure

With the optimized set of 5 exposures for FA MESI, the testing set animals underwent functional forepaw stimulation experiments described in the experimental protocol, with 7

responding experiments over 5 animals. Results showed that FA MESI, at a sampling rate of 5.2 Hz, was capable of measuring the functional blood flow response to piezo-electric forepaw stimulation (Figure 23).

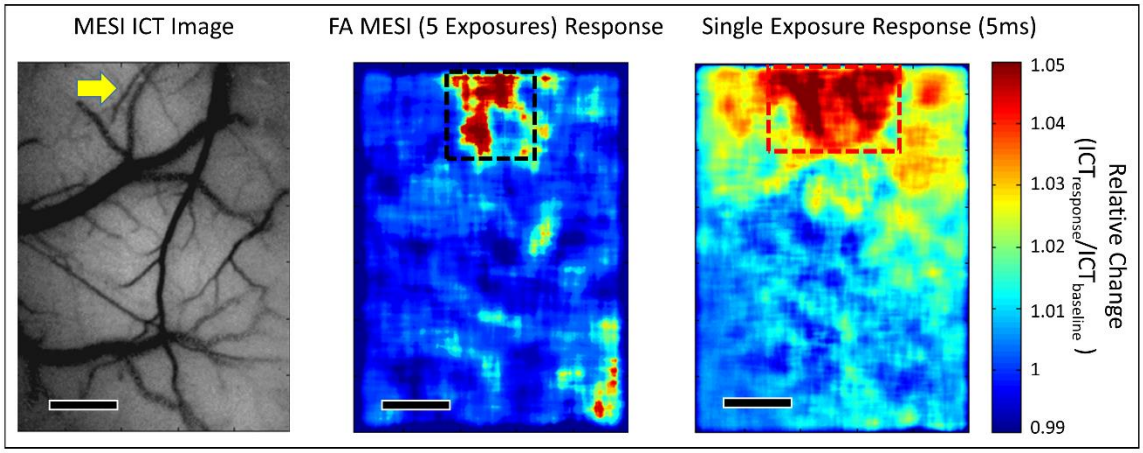

Figure 23: Multi-Exposure Speckle Imaging inverse correlation time images (MESI ICT) of vasculature (left). Yellow arrow denoting responding arteriole branch. Relative forepaw response maps for FA MESI (middle) and single exposure LSCI (right). Scale bar = 500 µm.

Responding areas of the vasculature were smaller spatially with FA MESI than with single exposure LSCI (Figure 23), though the time courses of their relative changes were very similar over the denoted responding regions (Figure 24). The temporal dynamics and magnitudes of the relative ICT changes to the forepaw stimulation were very similar with these interleaved functional experiments, with single exposure LSCI showing a slightly higher peak response (Figure 24). One period where the FA MESI and single exposure time courses did not match was during the period of flow decline following the end of the 5 second stimulus. While single exposure LSCI showed a decrease in flow below baseline following the stimulus, FA MESI did not measure this dip in flow.

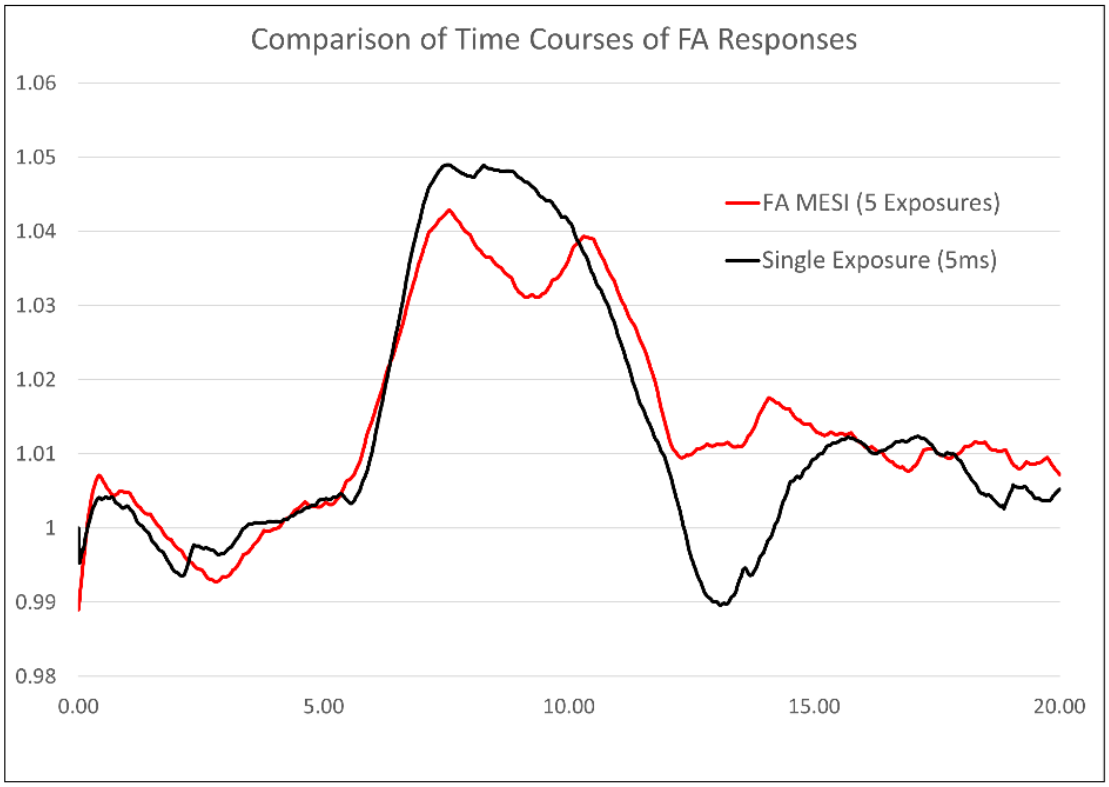

Figure 24: Plot of time courses for functional activation responses from FA MESI and single exposure LSCI in Figure 23 denoting the average relative change compared to baseline over the 20 second imaging interval.

The optimized 5-exposure FA MESI could also be split into individual exposures for independent mapping to display the sensitivity of each exposure to the flow distributions making up the functional response. Each of these individual exposures were sampled at the FA MESI rate of 5.2 Hz (Figure 25).

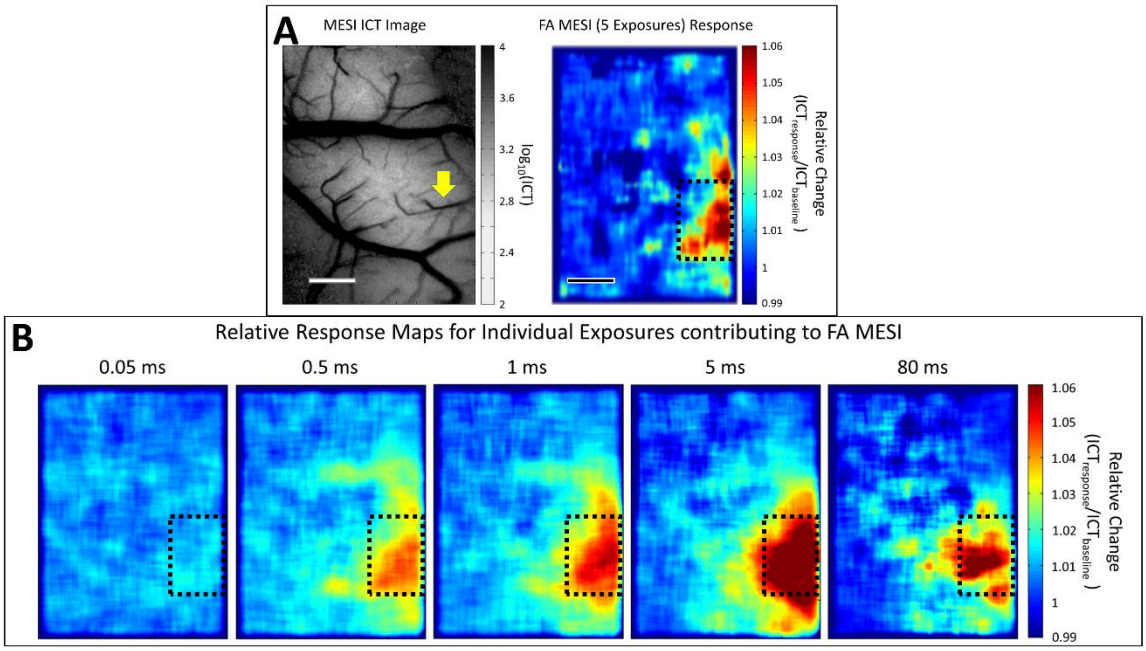

Figure 25: (A) Multi-Exposure Speckle Imaging inverse correlation time image (MESI ICT) of vasculature (left). Relative change of ICT values measured with FA MESI during functional forepaw stimulation (right). Yellow arrow denoting responding arteriole branch. Scale bar = 500 µm. (B) Maps of relative change during functional forepaw stimulation of each individual exposure contributing to FA MESI. Scale bar = 500 µm.

The 5 ms exposure showed the largest peak response in relative response reaching almost 2% higher than all other individual exposures (Figure 26), as well as the largest spatial response for this animal (Figure 25). The temporal dynamics of the response were similar in all exposures except for the 0.05 ms exposure, which measured a slow increase in relative change at the stimulus onset followed by a slow decrease when the stimulus stopped (Figure 25).

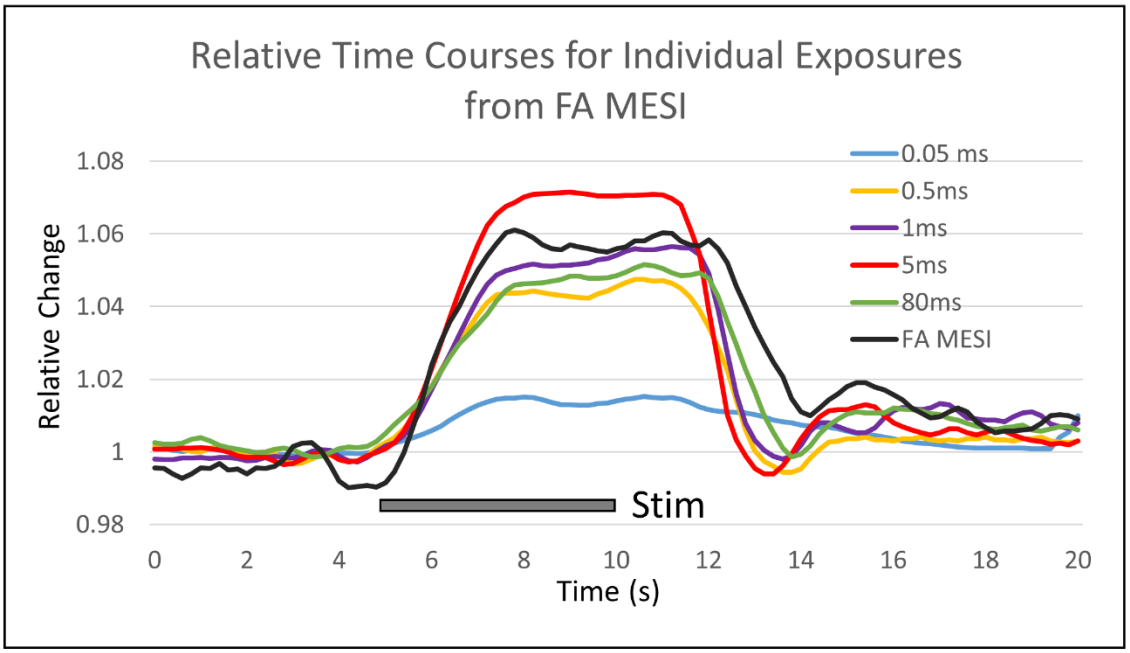

Figure 26: Plot of relative time courses of Figure 25 for blood flow responses from FA MESI and each individual exposure that contributes to FA MESI.

Overall the FA MESI response again had a smaller spatial extent, a trend which continued for all measured responses, with similar temporal dynamics to the longer 4 single exposure responses (Figure 26). The FA MESI time course differed following the stimulus offset, where the FA MESI peak extends around half a second longer than the individual exposures, excluding 0.05 ms, and again doesn't register a dip below baseline as is seen in the longer 4 single exposures (Figure 26). The spatial extent of the responses measured for the 0.5, 1, and 5 ms exposures were very similar in this animal, with 5 ms displaying a higher magnitude response (Figure 25). The 0.05 ms spatial response was not confined to the FA area, showing a global increase of ~1% throughout the craniotomy, while the 80 ms response localized slightly downstream of the responding arteriole compared to the previous exposures (Figure 25). Two-dimensional Gaussians were fit to responding areas

for all animals in order to compare the spatial extent of each exposure's response with that of the FA MESI response.[76] Figure 27 illustrates that over all functional responding animals, the means of the responding areas of the single exposures (excluding 0.05 ms) were larger than the mean of the FA MESI response, with significant differences between each of the single exposure areas and the FA MESI area ($p<0.01$, t-test).

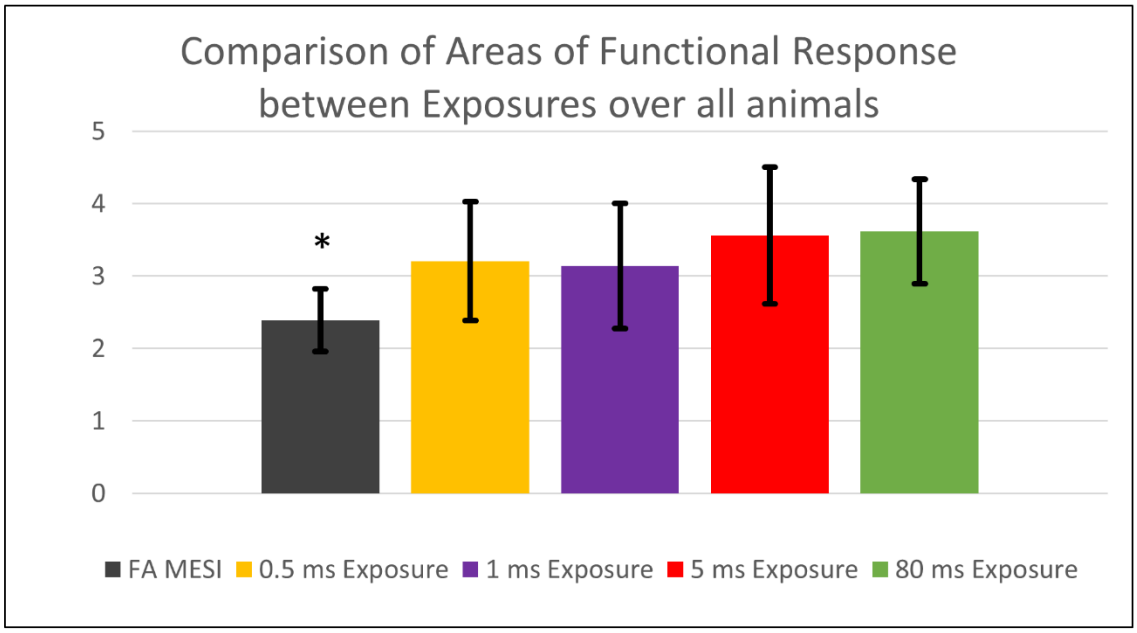

Figure 27: Plot of mean functional response areas for individual exposures (excluding 0.05 ms) and FA MESI over all functional responses. Asterisk denoting significant difference for FA MESI from each of the single exposures ($p<0.01$, t-test) (n=7, Mean ± SD).

4.4 Discussion

The data presented shows that absolute measurements of the functional blood flow response to forepaw stimulation are able to be captured with FA MESI. The differences in dynamics to those measured with single exposure LSCI are explored in more detail below,

as well as the implications for using a more complicated quantitative measurement of functional response.

4.4a Evaluation of Optimization *In Vivo*

The optimization of MESI exposures for functional forepaw responses allows for a higher sampling rate to be achieved with only a small reduction in the quantitative accuracy falling well within the pre-determined threshold. By imaging the testing set animals with this optimized FA MESI technique, the results displayed the feasibility of mapping the functional forepaw response to a 5 second piezo-electric stimulation with a sampling rate of 5.2Hz. The FA MESI results were compared to interleaved single exposure LSCI results imaged at a higher sampling rate. The time courses of the relative responses showed very similar changes in rate of flow increase during the onset of the stimulus within the functionally responding regions (Figures 24 and 26). As this portion of the time course measures of the highest rate of change, this suggests the 5.2 Hz sampling rate of the FA MESI to be temporally sufficient to capture the full functional forepaw response. Following the stimulus offset, FA MESI shows a slight temporal lag behind the 5 ms single exposure LSCI (Figures 24 and 26). This slight delay in the return to baseline with FA MESI might result from contributions of the remaining exposures, such as 0.05 ms, which have slightly different shapes in their return to baseline, particularly the slow fall in the relative change of the 0.05 ms exposure (Figure 26). As the 0.05 ms exposure is sampling only the fastest flows observed in the largest surface vessels, in particular the surface vein and arteriole seen in the measured ROI for the animal presented in Figure 25, the functional

response of these comparatively large vessels are not expected to show the same temporal dynamics as the surrounding vessels within the parenchyma.

The spatial extent of the FA MESI response displays a significant difference compared to the single exposure responses (Figure 27). This effect is mainly attributed to each single exposure measuring slightly different regional responses from different vascular flow distributions. In each FA MESI functional map, the area is much more regionally confined around the activated surface arteriole, denoted with a yellow arrow in the ICT map of Figure 4A, than seen with single exposures (Figure 25). The arteriole within the denoted function region of Figure 25 is sampled by every exposure in the optimized FA MESI technique, weighting it more than the surrounding parenchyma and smaller vessels, which are only sampled by the longer exposures. Though the spatial extent of the FA MESI response is smaller, the center of the response is very similar to the center of each single exposure. The particular arteriole branch from which the response is originating is much easier to recognize with FA MESI than with single exposure LSCI, with Figure 23 serving as a prime example. In this figure, the denoted arteriole near the top of the MESI ICT image is the vessel responding to functional stimulation, and has left and right arteriole branches. While the FA MESI localized the main response to the left branch, the single exposure response displays that both branches are responding about equally. This suggests FA MESI as a technique capable of localizing the surface vasculature supplying the functional region being stimulated, as each animal's functional blood flow response was more spatially confined with FA MESI than single exposure LSCI (Figure 27). This localization by FA MESI would be optimal for future studies looking to

perturb the blood flow of the functional forepaw area, such as with a targeted photo-thrombotic stroke.[118,134]

4.4b Implications of Chronic Functional Activation Imaging

With FA MESI, absolute measurements of functional response are able to be observed, allowing for comparison of responses both within a single animal over different time points and also between animals. This could not be fairly compared with single exposure LSCI due to the relative nature of its measurements. Current studies are being undertaken utilizing this optimized FA MESI technique observing functional forepaw responses pre- and post- occlusion. Preliminary results show that following the occlusion, Day 2 post-stroke functional measurements within the original pre-stroke functionally responding area show a similar relative ICT change (~5%) when stimulated, but the absolute change in ICT is <50% of the pre-stroke functional blood flow response due to the post-stroke area having a much lower starting baseline ICT. This suggests the possibility that large deviations between relative and absolute functional blood flow responses can be measured for studies perturbing the vasculature, providing inaccurate results of functional outcomes. The ability to compare different time points is of particular interest when measuring the functionally responding areas of the brain in conjunction with neurovascular recovery, allowing for chronic studies which could incorporate processes to modulate or probe recovery such as rehabilitation and pharmacological agents. The advantages of this technique allow for documentation in the progression of both the absolute temporal and spatial dynamics of the functional response over long experimental

durations of weeks to months, while still presenting an experimental duration on the same time scale as seen in single exposure LSCI or imaging of optical intrinsic signals.

For acute studies of functional activation within the mouse cortex, the benefits provided by FA MESI over single exposure LSCI may not outweigh the additional complexity introduced to both the imaging system and required computation. Though the spatial extent of the FA MESI response differed from the 5 ms exposure response, the center of these areas seemed to be similar. While absolute changes in flow cannot be taken from single exposure LSCI, the data presented showed that the magnitude and temporal dynamics of the responding areas were very comparable between the two techniques. In some cases, the increased signal-to-noise ratio from the 5 ms exposure LSCI technique sampling at 50 Hz or more may offer a larger benefit to experiments looking at very small changes in flow than benefits provided by FA MESI.

The optimization process of MESI for functional forepaw mapping shows that users can minimize one of the main drawbacks of MESI, the decreased sampling rate, by optimizing the subset of exposures for the flows they are interested in. By cutting out some of the redundancy in exposures sampling either similar subsets of flow distributions or flow velocities in which the user is not interested for their particular experiment, an increase in sampling rate and decrease in computational complexity can be achieved with FA MESI. The optimized exposure set presented in this paper was specifically for studying mouse functional forepaw response to the stimulation paradigm described.

4.5 SUMMARY

By optimizing a set of 5 exposures from MESI for functional forepaw activation measurements, sampling rates were more than doubled from 2.48 Hz to 5.2 Hz with an approximate deviation of 5.1 ± 4.2 % from the full 15 exposure set. The ability to map the functional response to forepaw stimulation within the mouse cortex using this optimized exposure set was presented, allowing for absolute responses to be measured with FA MESI where previously only relative responses could be taken using single exposure LSCI. The area of the response seen by FA MESI was significantly smaller than seen in single exposure LSCI responses, though the temporal dynamics and magnitude of the relative changes were very similar to exposures previously used for functional mapping with LSCI. With the ability to measure absolute functional responses, the presented FA MESI technique can be used in acute studies sampling large changes in resting and activated state cerebral blood flows and in chronic studies to track temporal and spatial changes in the functionally responding regions over the course of weeks to months.

Chapter 5: Progression of Functional Blood Flow Dynamics after Stroke

Monitoring the progression of the regional cerebral blood flow (CBF) and functional blood flow dynamics after brain injury is vital to understanding the neurovascular recovery process. An extension of Multi-Exposure Speckle Imaging (MESI), termed Functional Activation MESI (FA MESI), presents a quantitatively accurate technique for measuring CBF dynamics during functional activation of the mouse cortex. In this paper, we present hemodynamic outcomes extending 21 days after photo-thrombotic occlusion, tracking the progression of the CBF and the temporal dynamics of the functional forepaw response throughout this period for 5 animals. Following the occlusion, MESI shows increases in baseline CBF perfusion starting at Day 2 post-stroke and reaching near pre-stroke values by Day 21. Absolute changes in the functional blood flow response were measured with FA MESI over the same time period, with functional outcomes differing from those of the regional CBF perfusion. The magnitude of the functional blood flow response to forepaw stimulation was observed to have further decreased between Days 2 to 7 post-occlusion, followed by an increase between Days 7 and 21 where the blood flow response to stimulation reached just over half of the pre-stroke magnitude. With the combination of a chronic mouse model and relatively non-invasive optical imaging techniques, we present an imaging protocol for long-term monitoring of the baseline CBF and functional flow dynamics of the forepaw response after photo-thrombotic occlusion.

5.1 INTRODUCTION

Laser speckle contrast imaging (LSCI) has been shown as a full-field imaging technique capable of capturing the cerebral blood flow (CBF) dynamics associated with functional activation.[45,46,76,77,117] Advances in LSCI have resulted in the development of an extension termed Multi-Exposure Speckle Imaging (MESI), which uses an improved mathematical model and instrumentation to better separate the non-flow related contributions to the speckle contrast measurements.[59,79,81] By using multiple camera exposures, MESI is able to more precisely sample and map the wide range of flow distributions prevalent in the rodent vasculature.[79] Previous studies have shown MESI to accurately estimate a wide range of flows *in vivo*, including complete flow reduction during middle cerebral artery occlusions.[81] This technique has also shown the ability to determine spatially integrated perfusion measurements from unresolvable microvasculature within the parenchyma,[101] and to highlight perfusion boundaries for post-occlusion studies to determine the extent of the damage and chronically track the CBF progression.[79]

Traditional techniques for chronic tracking of functional responses include functional magnetic resonance imaging,[118–123] behavioral tests,[124–131] micro-stimulation and histological analyses,[2,132,133] and imaging of intrinsic optical signals.[134] A newly optimized FA MESI technique was recently developed, utilizing a subset of exposures taken from 15-exposure MESI that were specifically designed to sample the flow distributions found within regions of the cortex responding to functional forepaw stimulation. Chapter 4 establishes that the technique is able to measure an absolute baseline for the CBF, allowing for comparison of results over chronic measurements within and

between animals. The technique is capable of monitoring the blood flow dynamics of the functional response to forepaw stimulation, resulting in the functional health of the regional response being chronically tracked. This technique can be used to measure the long-term effects of any neurovascular perturbations, such as ischemic stroke, on the functional health of the mouse cortex. While post-occlusion microvascular blood flow has been shown to be a significant indicator of overall tissue outcome,[92,93] the functional health of the occluded region is an important factor in the neurovascular progression that must also be monitored. A short period of post-stroke neuroplasticity occurring within the region of tissue surrounding the occlusion known as the penumbra has been shown as the beginning of the vascular recovery process.[94,95,137] Previous studies using MESI have identified a period of around 1 week following the occlusion as a significant recovery period, with the CBF reaching baseline measurements on the order of 3 weeks post-occlusion for the small-scale photo-thrombotic occlusion model utilized in this paper.[79] This study presents a protocol using 15-exposure MESI and 5-exposure FA MESI as noninvasive, quantitatively accurate imaging techniques capable of chronically tracking the progression of the post-occlusion cerebral blood flow and functional blood flow dynamics of the forepaw response.

5.2 METHODS

This study utilized 15-exposure Multi-Exposure Speckle Imaging (Figure 20) for baseline measurement of the resting-state baseline CBF, as well as Functional Activation Multi-Exposure Speckle Imaging (Figure 28) to chronically compare forepaw stimulation blood flow responses from the mouse cortex. The same surgical preparation and post-

surgical upkeep of the chronic mouse model from Chapters 3 and 4 was used, with photo-thrombotic strokes delivered in the functionally responding area of the mouse to induce flow changes.

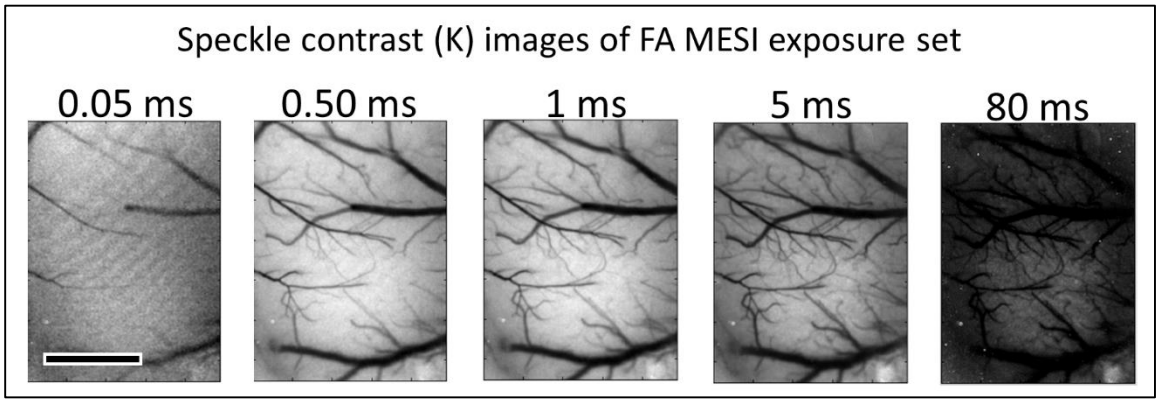

Figure 28: Exposure durations used for Functional Activation MESI. Scale bar = 1 mm.

Animals (n=5) with clear and healthy cranial windows after the recovery period of 3-4 weeks were anesthetized with 70% N_2/O_2 vaporized isoflurane via nose-cone and affixed to a stereotaxic frame. Vitals were recorded via pulse oximetry and temperature was maintained by feedback heating. Multi-Exposure Speckle Imaging was performed over a 2.7 × 2.0 mm field of view centered on the region of interest by collecting 300 frames at each exposure. This imaging technique provided ICT maps of the imaged region, giving a global perfusion index of the area, and was repeated 3 times for each animal to ensure a stable baseline. Heart rate for each experiment was adjusted to be within 10% of the animal's baseline heart rate by small changes in the animal's depth of anesthesia in attempts to control for physiologic variability in the cardiac output within each animal.

After establishing a repeatable baseline with MESI, functional forepaw stimulation measurements were taken using 5-exposure FA MESI. Isoflurane anesthesia was delivered

at 1.0 – 1.5% for functional measurements. A piezoelectric stimulator placed under the forepaw contralateral to the cranial window being imaged (Figure 21). A 35 second stimulation paradigm (Figure 21) was utilized, consisting of 5 seconds of baseline, 5 seconds of 100 Hz piezoelectric stimulation, and 10 seconds of post-stimulation measurements followed by a 15 second break preceding the next stimulation block. This paradigm was repeated for 25 stimulation blocks in attempts to average out any physiological variables not associated with the stimulation. Relative CBF maps of the responding areas (Figure 29) were created by dividing inverse correlation time images averaged within the response window (Figure 21, 5 – 10 s) by images averaged within the baseline window (Figure 21, 0 – 5 s).

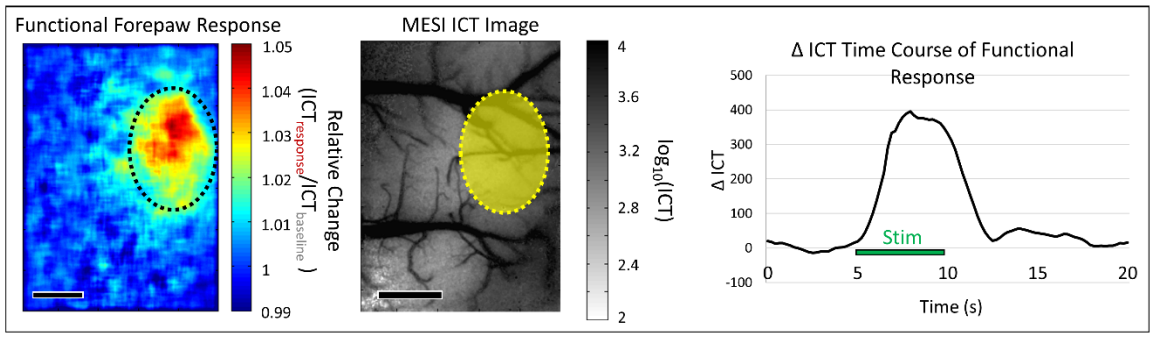

Figure 29: Map of relative change in ICT (left) from Functional Activation Multi-Exposure Speckle Imaging, averaged over 25 stimulation blocks. Multi-Exposure Speckle Imaging inverse correlation time (MESI ICT) image with functionally responding region denoted (middle). Scale bar = 500 µm. Time course (right) of Δ ICT for denoted responding region.

After a pre-stroke functional map was established with FA MESI, a photo-thrombotic stroke was delivered, targeting a descending arteriole within the functionally responding region. Post occlusion imaging sessions included both 15-exposure MESI for baseline CBF monitoring as well as FA MESI for functional monitoring. These sessions

were taken four times within the first week of post-stroke experiments at time points of 0, 2, 4 and 7 days post-occlusion. Following the first week, the animals underwent two more imaging sessions at Days 14 and 21 of their respective post-stroke time points.

A pre-stroke baseline ICT value was established for each animal by taking the mean of ICT measurements within their functionally responding region. This value was used to create a color map by which perfusion boundaries of the damaged regions of the cortex could be identified post-occlusion. Measurements of absolute CBF change were taken within the area of the craniotomy corresponding to original pre-stroke functionally responding region for all time points to compare the changes in temporal dynamics and magnitude of response within this region over time. All experiments were approved by the Institutional Animal Care and Use Committee (IACUC) at The University of Texas at Austin under guidelines and regulations consistent with the Guide for the Care and Use of Laboratory Animals, the Public Health Service Policy on Humane Care and Use of Laboratory Animals (PHS Policy) and the Animal Welfare Act and Animal Welfare Regulations.

5.3 RESULTS

5.3a Post-Occlusion Dynamics of Functional Forepaw Response

Measurements of the functional forepaw response to the previously described stimulation paradigm were taken for pre- and post-occlusion time points. Figure 3 displays results from one of the animals in the study. The pre-stroke functional map of the animal showed the responding region to be localized to the bottom of the field of view (Figure

30A). This area was then targeted for photo-thrombotic occlusion to disrupt blood flow and observe subsequent changes in functional blood flow response. Measurements of the baseline ICT with MESI display progression outcomes of the CBF extending to 21 days post-occlusion (Figure 3B). Maps of the ICT values for this animal show a Day 2 post-stroke reduction in flow within the original FA region to 55% of the pre-stroke baseline, with increases in the ICT values for the following time points. At Day 21 post-stroke, ICT measurements recovered to a mean of 80% of the pre-stroke values.

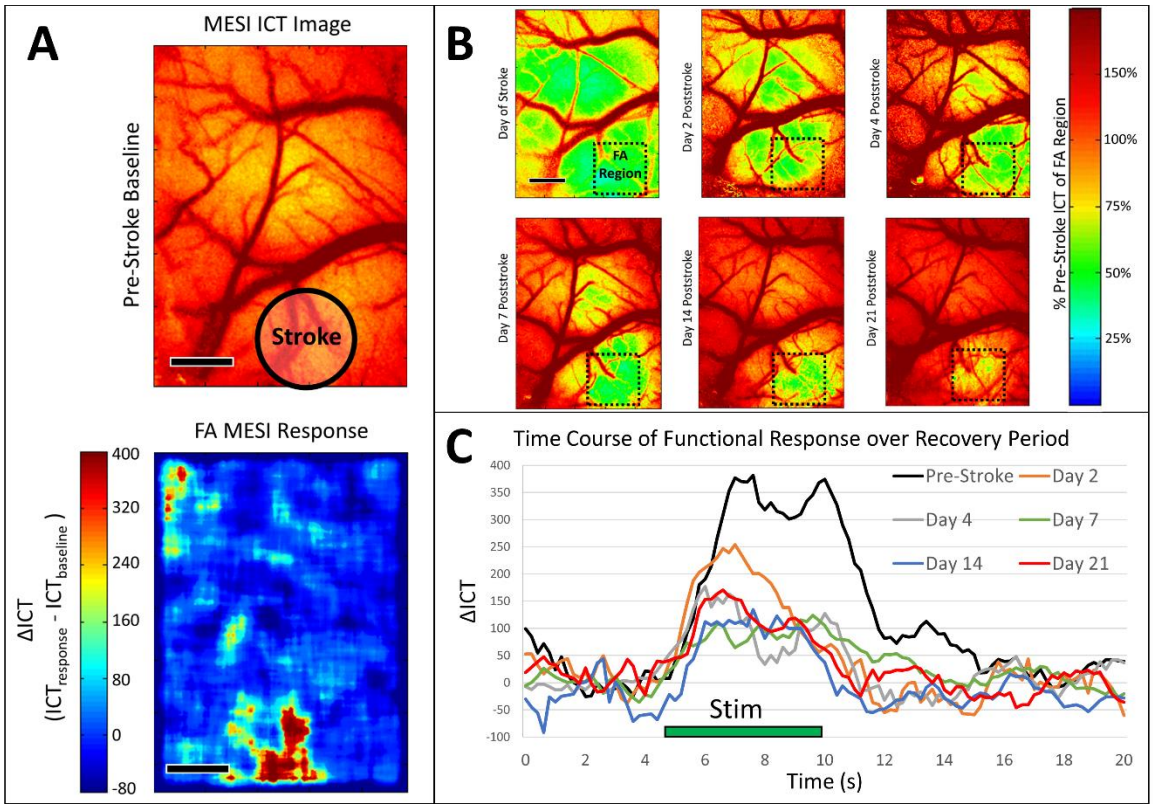

Figure 30: (A) Multi-Exposure Speckle Imaging inverse correlation time (MESI ICT) image before occlusion (top) with targeted area denoted. Map of the functional response (bottom) to forepaw stimulation for pre-stroke measurements. Scale bar = 500 µm. (B) Multi-Exposure Speckle Imaging inverse correlation time images of the baseline CBF values at each time point in the experiment with boxes denoting the FA Region where time courses for (C) were taken. Color map scaled to the mean pre-stroke ICT value of the FA region. Scale bar = 500 µm. (C) Plot of time courses of the changes in ICT value (ICT(x) – ICT(baseline)) for each time point with 5 second stimulus denoted.

Time courses of the functional responses were taken in the regions denoted in Figure 30B corresponding to the original pre-stroke FA region (Figure 30C). These time courses display the absolute change in the CBF response by establishing a quantitative baseline for each time point. Results from this animal show the original pre-stroke

response to have a ΔICT over 350 for seconds 7 to 11 of the response, which corresponds to a 5% increase in flow from baseline for the stimulated time period (Figure 30C). Following the occlusion the ΔICT of the response fell to a peak magnitude of around 200 for Day 2 post-stroke measurements, or just over half of the pre-stroke peak ΔICT magnitude (Figure 30C). When comparing relative responses, this Day 2 value was very similar to the pre-stroke value at a 5% increase in flow, though MESI shows us that the overall resting state baseline CBF was only about half of the pre-stroke baseline (Figure 30B). Measurements of ΔICT for the rest of the time points showed a decrease in magnitude from Day 2 to Day 7 post-stroke, followed by a small increase from Day 14 to Day 21 (Figure 30C). Though Figure 30B shows the CBF of the denoted region is undergoing increases in ICT to near pre-stroke values, the functional responses do not follow this same trend.

Another observation from the post-occlusion functional blood flow responses is the reduced temporal length of the response when compared to the pre-stroke response (Figure 30C). In order to compare the temporal length of functional responses for all animals (n=5) across all time points, the temporal extent of the full width half maximum (FWHM) was used. The mean ΔICT value of the FWHM was also utilized to describe the magnitudes of response changes. Figure 31 displays results comparing the relative magnitude of ΔICT change of functional response, relative temporal length of the functional response, and relative health of the baseline ICT measurements at each time point averaged over the FA region for all animals compared to the pre-stroke measurements (Figure 31).

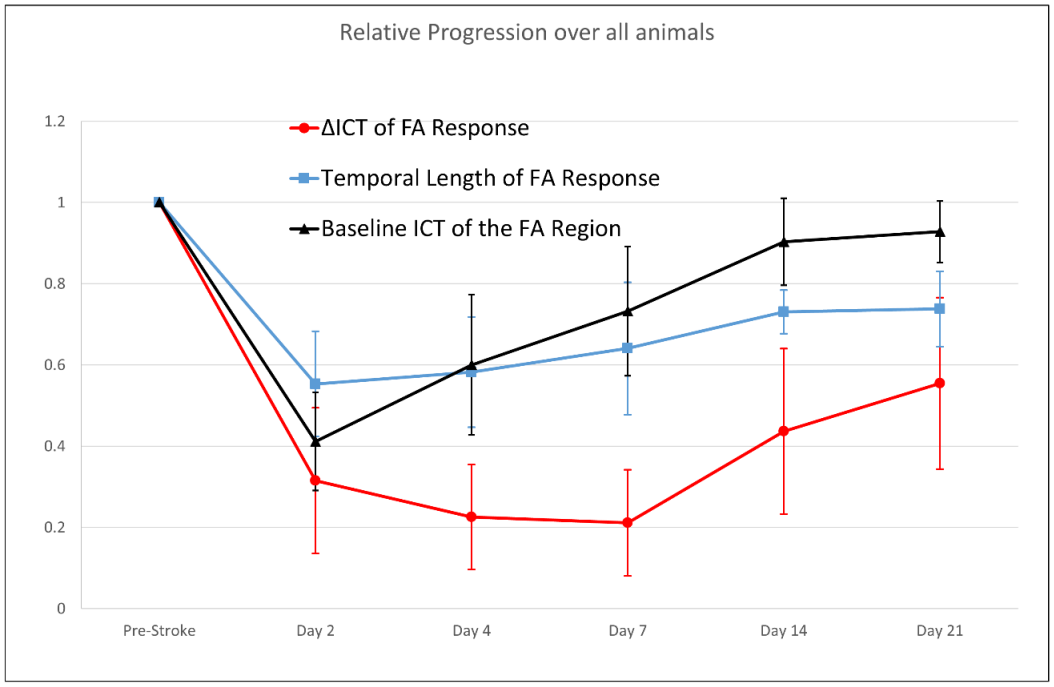

Figure 31: Plot of the relative magnitude of ΔICT change of functional response, relative temporal length of the functional response, and relative mean baseline ICT measurements over the FA region for all animals (mean ± SD) (n=5).

While the mean baseline ICT of the FA region, describing the regional CBF health, begins increasing after Day 2 post-stroke and reaches 93% of the pre-stroke measurement by Day 21, the functional progression of ΔICT does not follow the same trend. Instead, the mean ΔICT of all animals shows a large reduction in magnitude immediately after occlusion, followed by further reductions from Day 2 to Day 7 post-stroke, before a relative increase to 55% of the pre-stroke magnitude by Day 21 (Figure 31). The overall temporal length of the FWHM of the animal's responses, which exhibited a mean of 5.15 seconds for pre-stroke measurements, dropped to 2.85 seconds, or a relative value of 55%, for Day 2 post-occlusion measurements (Figure 31). The temporal length measurements show

small increases for each subsequent time point, reaching a value of 3.8 seconds at Day 21, corresponding to 74% of the pre-stroke measurement (Figure 31).

5.3b Performance of Imaging Technique

Measurements of ICT were taken within the FA region under baseline conditions with both 15-exposure MESI and 5-exposure FA MESI. These baseline values of pre- and post-stroke measurements were compared between techniques to determine the accuracy of FA MESI, using 15-exposure MESI as a reference, as it has been shown previously to accurately determine all flow ranges seen in this occlusion model.[79] Each experiment contributed one data point to Figure 32 for a total of 30 data points over 5 animals. Baseline FA MESI ICT values were taken by averaging the first 5 seconds of all stimulation blocks together.

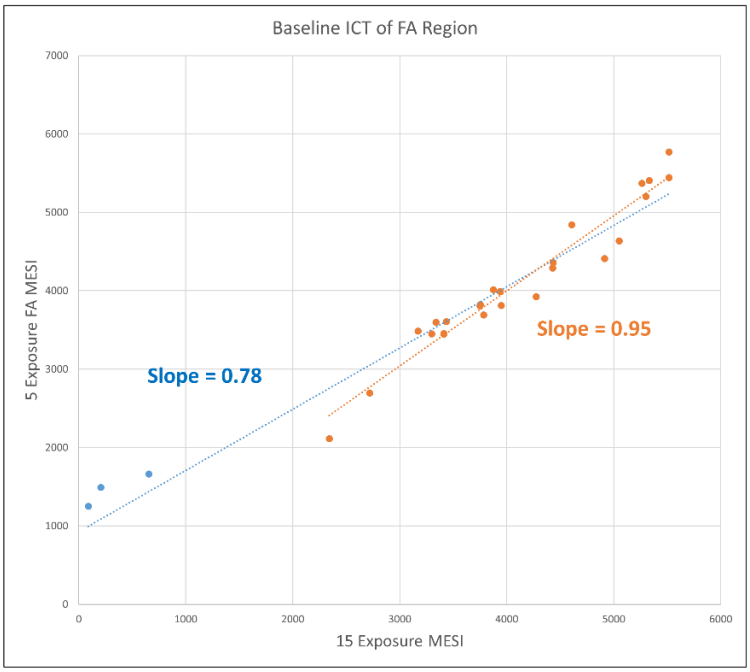

Figure 32: Plot comparing the measured baseline ICT values of 5-Exposure FA MESI and 15-Exposure MESI over all animals (n=5) for all time points (30 total data points). Orange slope (0.95) denoting the regional trend line of the orange data points. Blue slope (0.78) denoting the trend line for all data points.

Results of the comparison shows that the trend line slope for all data points is 0.78, with a slope of 1 denoting matching values between techniques (Figure 32). Figure 32 shows that FA MESI was not accurate in estimating very low CBF flows in three of the post-occlusion data points originating from an animal who developed a much larger occlusion than the remaining 4 animals. In each of these three cases, FA MESI overestimated the ICT value of the FA region of the animal. By excluding these outlying points and observing the regional trend line of the remaining 27 points, a slope of 0.95 was measured. This regional trend line denoted a more accurate range of flow distributions measured with FA MESI.

5.3c Individual Exposure Contributions to Functional Response

In addition to overall FA MESI response, relative time courses from each of the 5 single exposures contributing to the FA MESI signal were plotted for pre-stroke and Day 7 post-stroke measurements (Figure 33), as this time point averaged the lowest ΔICT magnitude over all animals (Figure 31). Shifts in the flow distributions present in the post-occlusion FA region, which had a mean regional ICT value of 67% of the pre-stroke ICT in this animal, resulted in changes to the relative responses of each individual exposure (Figure 33A).

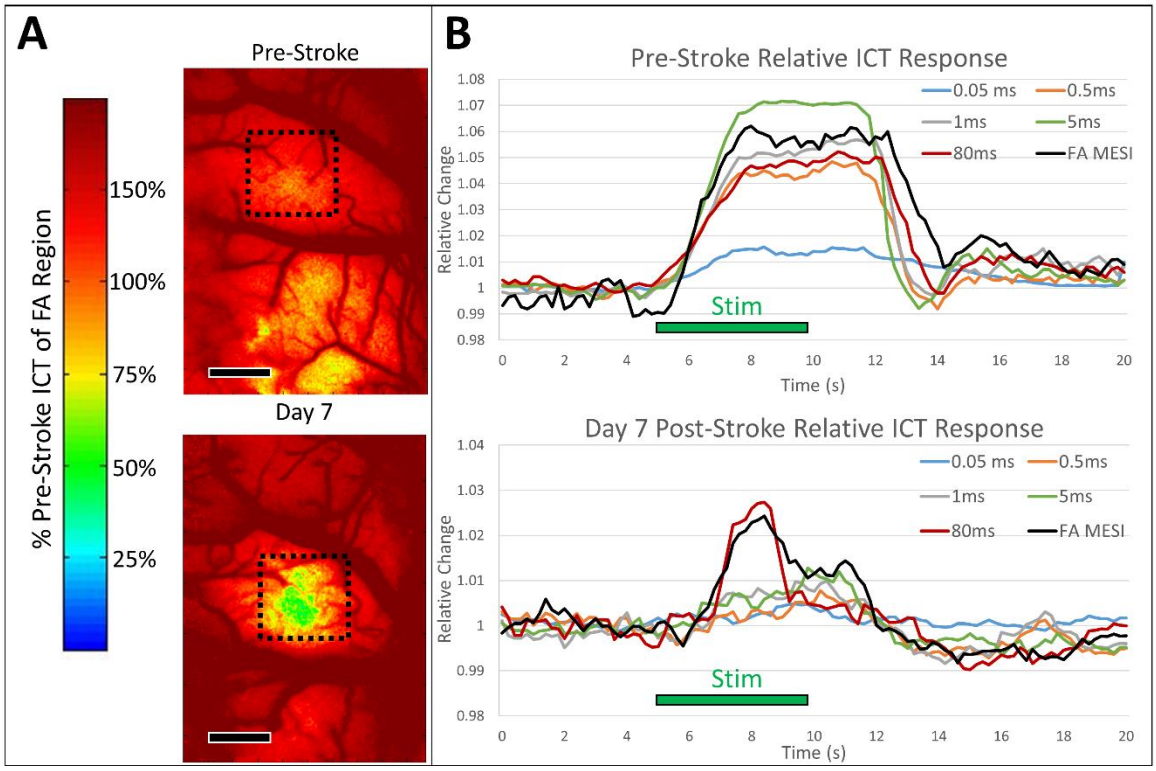

Figure 33: (A) Multi-Exposure Speckle Imaging inverse correlation time (MESI ICT) images of the baseline CBF values at pre-stroke (top) and Day 7 (bottom) time points. Color map scaled to the mean pre-stroke ICT value of the denoted FA region. Scale bar = 500 µm. (B) Plot of relative time courses from each individual exposure contributing to FA MESI response within regions denoted in (A) for pre-stroke and Day 7 post-stroke time points with stimulus denoted.

While the pre-stroke experimental results showed a similar response for the single exposures from 0.5 - 80 ms, the Day 7 post-stroke measurements had higher variability between these exposures (Figure 33B). The highest relative response from this exposure set for the pre-stroke vasculature was 5 ms, which has been shown as an optimal exposure for capturing functional responses using LSCI in previous rodent studies,[76] though each of the remaining exposures longer than 0.05 ms showed prominent relative responses (Figure

33B). Seven days after the occlusion, when flows were lower regionally, the highest relative response occurred in the 80 ms exposure for this animal, with much lower relative responses in the remaining exposures (Figure 33B).

Temporal differences in the relative responses were also observed for post-occlusion measurements, particularly within the 80 ms response, which rose to a peak for approximately 2 seconds but declined while the piezo-electric transducer was still actively stimulating (Figure 33B). The onset time for the Day 7 FA MESI measurement starting at ~6 seconds into the paradigm was also slightly later than the pre-stroke onset at ~5.5 seconds, though both FA MESI responses displayed comparable times to peak response (Figure 33B).

5.3d Comparing Absolute and Relative Responses

The progression of relative responses were compared with absolute functional blood flow responses over the same time period by dividing the ΔICT by the Baseline ICT for each individual experiment and averaging over all animals. Figure 34 displays the results of this comparison, with the largest deviation between the absolute and relative measurements occurring on the first post-stroke measurement at Day 2. The absolute functional blood flow response of the Day 2 post-stroke measurement only averaged 31% of the pre-stroke magnitude, while the relative response was almost 80% at this same time point. The remaining post-occlusion time points were much closer, with the two progressions trending similarly during the period between Day 7 and Day 21 post-stroke.

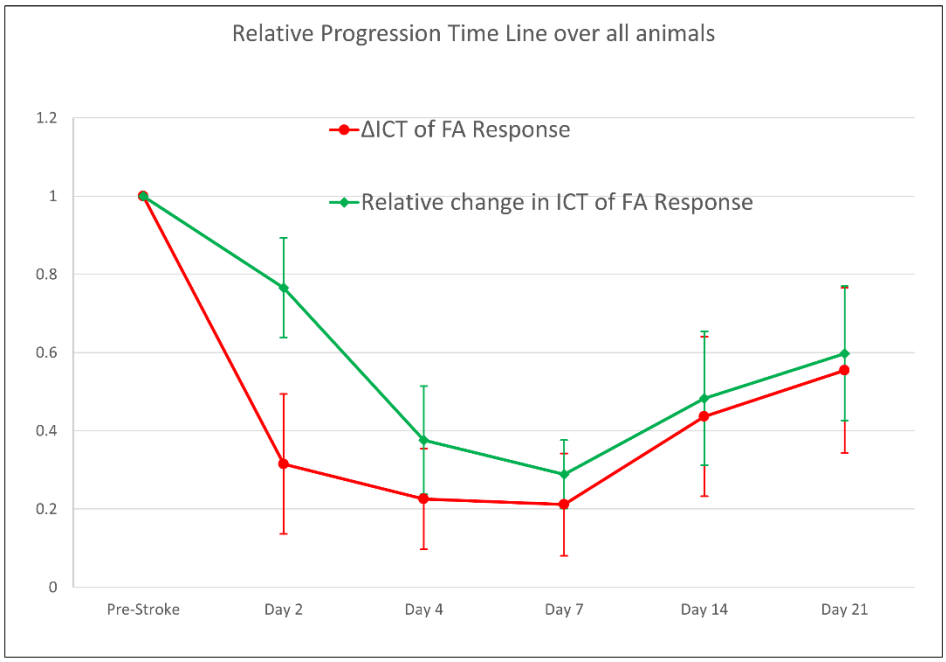

Figure 34: Plot comparing the progression of the relative and absolute changes in ICT during functional stimulation over all animals at each time point. (Mean ± SD) (n=5).

Relative responses for the animal in Figure 30, with the time courses displayed to compare those of the absolute functional blood flow response (Figure 35). Each of the 5 relative post-stroke time points shows a response that appears to be at or near the pre-stroke magnitude, though the absolute measurements display a diminished post-stroke response.

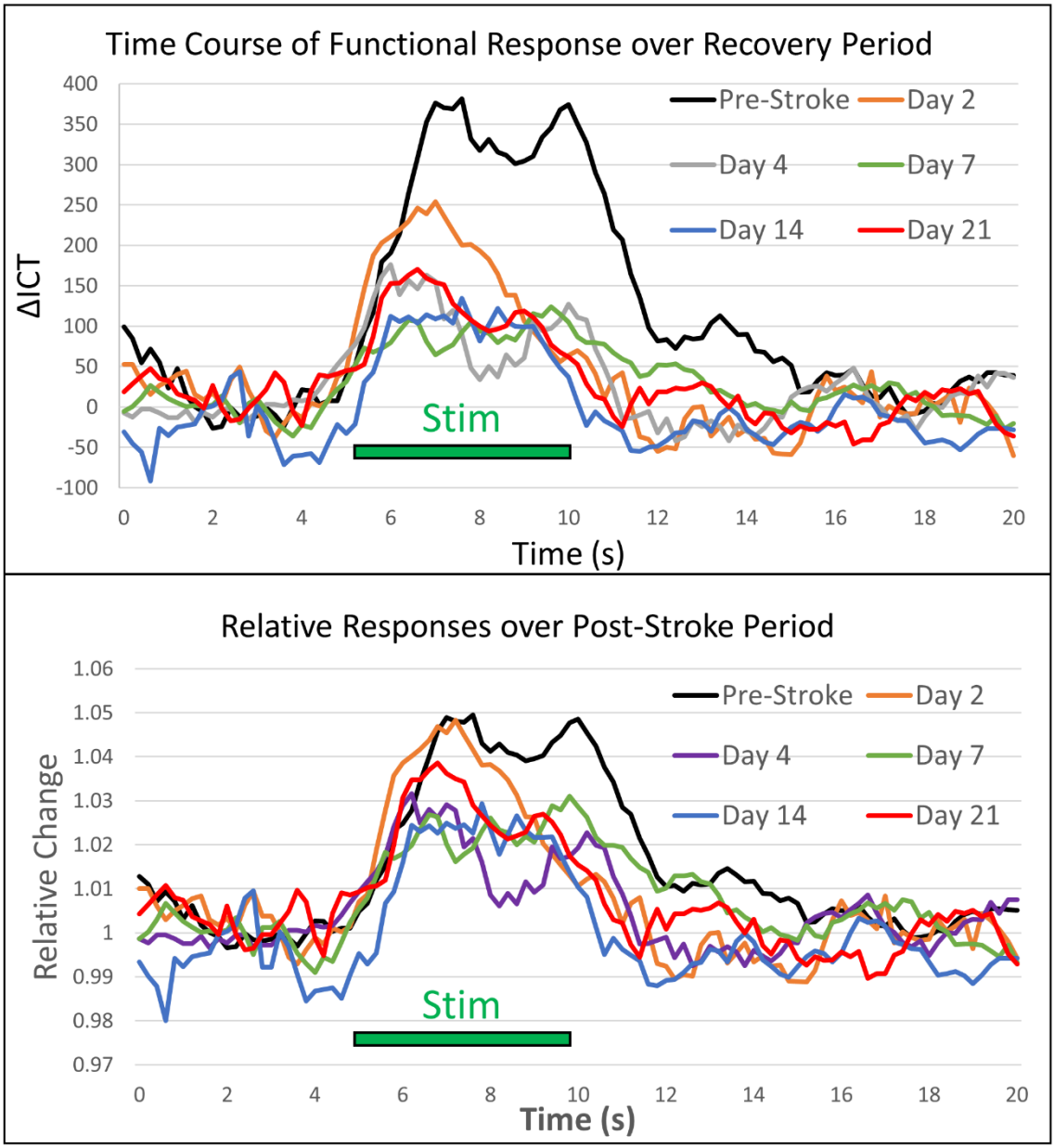

Figure 35: Plot of time courses of the absolute changes in ICT value (ICT(x) – ICT(baseline)) for each time point with 5 second stimulus denoted (top). Plot of time courses of the relative changes in ICT value (ICT(x)/ ICT(baseline)) for each time point with 5 second stimulus denoted (bottom).

5.4 DISCUSSION

The data presented demonstrates a protocol for a long-term *in vivo* study monitoring the dynamics of the CBF response to functional forepaw stimulation after ischemic stroke using two variations of Multi-Exposure Speckle Imaging. Over the 21 day post-occlusion period, animals underwent increases to near pre-stroke levels in their resting state baseline ICT measurements, with the progression captured by MESI. Using FA MESI over the same time period, the magnitudes of the absolute functional blood flow responses reached only 55% of their pre-stroke measurements. By pairing these relatively non-invasive imaging techniques with a chronic mouse model, this protocol could be further adapted to incorporate additional long-term pathophysiologic and pharmacologic studies of stroke recovery.

5.4a Absolute Changes in Functional Blood Flow Response

With FA MESI, absolute baselines were able to be quantified for pre- and post-stroke measurements of the CBF during each stimulation block, allowing for the changes in functional blood flow response due to the occlusion damage to be monitored over a long-term period of weeks to months. While previous optical techniques for measuring functional responses display only relative measurements, FA MESI's capability to measure absolute changes presents a chronic platform from which different experiment days can be fairly compared. If experimenters were to compare only the relative magnitudes of the pre- and post-stroke functional responses from Figure 34, average Day 2 post-stroke measurements would present a response at 77% of the magnitude of the pre-stroke

response. This means the magnitude of the relative response would display over twice the estimate of the absolute change, 31%, measured with FA MESI, and would suggest the photo-thrombotic occlusion to have a much less pronounced effect on the functional health of the region, giving an inaccurate representation of the CBF recovery process (Figure 31).

Progression outcomes from this small scale photo-thrombotic occlusions indicate that the functional health of the forepaw region does not directly mirror the overall CBF health. While the baseline ICT around the occlusion site for Day 21 post-stroke measurements show the CBF reaching 93% of the pre-stroke values, the functional blood flow response of this region, or ΔICT, only reaches 55% of the pre-stroke magnitudes (Figure 31). This suggests the need for further extending the post-stroke experimental period to monitor the progression of the functional response past the time when baseline ICT measurements have reached their pre-stroke values. Results also showed that though the baseline regional CBF saw large increases at Days 4 and 7 post-stroke time points, the functional health did not follow this trend, and instead slightly worsened over the same period. The lack of increases in the functional blood flow responses over this time period between Days 2 and 7 could be the result of a diminished functional capacity to raise blood flow or the lack of restoration of the neuropil's demand for blood flow. The temporal length of the functional response was also impacted for all post-occlusion measurements, though the onset and time to peak of the blood flow responses had similar latencies for most animals (Figure 30C). The combination of these observations suggests that perhaps the regional vasculature cannot recruit enough supply to maintain the functional response for the full stimulation duration of 5 seconds.

5.4b Performance of FA MESI determining baseline ICT

When comparing the baseline ICT values measured with 15-exposure MESI and 5-exposure FA MESI, results showed inaccurate estimations from FA MESI when the flow range measured <15% of the pre-stroke values. These three data points originated from a single animal's Day 2, 4, and 7 post-occlusion measurements, and were the result of a much larger occlusion than was seen for the remaining 4 animals. By Day 14 of this animal's post-stroke period, ICT values rose enough to fall into the more accurately sampled flow distributions for FA MESI. These results suggest that studies looking to cause high impact strokes and measure functional responses during these days should incorporate a different subset of MESI exposures to account for the much slower flow distributions present. An increased number of longer exposure durations, particularly between 5 ms and 80 ms, are needed to better sample the speckle visibility curve for the slow flowing post-occlusion vasculature after high-impact strokes. For the remaining 27 data points on Figure 32, a regional trend line slope of 0.95 presents a strong indicator of the accuracy of FA MESI over these flow ranges compared to traditional 15-exposure MESI. As the baseline values for FA MESI were taken by averaging the 5 seconds before the stimulus over all 25 stimulation blocks, small inaccuracies could have resulted from any baseline drift over the experimental period. The FA MESI measurements were also taken immediately following 15-exposure MESI in all animals, resulting in the animal being on anesthesia for a slightly longer period (~5 minutes) at the start of FA MESI, which could account for slightly lower baseline ICT values measured with FA MESI.

5.4c Changes in Measured Flow Distributions

After the occlusion, when flow distributions have shifted toward lower flows, contributions from each single exposure in FA MESI were expected to re-organize with more emphasis placed on the longer 80 ms exposure and less on the shorter exposures. Figure 6 showed that this was indeed occurring in a Day 7 post-stroke measurement where regional ICT was still at 67% of the pre-stroke values. The Day 7 measurements show the 80 ms exposure having the most prominent relative change when the stimulus occurs, and illustrates how the overall FA MESI response is weighted by this chosen exposure (Figure 33B). Once again the limited ability of the vascular region to sustain hyperemic signals is prominent for this exposure, as the 80 ms relative response drops swiftly toward baseline while the stimulus is still being delivered (Figure 33B). The re-organization of the single exposure contributions shows the necessity for having multiple exposures when measuring any perturbation in flow, as the accuracy of any single exposure when looking at large changes diminishes when the flow distributions fall out of the particular accurate range of the exposure. With multiple exposures sampling the same region, these inaccuracies are resolved by the combination of exposures having accurate ranges across all possible flows for the particular experiment.

5.4d Progression of Absolute and Relative Flow Responses

Though the absolute functional blood flow response of the Day 2 post-stroke measurement only averaged 31% of the pre-stroke magnitude, the relative response was almost 80% at this same time point (Figure 34). This suggests that this region of the brain

is still able to recruit at or near the same percentage of available CBF at Day 2 post-stroke. While relative results may misinterpret this response as showing minimal change from pre-stroke values, the establishment of an absolute baseline with FA MESI is able to illustrate just how large of a drop in flow response actually occurs. This large difference between the relative and absolute responses seems to lessen after this Day 2 post-stroke time point, and trends fairly similarly between Days 7 and 21 post-stroke. This suggests the possibility that the period of 7 days after occlusion with diminished cerebral blood flow reduced either the number of cells or capacity of the cells to recruit the available flow for a functional response.

5.5 SUMMARY

A long-term stroke progression study using a photo-thrombotic occlusion model was used to evaluate an optical imaging protocol for monitoring chronic functional blood flow measurements of the forepaw region of the mouse cortex. After occlusion, Multi-Exposure Speckle Imaging was used to measure regional CBF perfusion of the stroked area, with increases to CBF occurring after Day 2 and reaching 93% of pre-stroke values by Day 21 of the post-stroke period. During this same time span, Functional Activation MESI measured the absolute change in functional blood flow response to forepaw stimulation within the damaged area. The occlusion delivered within the pre-stroke functionally responding area resulted in both a lower magnitude and shorter temporal length of the post-stroke response. Functional outcomes of the study observed Day 21 response measurements reaching 55% of the pre-stroke magnitude and 74% of the pre-

stroke temporal length of the functional blood flow response. Though increases in the regional CBF began after Day 2, the magnitude of functional blood flow responses did not mirror this recovery time line, instead regressing from Days 2 to 7, after which it began to increase toward pre-stroke values. With the ability to measure absolute functional responses, the presented FA MESI technique has been shown to chronically track the temporal dynamics of the blood flow within functionally responding areas over the course of weeks, and can also be used in acute studies to more accurately sample large changes in resting and activated state cerebral blood flows.

Chapter 6: Conclusions

6.1 SUMMARY

Optical imaging techniques have played important roles in understanding the progression of the complex hemodynamics in the brain by observing changes in physiological parameters associated with neurovascular disease. Rodent models of these diseases have been studied with these techniques in hopes of elucidating the neurovascular response and treatment outcomes of analogous clinical pathologies. These optical methods present significant advantages over other imaging techniques due to their combination of non-invasiveness, excellent spatial and temporal resolution, and relatively low cost. One of the main previous limitations of optical techniques is that they typically only determine relative changes in the physiological parameter of interest, limiting studies to acute measurements. Multi-Exposure Speckle Imaging offers a technique capable of establishing a quantitative baseline, thus eliminating the limitation of relative measurements.

With the combination of a chronic mouse model, MESI measurements of cerebral blood flow, and two-photon fluorescence microscopy measurements of vascular structure, we have demonstrated a protocol for a long-term study monitoring the progression of the vasculature in the rodent cortex after photo-thrombotic stroke. We have shown the occurrence of significant vascular reorientation over a 35 day post-occlusion period, beginning as early as 7 days after the occlusion delivery. Flow estimates from MESI within the un-resolvable parenchyma were shown to have high correlations with two-photon microscopy sub-surface volume fractions within areas of recovering vasculature in the peri-infarct region. This imaging protocol presents the potential to test the efficacy of rehabilitation and pharmacological therapies on neurovascular disease.

We have demonstrating the ability to optimize MESI for measuring functional blood flow responses with sufficient temporal resolution, providing an absolute baseline that can be utilized for chronic studies monitoring the progression of the response. A subset of 5 exposures was found to sample the flows distributions prevalent in functional blood flow response to forepaw stimulation. This allowed FA MESI to double the sampling rate of 15-exposure MESI while maintaining a comparable accuracy. The feasibility of capturing functional blood flow responses was demonstrated with FA MESI, allowing for absolute changes in CBF to be measured. By developing this imaging modalities to provide absolute flow changes rather than relative measurements, it allows for studying the progression of the functional response after ischemic stroke with the chronic mouse model. This development also illustrates the ability to adapt MESI for other experiments by optimizing the subset of exposures for the flows of interest, minimizing the main drawbacks of decreased sampling rate and computational complexity.

Finally, we deployed FA MESI in a chronic study monitoring the progression of the functional blood flow response and regional CBF of the cortex after photo-thrombotic occlusion within the functionally responding region to forepaw stimulation. Following the occlusion, increases in the baseline CBF perfusion begin at Day 2 post-stroke and reach near pre-stroke baseline values by Day 21. Absolute changes in the functional blood flow response over the same animals show the magnitude of the response to decrease further between Days 2 and 7 post-stroke, followed by an increase between Days 7 and 21. While the CBF perfusion values reached over 90% of the pre-stroke measurements, the magnitude of the functional blood flow response only reached 55% of the pre-stroke magnitude.

Absolute changes in the flow response were compared to relative changes, showing large discrepancies for Day 2 and Day 4 post-stroke measurements, demonstrating the need for measurements of absolute response in experiments such as these to accurately measure functional outcomes. The performance of FA MESI technique was validated over the sampled flow distributions by comparing baseline measurements of ICT to those from 15-exposure MESI at the same time points.

By combining these non-invasive optical systems capable of measuring absolute outcomes of cerebral blood flow, functional response, and vascular structure with a chronic mouse model, we can work to determine each parameters role during pathophysiological events, helping elucidate the progression of neurovascular diseases

6.2 Future Work

Combining a chronic mouse model with long-term studies of vascular progression after ischemic stroke has opened many pathways that can be taken for future work. Two that will be discussed in more detail are adding chronic monitoring of oxygen tension to protocols from this dissertation in order to address the impact of oxygen gradients on the health of the vasculature and blood flow, and altering the damage model from the photo-thrombotic stroke toward a technique that results in a larger penumbral area and smaller ischemic core. By introducing a disease model with less damage to the area of interest, the impact of the flow decrease in the penumbra on the functional health of the tissue can be better separated from the damage in the ischemic core. A large limitation of the current model used in Chapters 3 and 5 is that the photo-thrombotic occlusion results in a large

ischemic core but creates only a relatively small area of penumbra surrounding the core, which may not be the most clinically relevant stroke model to study.

6.2a Monitoring Oxygen Tension Chronically after Stroke

Phosphorescence quenching provides an optical technique for *in vivo* measurements of the partial pressure of oxygen, or pO_2.[138,139] This technique works by dissolved oxygen within the region of interest quenching the phosphorescence of molecules and altering their excited state lifetimes (Illustration 5).[140–142]

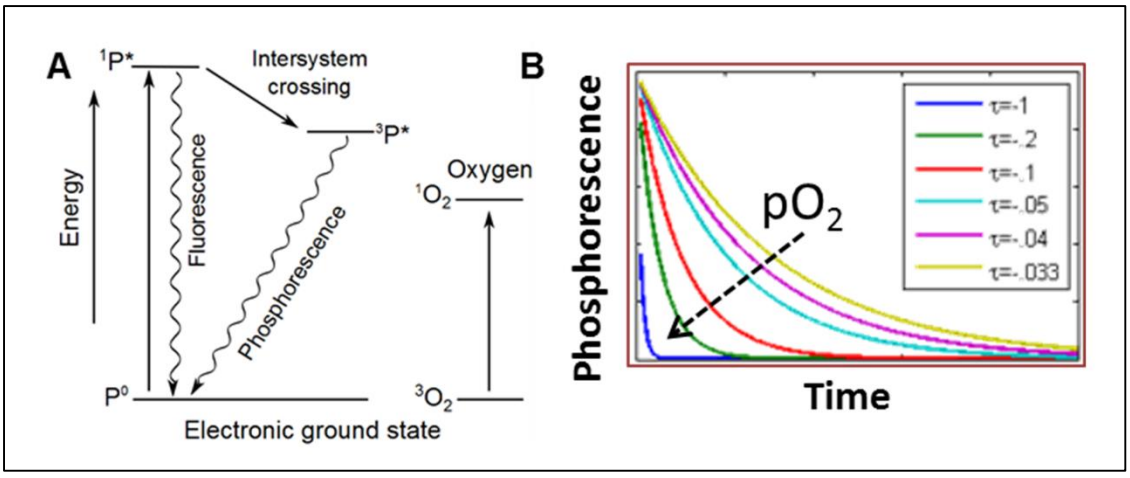

Illustration 5: A) Jablonski diagram of phosphorescence quenching. B) Reduction in excited state lifetimes due to phosphorescence quenching.

The pO_2 can be quantified from the measured lifetime using the Stern-Volmer relationship below.

$$\tau_o/\tau = 1 + k_q\tau_o[pO_2], \qquad \text{(Eqn. 4)}$$

For this equation, τ is the measured excited state lifetime, τ_o is the unquenched lifetime and k_q is a quenching constant dependent on the probe's energy transfer efficiency

and kinetics within its microenvironment. This technique has been demonstrated in a wide range of tissues including retina,[143] brain,[144,145] and muscle,[146] and is especially useful for studying the cortical oxygenation before and after occlusion.[97]

Preliminary studies were undertaken attempting to monitor the progression of pO_2 after photo-thrombotic occlusion within the region of the cortex functionally responding to forepaw stimulation in several animals. Measurements of oxygen tension were taken with the two-photon microscope used in Chapter 3, as it provides a depth-resolved technique capable of describing the oxygen concentrations in very small volumes of vasculature. The goal of this study was to link the progression of the pO_2 in the post-occlusion region with the CBF, volume fraction, and relative functional blood flow response. These studies were intended to be a follow-up to the work presented in Chapter 3, before the development of FA MESI. Specifically, we wanted to investigate the oxygen tension gradients within the infarct core along the direction of vascular reorientation previously documented. A similar stimulation paradigm to the paradigm described in Chapters 4 and 5 was used to identify the pre-stroke functionally responding forepaw region in all animals (n=5) (Figure 36).

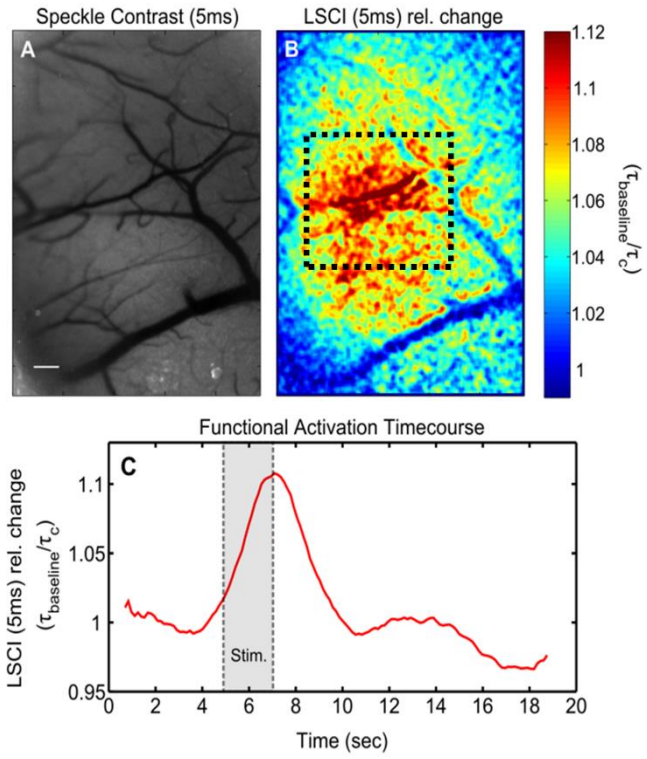

Figure 36: A) Speckle contrast image (5 ms exposure) of cortical microcirculation. Scale bar = 300 µm. B) Relative response map of inverse correlation times at 5 ms exposure. C) Time course of ICT dynamics from an 800µm square region bounding the area with maximal response in (B).

Two-photon microscopy was used to identify a descending arteriole supplying the functionally responding region, denoted by an arrow in Figure 37A. After identification of the vessel of interest, a photo-thrombotic occlusion was delivered to the animal, and chronic monitoring of the post-occlusion dynamics commenced. The flow reductions in the CBF were monitored with MESI and classified into vascular or parenchymal regions. This classification was done both for the entire field of view as well as the area of the ischemic core (Figure 37).

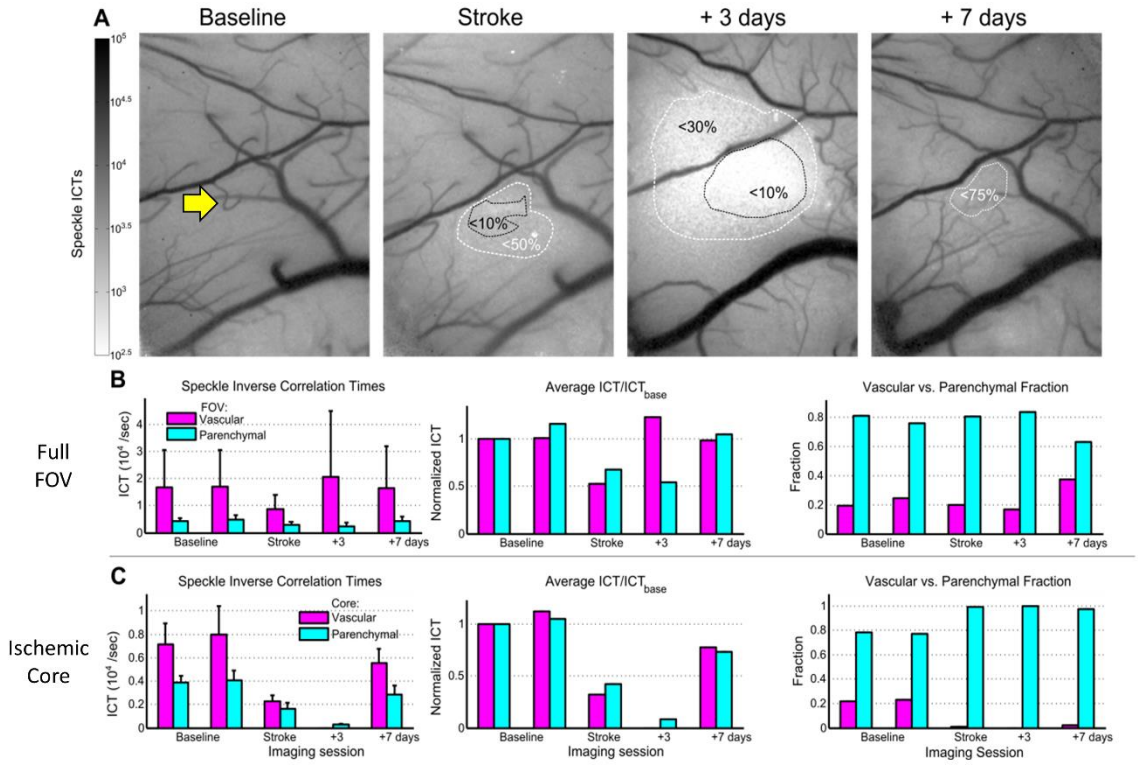

Figure 37: A) Progression of MESI ICT maps pre- and post-occlusion. Core regions with flow <10% of baseline are identified by black outline. Areas of reduced flow are bounded by white outline. Vessel and parenchymal segmented perfusion analysis of the entire FOV (B) and in the ischemic core (C).

Results from the animal in Figure 37 suggest that the vascular ICT measurements increased above baseline values by Day 3 post-stroke within the full FOV, while parenchymal ICT measurements were only ~50% of their pre-stroke baseline (Figure 37B). The full FOV ICT measurements within the parenchyma reached pre-stroke baseline values by the next measurement point 7 days after occlusion. The dynamics of the vascular and parenchymal volume fractions within the field of view were also studied, showing substantial increases in the amount of surface vasculature at Day 7 post-stroke (Figure 37B). Within the ischemic core, measurements of parenchymal ICT reach only ~75% of

the pre-stroke baselines by Day 7 post-stroke, with little surface vascular volume fraction remaining after the occlusion (Figure 37C).

The vascular structure and partial pressure of molecular oxygen within ischemic core area were studied with two-photon lifetime microscopy to further characterize the region before and after photo-thrombotic occlusion (Figure 38). Three time points were used for chronic two-photon imaging of the targeted area: baseline, day of stroke, and 7 days post-stroke.

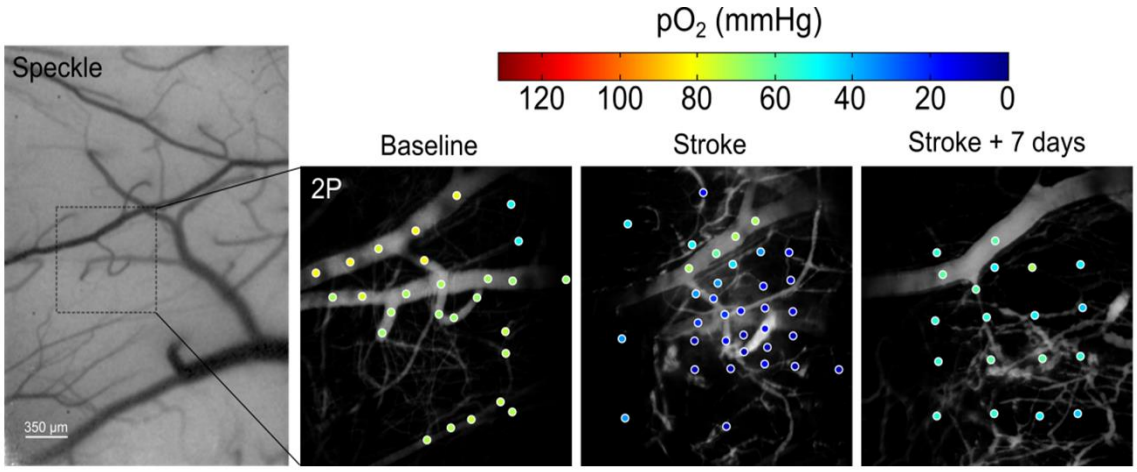

Figure 38: Chronic two photon lifetime microscopy of functionally responding region identified with speckle imaging. Oxygen tension values in terms of the partial pressure of molecular oxygen (pO_2) are overlaid over two photon intensity projections of fluorescein labeled vasculature.

Baseline measurements of pO_2 were restricted to within vasculature, while post-stroke measurements could also sample the surrounding tissue, as the phosphorescent probe was small enough (MW=65 kDa) to escape the post-occlusion leaky vasculature. Baseline measurements of the oxygen tension were taken at two pre-stroke time points separated by 4 days with no significant differences. The small fluorescent dye (MW=70 kDa) used in Chapter 3 was replaced with a larger dextran conjugated plasma fluorescent

dye (MW=2MDa) in attempts to minimize the effects extravasation on post-stroke imaging. This improvement resulted in much better SNR for Day 7 post-stroke imaging than was previously seen in the Chapter 3 experiments. The oxygen tension within the targeted arteriole branch showed a 60 mmHg drop (70mmHg baseline, 10-15 mmHg post-occlusion), with even lower oxygen tension in the surrounding tissue of the ischemic core area. This surrounding tissue measured pO_2 values as low as 7 mmHg immediately after stroke, suggesting that the oxygen delivery to this area was severely disrupted by the photo-thrombotic occlusion (Figure 38). Measurements of oxygen tension 7 days after the stroke showed slight perfusion into the targeted arteriole branch, though much less than pre-stroke baseline. This slight perfusion was enough to raise pO_2 values in this vessel of ~60 mmHg. Though the extravasation seemed to have stopped for the large fluorescent probe, the small phosphorescent probe was still able to be measured in the extravascular space at Day 7, and showed comparative pO_2 values to those measured in capillaries of the pre-stroke baseline vasculature. Results from this study suggest the recovery of the oxygen tension on the surface of the vasculature to be on a similar timeline to the CBF recovery for this photo-thrombotic model.

The major limitation of this study was the time required to make these point-by-point measurements of pO_2. While the main benefit of two-photon microscopy is the ability to resolve deeper vasculature, this advantage was not able to be capitalized for this study due to experimental times lasting much longer than is healthy for the chronic animal model. Minimizing anesthesia exposure of the chronic animals in these studies is an important factor in maintaining the general health of the animal and measuring results that

aren't biased by the effects of anesthesia. While the experimental time line for this study was expected to measure the progression on the order of 35 days post-occlusion, only one of the five animals that made it to the occlusion stage reached the Day 7 post-stroke time point. The experimental time of ~2-3 hours for two-photon lifetime microscopy was not conducive to a chronic study with time points as close together as this. Measurements of functional blood flow response to forepaw stimulation did not progress at all over this small post-stroke window.

Future work looking to add oxygen tension measurements into a chronic study of the cortex after photo-thrombotic occlusion could potentially move toward a much faster but less regionally confined surface measurement. The same phosphorescent decays can be measured by selectively illuminating the surface with a digital micro-mirror device (DMD) and taking the resulting depth-integrated signals to map the pO_2 of the region (Figure 39).

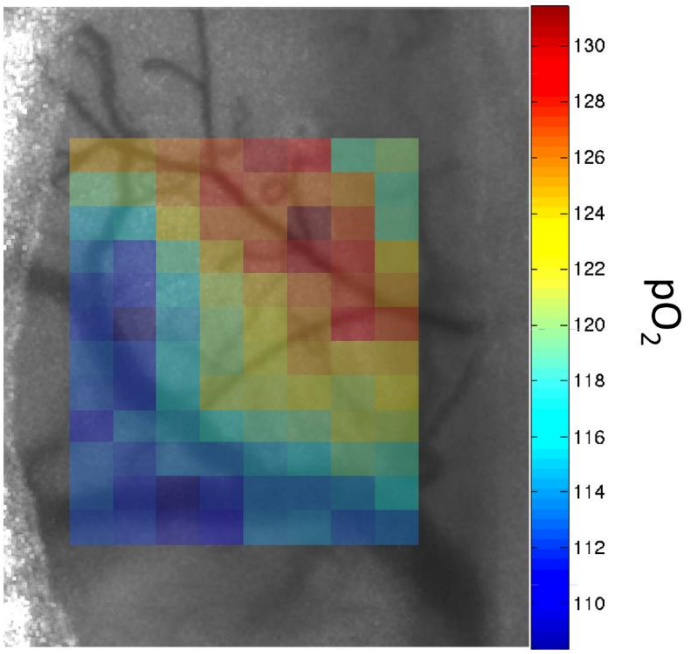

Figure 39: Map of depth-integrated pO_2 measurements of the surface vasculature using selective illumination from DMD.

This technique presents a much faster alternative to two-photon lifetime microscopy due to the selectively ability to illuminate a relatively large region and recover signal with good SNR. The drawbacks being that it is a spatially averaged result in all three dimensions. These drawbacks are relatively minor for this particular study looking at oxygen gradients along the perfusion boundaries highlighted with MESI, as the spatial resolution could prove to be sufficient for this application.

6.2b Alternate Physiologically Relevant Disease Models

The chronic mouse model which was originally hoped to last 1-2 months has shown that with a good preparation and upkeep they can potentially last 4-6 months, allowing for

a much slower damage model as well as a much longer post-occlusion window to look at. This longer window would be useful in both the experiments done in Chapters 3, where the full vascular progression into the infarct was not able to be captured with two-photon microscopy over our experimental duration. In addition to this, questions could be answered on the remodeling effect of the vessels perfusing into this area, and whether there is a return to a homogenous orientation as was seen pre-stroke. The extended post-occlusion window would see similar effects in the Chapter 5 study, as more information could be gleaned into the recovery of the functional blood flow response to forepaw stimulation, as the magnitude of the response was still increasing at the experimental end point. Longer periods would allow for more information on whether the magnitude of the response does indeed recover to pre-stroke values within the affected region, or if perhaps the spatially responding area will migrate toward a healthier region of the cortex given more time to recover.

The photo-thrombotic occlusion used throughout the studies presented in this dissertation resulted in a quickly developing ischemic core area matching the focal spot size of the photo-activation laser (0.6 mm diameter circle). Though a penumbral area of reduced blood flow surrounding this core was created in the animals, it was much smaller on average than the core area itself. This results in the vascular progression outcomes presented being specifically tailored only to this stroke model where in addition to the main occlusion of the descending arteriole, there are micro-scale occlusions throughout the sub-surface vasculature reached by the photo-activation laser. This model may not present the

most clinically relevant model, as many clinical therapies are targeting the recovery of the penumbral area.

The potential exists for a more precise photo-thrombotic occlusion, resulting in minimized damage to the surrounding tissue by only occluding surface vessels. By using a DMD to selectively illuminate only the targeted vessels, a photo-thrombotic occlusion can be delivered within individual vessels with much lower laser powers (Illustration 6). This selective illumination allows for the experimenter to better tailor the impact of the occlusion to fit an experiment, as well as create a larger penumbra area with a small core by only damaging a vessel supplying flow to a region.

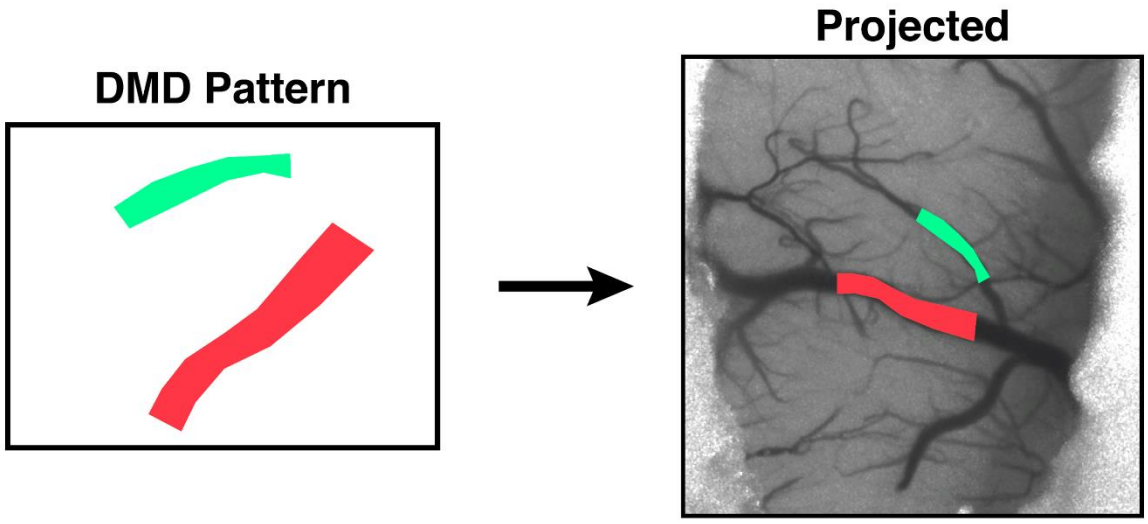

Illustration 6: Selective illumination pattern for digital micro-mirror device (DMD) to project light for phosphorescence measurements or photo-thrombotic stroke.

Preliminary work using this DMD has shown the ability to create strokes with low laser powers, occluding the targeted vessel for 1-2 days after which the flow returns as the thrombus is cleared. Combining this short term occlusion method with the longer-lasting

chronic mouse model gives the potential for a damage model based on repeated small-scale vascular occlusions that could be delivered every week or two with the chronic effects being monitored for months. This damage model would result in very little to no ischemic core, as the vessel would reperfuse itself after hours to days, but would induce a deprivation of the blood flow and oxygen supply to the surrounding tissue if targeting a descending arteriole, creating a penumbral region. By using this model in combination with MESI and surface-integrated phosphorescence quenching, much information could be gleaned about the role of CBF in creating local oxygen gradients. Repeatedly occluding the supplying vessels would also detail the cumulative effect of these strokes on the vasculature over a longer period of time.

Though delivery of traditional stroke models such as endothelin-1 (ET1),[147–151] a potent vasoconstrictor used in animal studies of cerebral ischemia, or middle cerebral artery occlusion (MCAo)[152–154] present problems in delivery with this chronic mouse, both present alternate techniques with the capability to produce a large penumbra area with minimal additional damage. It is possible that these alternate techniques present more clinically relevant disease models to mimic the localization and progression of stroke than a scalable photo-thrombotic occlusion, which must be further validated. Ultimately, all pre-clinical studies of neurovascular disease require imaging techniques such as those developed and utilized in this thesis to interrogate and predict the efficacy of potential interventions.

Appendices

The information presented in the Appendices is intended for further description of the animal preparation and maintenance protocol developed for the evaluation of the chronic *in vivo* optical imaging techniques.

APPENDIX 1. STERILE CRANIAL WINDOW SURGICAL PREPARATION

The optical techniques of MESI and 2PLM are noncontact to the extent that optical access to the tissue can be obtained, for which a chronic cranial window implantation technique is outlined as follows.

Mice (CD-1, male, 30 g, Charles River) were anesthetized with isoflurane (2.0%) via a nose-cone. Body temperature was maintained at 37°C throughout surgery and imaging using a feedback temperature control system (FHC Bowdoin, ME, USA). All animal surgeries were performed in sterile conditions. Vitals, including heart rate, breath rate, and arterial oxygen saturation were monitored with a pulse oximeter (MouseOX, Starr Life Sciences Corp., Oakmont, PA, USA). After induction, mice were placed in a stereotaxic frame (Narishige Scientific Instrument Lab, Tokyo, Japan) and administered injections of carprofen (5 mg/kg, subcutaneous) and dexamethasone (2 mg/kg, intramuscular) to reduce inflammation of the brain after skull removal during the craniotomy.

Surgical instruments and artificial cerebral spinal fluid (ACSF, buffered pH 7.4) exposed to incision area were sterilized via autoclave. The mouse was placed supine and the head fixed to a stereotaxic frame. The scalp and topical anesthetic applied to the skin.. A 4 x 3 mm portion of skull was removed via dental drill (Ideal Microdrill, 0.5mm burr;

Fine Science Tools, Foster City, CA, USA) with constant perfusion of sterile artificial cerebral spinal fluid (buffered pH 7.4). A thin layer of cyanoacrylate (Vetbond, 3M, St. Paul, MN, USA) was applied to the areas of exposed skull in order to facilitate the adhesion of dental cement in a following step. A 5-8 mm round coverglass (#1.5, World Precision Instruments, Sarasota, FL, USA) was placed on the brain with a layer of artificial cerebral spinal fluid separating the two. While applying gentle pressure to the coverglass, a dental cement mixture was wicked around the perimeter of the coverglass and sealed to skull. This process ensured a sterile air-tight seal around the craniotomy and restored intracranial pressure. A second layer of cyanoacrylate was then applied over the dental cement mixture to further seal the cranial window. Animals were allowed to recover from anesthesia on the heating pad and were monitored for cranial window integrity and behavior normality for 4-6 weeks before imaging.

APPENDIX 2. Chronic Animal Maintenance

Following the surgical preparation described in Appendix 1, animals were administered carprofen injections subcutaneously (5 mg/kg) 2, 4, and 7 days post-surgery. This helps relieve chronic pain from the preparation as well as inflammation of the brain. Daily checks on the animals were made to monitor the integrity of the cranial window as well as the behavior of the animals. Surgical preparations were done in batches of 5 over a period of 2-3 days to keep all animals in the same housing. By keeping the animals socially housed, it reduced the amount of overeating that is seen when solo housing, thus reducing possible growth in the animal's size, which helps to keep the cranial window

intact. Any aggression from the mice resulted in separation of the animals, though this did not occur very often post-surgery.

After 4-6 weeks recovery, animals were used for chronic imaging experiments. Cranial windows were cleaned before each imaging experiment with a cotton swab containing a few drops of 70% ethanol by swiping the swab over the window. Any signs of discoloration on or around the cranial implant were documented and further observed for possible infections. Behavior abnormalities were also documented before and after each experiment, particularly following delivery of the photo-thrombotic occlusion and post-stroke measurements. Any cracks or breaking of the windows was also documented, resulting in the removal of this animal from the experiment and subsequent euthanasia. In some cases, the connection between the dental cement and the surrounding skin of the animal's head was bolstered by the application of another layer of sterile cyanoacrylate.

References

1 Go AS, Mozaffarian D, Roger VL, Benjamin EJ, Berry JD, Blaha MJ *et al.* Heart Disease and Stroke Statistics—2014 Update A Report From the American Heart Association. *Circulation* 2013; : 01.cir.0000441139.02102.80.

2 Carmichael ST. Cellular and molecular mechanisms of neural repair after stroke: Making waves. *Ann Neurol* 2006; **59**: 735–742.

3 Astrup J, Symon L, Branston NM, Lassen NA. Cortical evoked potential and extracellular K+ and H+ at critical levels of brain ischemia. *Stroke* 1977; **8**: 51–57.

4 Ramos-Cabrer P, Campos F, Sobrino T, Castillo J. Targeting the Ischemic Penumbra. *Stroke* 2011; **42**: S7–S11.

5 Wardlaw JM, Murray V, Berge E, del Zoppo G, Sandercock P, Lindley RL *et al.* Recombinant tissue plasminogen activator for acute ischaemic stroke: an updated systematic review and meta-analysis. *The Lancet* 23; **379**: 2364–2372.

6 Cronin CA. Intravenous Tissue Plasminogen Activator for Stroke: A Review of the ECASS III Results in Relation to Prior Clinical Trials. *J Emerg Med* 2010; **38**: 99–105.

7 Endres M. Statins and stroke. *J Cereb Blood Flow Metab* 2005; **25**: 1093–1110.

8 Council TS. Statins After Ischemic Stroke and Transient Ischemic Attack An Advisory Statement From the Stroke Council, American Heart Association and American Stroke Association. *Stroke* 2004; **35**: 1023–1023.

9 Vaughan CJ. Prevention of stroke and dementia with statins: effects beyond lipid lowering. *Am J Cardiol* 2003; **91**: 23–29.

10 Structure, Process, and Outcomes in Stroke Rehabilitation : Medical Care. http://journals.lww.com/lww-medicalcare/Fulltext/2002/11000/Structure,_Process,_and_Outcomes_in_Stroke.5.aspx (accessed 9 Jul2013).

11 Jette DU, Latham NK, Smout RJ, Gassaway J, Slavin MD, Horn SD. Physical Therapy Interventions for Patients With Stroke in Inpatient Rehabilitation Facilities. *Phys Ther* 2005; **85**: 238–248.

12 Coupar F, Pollock A, van Wijck F, Morris J, Langhorne P. Simultaneous bilateral training for improving arm function after stroke. *Cochrane Database Syst Rev* 2010; : CD006432.

13 Stroke Stopper -- Interventional Neuroradiologists Treat Brain Strokes with New Kind of Stent. http://www.sciencedaily.com/videos/2006/0407-stroke_stopper.htm (accessed 9 Jul2013).

14 De la Torre JC. Alzheimer Disease as a Vascular Disorder. *Stroke* 2002; **33**: 1152 – 1162.

15 De la Torre JC. Is Alzheimer's disease a neurodegenerative or a vascular disorder? Data, dogma, and dialectics. *Lancet Neurol* 2004; **3**: 184–190.

16 Schaffer CB, Friedman B, Nishimura N, Schroeder LF, Tsai PS, Ebner FF *et al.* Two-Photon Imaging of Cortical Surface Microvessels Reveals a Robust Redistribution in Blood Flow after Vascular Occlusion. *PLoS Biol* 2006; **4**: e22.

17 Nishimura N, Schaffer CB, Friedman B, Lyden PD, Kleinfeld D. Penetrating arterioles are a bottleneck in the perfusion of neocortex. *Proc Natl Acad Sci* 2007; **104**: 365 –370.

18 Sacco S, Marini C, Totaro R, Russo T, Cerone D, Carolei A. A population-based study of the incidence and prognosis of lacunar stroke. *Neurology* 2006; **66**: 1335–1338.

19 Devor A, Ulbert I, Dunn AK, Narayanan SN, Jones SR, Andermann ML *et al.* Coupling of the cortical hemodynamic response to cortical and thalamic neuronal activity. *Proc Natl Acad Sci U S A* 2005; **102**: 3822–3827.

20 Jones PB, Shin HK, Boas DA, Hyman BT, Moskowitz MA, Ayata C *et al.* Simultaneous multispectral reflectance imaging and laser speckle flowmetry of cerebral blood flow and oxygen metabolism in focal cerebral ischemia. *J Biomed Opt* 2008; **13**: 044007.

21 Bahar S, Suh M, Zhao M, Schwartz TH. Intrinsic optical signal imaging of neocortical seizures: the 'epileptic dip'. *Neuroreport* 2006; **17**: 499–503.

22 Koronyo-Hamaoui M, Koronyo Y, Ljubimov AV, Miller CA, Ko MK, Black KL *et al.* Identification of amyloid plaques in retinas from Alzheimer's patients and noninvasive in vivo optical imaging of retinal plaques in a mouse model. *NeuroImage* 2011; **54 Suppl 1**: S204–217.

23 Waerzeggers Y, Monfared P, Viel T, Winkeler A, Jacobs AH. Mouse models in neurological disorders: applications of non-invasive imaging. *Biochim Biophys Acta* 2010; **1802**: 819–839.

24 Calamante F, Thomas DL, Pell GS, Wiersma J, Turner R. Measuring cerebral blood flow using magnetic resonance imaging techniques. *J Cereb Blood Flow Metab Off J Int Soc Cereb Blood Flow Metab* 1999; **19**: 701–735.

25 Manole MD, Foley LM, Hitchens TK, Kochanek PM, Hickey RW, Bayir H *et al.* Magnetic resonance imaging assessment of regional cerebral blood flow after asphyxial cardiac arrest in immature rats. *J Cereb Blood Flow Metab* 2008; **29**: 197–205.

26 Sung K-K, Jang D-P, Lee S, Kim M, Lee S-Y, Kim Y-B *et al.* Neural responses in rat brain during acute immobilization stress: a [F-18]FDG micro PET imaging study. *NeuroImage* 2009; **44**: 1074–1080.

27 Blomqvist G, Seitz RJ, Sjögren I, Halldin C, Stone-Elander S, Widén L *et al.* Regional cerebral oxidative and total glucose consumption during rest and activation studied with positron emission tomography. *Acta Physiol Scand* 1994; **151**: 29–43.

28 Sarkar S, Ghosh S, Ghosh SK, Collier A. Role of transcranial Doppler ultrasonography in stroke. *Postgrad Med J* 2007; **83**: 683–689.

29 Cui X, Bray S, Bryant DM, Glover GH, Reiss AL. A quantitative comparison of NIRS and fMRI across multiple cognitive tasks. *NeuroImage* 2011; **54**: 2808–2821.

30 Terborg C, Bramer S, Harscher S, Simon M, Witte OW. Bedside assessment of cerebral perfusion reductions in patients with acute ischaemic stroke by near-infrared spectroscopy and indocyanine green. *J Neurol Neurosurg Psychiatry* 2004; **75**: 38–42.

31 Grinvald A, Lieke E, Frostig RD, Gilbert CD, Wiesel TN. Functional architecture of cortex revealed by optical imaging of intrinsic signals. *Nature* 1986; **324**: 361–364.

32 D Malonek AG. Vascular regulation at sub millimeter range. Sources of intrinsic signals for high resolution optical imaging. *Adv Exp Med Biol* 1997; **413**: 215–20.

33 Masino SA, Kwon MC, Dory Y, Frostig RD. Characterization of functional organization within rat barrel cortex using intrinsic signal optical imaging through a thinned skull. *Proc Natl Acad Sci* 1993; **90**: 9998–10002.

34 Masino SA, Frostig RD. Quantitative long-term imaging of the functional representation of a whisker in rat barrel cortex. *Proc Natl Acad Sci* 1996; **93**: 4942–4947.

35 Ts'o DY, Frostig RD, Lieke EE, Grinvald A. Functional organization of primate visual cortex revealed by high resolution optical imaging. *Science* 1990; **249**: 417–420.

36 Briers JD. Laser Doppler, speckle and related techniques for blood perfusion mapping and imaging. *Physiol Meas* 2001; **22**: R35–66.

37 Choi B, Kang NM, Nelson JS. Laser speckle imaging for monitoring blood flow dynamics in the in vivo rodent dorsal skin fold model. *Microvasc Res* 2004; **68**: 143–146.

38 Ruth B. Measuring the steady-state value and the dynamics of the skin blood flow using the non-contact laser speckle method. *Med Eng Phys* 1994; **16**: 105–111.

39 Hecht N, Woitzik J, König S, Horn P, Vajkoczy P. Laser speckle imaging allows real-time intraoperative blood flow assessment during neurosurgical procedures. *J Cereb Blood Flow Metab Off J Int Soc Cereb Blood Flow Metab* 2013; **33**: 1000–1007.

40 Dunn AK, Bolay H, Moskowitz MA, Boas DA. Dynamic Imaging of Cerebral Blood Flow Using Laser Speckle. *J Cereb Blood Flow Metab* 2001; **21**: 195–201.

41 Fercher AF, Briers JD. Flow visualization by means of single-exposure speckle photography. *Opt Commun* 1981; **37**: 326–330.

42 Zhang S, Murphy TH. Imaging the Impact of Cortical Microcirculation on Synaptic Structure and Sensory-Evoked Hemodynamic Responses In Vivo. *PLoS Biol* 2007; **5**.http://dx.doi.org/10.1371/journal.pbio.0050119 (accessed 30 Nov2011).

43 Ayata C, Dunn AK, Gursoy-Ozdemir Y, Huang Z, Boas DA, Moskowitz MA. Laser Speckle Flowmetry for the Study of Cerebrovascular Physiology in Normal and Ischemic Mouse Cortex. *J Cereb Blood Flow Metab* 2004; **24**: 744–755.

44 Armitage GA, Todd KG, Shuaib A, Winship IR. Laser speckle contrast imaging of collateral blood flow during acute ischemic stroke. *J Cereb Blood Flow Metab* 2010; **30**: 1432–1436.

45 Durduran T, Burnett MG, Yu G, Zhou C, Furuya D, Yodh AG *et al.* Spatiotemporal Quantification of Cerebral Blood Flow During Functional Activation in Rat Somatosensory Cortex Using Laser-Speckle Flowmetry. *J Cereb Blood Flow Metab* 2004; **24**: 518–525.

46 Dunn AK, Devor A, Bolay H, Andermann ML, Moskowitz MA, Dale AM *et al.* Simultaneous imaging of total cerebral hemoglobin concentration, oxygenation, and blood flow during functional activation. *Opt Lett* 2003; **28**: 28–30.

47 Parthasarathy AB, Weber EL, Richards LM, Fox DJ, Dunn AK. Laser speckle contrast imaging of cerebral blood flow in humans during neurosurgery: a pilot clinical study. *J Biomed Opt* 2010; **15**: 066030.

48 Hecht N, Woitzik J, Dreier JP, Vajkoczy P. Intraoperative monitoring of cerebral blood flow by laser speckle contrast analysis. *Neurosurg Focus* 2009; **27**: E11.

49 Cheng H, Duong TQ. Simplified laser-speckle-imaging analysis method and its application to retinal blood flow imaging. *Opt Lett* 2007; **32**: 2188–2190.

50 Fujii H. Visualisation of retinal blood flow by laser speckle flow-graphy. *Med Biol Eng Comput* 1994; **32**: 302–304.

51 Bonner R, Nossal R. Model for laser Doppler measurements of blood flow in tissue. *Appl Opt* 1981; **20**: 2097–2107.

52 Burnett MG, Detre JA, Greenberg JH. Activation–flow coupling during graded cerebral ischemia. *Brain Res* 2005; **1047**: 112–118.

53 Boas DA, Yodh AG. Spatially varying dynamical properties of turbid media probed with diffusing temporal light correlation. *J Opt Soc Am A* 1997; **14**: 192–215.

54 Durduran T, Yodh AG. Diffuse correlation spectroscopy for non-invasive, micro-vascular cerebral blood flow measurement. *NeuroImage* 2014; **85 Pt 1**: 51–63.

55 Briers JD, Webster S. Laser speckle contrast analysis (LASCA): a nonscanning, full-field technique for monitoring capillary blood flow. *J Biomed Opt* 1996; **1**: 174–179.

56 Tom WJ, Ponticorvo A, Dunn AK. Efficient processing of laser speckle contrast images. *IEEE Trans Med Imaging* 2008; **27**: 1728–1738.

57 Davis MA, Kazmi SMS, Dunn AK. Imaging depth and multiple scattering in laser speckle contrast imaging. *J Biomed Opt* 2014; **19**: 086001–086001.

58 Bandyopadhyay R, Gittings AS, Suh SS, Dixon PK, Durian DJ. Speckle-visibility spectroscopy: A tool to study time-varying dynamics. *Rev Sci Instrum* 2005; **76**: 093110.

59 Parthasarathy AB, Tom WJ, Gopal A, Zhang X, Dunn AK. Robust flow measurement with multi-exposure speckle imaging. *Opt Express* 2008; **16**: 1975–1989.

60 Bonner R, Nossal R. Model for laser Doppler measurements of blood flow in tissue. *Appl Opt* 1981; **20**: 2097–2107.

61 Boas DA, Yodh AG. Spatially varying dynamical properties of turbid media probed with diffusing temporal light correlation. *J Opt Soc Am A* 1997; **14**: 192–215.

62 Strong AJ, Bezzina EL, Anderson PJB, Boutelle MG, Hopwood SE, Dunn AK. Evaluation of laser speckle flowmetry for imaging cortical perfusion in experimental stroke studies: quantitation of perfusion and detection of peri-infarct depolarisations. *J Cereb Blood Flow Metab* 2005; **26**: 645–653.

63 Wang Z, Hughes S, Dayasundara S, Menon RS. Theoretical and experimental optimization of laser speckle contrast imaging for high specificity to brain microcirculation. *J Cereb Blood Flow Metab* 2006; **27**: 258–269.

64 Bandyopadhyay R, Gittings AS, Suh SS, Dixon PK, Durian DJ. Speckle-visibility spectroscopy: A tool to study time-varying dynamics. *Rev Sci Instrum* 2005; **76**: 093110.

65 Briers JD. Laser Doppler and time-varying speckle: a reconciliation. *J Opt Soc Am A* 1996; **13**: 345–350.

66 Dunn AK, Bolay H, Moskowitz MA, Boas DA. Dynamic Imaging of Cerebral Blood Flow Using Laser Speckle. *J Cereb Blood Flow Metab* 2001; **21**: 195–201.

67 Choi B, Ramirez-San-Juan JC, Lotfi J, Stuart Nelson J. Linear response range characterization and in vivo application of laser speckle imaging of blood flow dynamics. *J Biomed Opt* 2006; **11**: 041129–041129–7.

68 Parthasarathy AB, Tom WJ, Gopal A, Zhang X, Dunn AK. Robust flow measurement with multi-exposure speckle imaging. *Opt Express* 2008; **16**: 1975–1989.

69 Choi B, Ringold TL, Kim J. Methods to Enhance Laser Speckle Imaging of High-Flow and Low-Flow Vasculature. *Conf Proc Annu Int Conf IEEE Eng Med Biol Soc IEEE Eng Med Biol Soc Conf* 2009; **2009**: 4073–4076.

70 Nadort A, Woolthuis RG, van Leeuwen TG, Faber DJ. Quantitative laser speckle flowmetry of the in vivo microcirculation using sidestream dark field microscopy. *Biomed Opt Express* 2013; **4**: 2347.

71 Li H, Liu Q, Lu H, Li Y, Zhang HF, Tong S. Directly measuring absolute flow speed by frequency-domain laser speckle imaging. *Opt Express* 2014; **22**: 21079–21087.

72 Ayata C, Dunn AK, Gursoy-Ozdemir Y, Huang Z, Boas DA, Moskowitz MA. Laser Speckle Flowmetry for the Study of Cerebrovascular Physiology in Normal and Ischemic Mouse Cortex. *J Cereb Blood Flow Metab* 2004; **24**: 744–755.

73 Strong AJ, Bezzina EL, Anderson PJB, Boutelle MG, Hopwood SE, Dunn AK. Evaluation of laser speckle flowmetry for imaging cortical perfusion in experimental

stroke studies: quantitation of perfusion and detection of peri-infarct depolarisations. *J Cereb Blood Flow Metab* 2005; **26**: 645–653.

74 Towle EL, Richards LM, Kazmi SMS, Fox DJ, Dunn AK. Comparison of indocyanine green angiography and laser speckle contrast imaging for the assessment of vasculature perfusion. *Neurosurgery* 2012; **71**: 1023–1030; discussion 1030–1031.

75 Kazmi SMS, Parthasarthy AB, Song NE, Jones TA, Dunn AK. Chronic imaging of cortical blood flow using Multi-Exposure Speckle Imaging. *J Cereb Blood Flow Metab* 2013; **33**: 798–808.

76 Dunn AK, Devor A, Dale AM, Boas DA. Spatial extent of oxygen metabolism and hemodynamic changes during functional activation of the rat somatosensory cortex. *NeuroImage* 2005; **27**: 279–290.

77 Boas DA, Dunn AK. Laser speckle contrast imaging in biomedical optics. *J Biomed Opt* 2010; **15**: 011109.

78 Duncan DD, Kirkpatrick SJ. Can laser speckle flowmetry be made a quantitative tool? *J Opt Soc Am A* 2008; **25**: 2088–2094.

79 Kazmi SMS, Parthasarthy AB, Song NE, Jones TA, Dunn AK. Chronic imaging of cortical blood flow using Multi-Exposure Speckle Imaging. *J Cereb Blood Flow Metab* 2013. doi:10.1038/jcbfm.2013.57.

80 Parthasarathy AB, Kazmi SMS, Dunn AK. Quantitative imaging of ischemic stroke through thinned skull in mice with MultiExposure Speckle Imaging. *Biomed Opt Express* 2010; **1**: 246–259.

81 Parthasarathy AB, Kazmi SMS, Dunn AK. Quantitative imaging of ischemic stroke through thinned skull in mice with Multi Exposure Speckle Imaging. *Biomed Opt Express* 2010; **1**: 246–259.

82 Parthasarathy AB, Weber EL, Richards LM, Fox DJ, Dunn AK. Laser speckle contrast imaging of cerebral blood flow in humans during neurosurgery: a pilot clinical study. *J Biomed Opt* 2010; **15**: 066030.

83 Li Y, Baran U, Wang RK. Application of Thinned-Skull Cranial Window to Mouse Cerebral Blood Flow Imaging Using Optical Microangiography. *PLoS ONE* 2014; **9**: e113658.

84 Parthasarathy AB, Kazmi SMS, Dunn AK. Quantitative imaging of ischemic stroke through thinned skull in mice with MultiExposure Speckle Imaging. *Biomed Opt Express* 2010; **1**: 246–259.

85 Atchia Y, Levy H, Dufour S, Levi O. Rapid multiexposure in vivo brain imaging system using vertical cavity surface emitting lasers as a light source. *Appl Opt* 2013; **52**: C64–C71.

86 Dunn AK. Laser Speckle Contrast Imaging of Cerebral Blood Flow. *Ann Biomed Eng* 2012; **40**: 367–377.

87 Göppert-Mayer M. Über Elementarakte mit zwei Quantensprüngen. *Ann Phys* 1931; **401**: 273–294.

88 Denk W, Strickler J, Webb W. Two-photon laser scanning fluorescence microscopy. *Science* 1990; **248**: 73–76.

89 Oheim M, Beaurepaire E, Chaigneau E, Mertz J, Charpak S. Two-photon microscopy in brain tissue: parameters influencing the imaging depth. *J Neurosci Methods* 2001; **111**: 29–37.

90 Wilson CA, Hatchell DL. Photodynamic retinal vascular thrombosis. Rate and duration of vascular occlusion. *Invest Ophthalmol Vis Sci* 1991; **32**: 2357 –2365.

91 Watson BD, Dietrich WD, Busto R, Wachtel MS, Ginsberg MD. Induction of reproducible brain infarction by photochemically initiated thrombosis. *Ann Neurol* 1985; **17**: 497–504.

92 Dalkara T, Arsava EM. Can restoring incomplete microcirculatory reperfusion improve stroke outcome after thrombolysis? *J Cereb Blood Flow Metab* 2012; **32**: 2091–2099.

93 Gursoy-Ozdemir Y, Yemisci M, Dalkara T. Microvascular protection is essential for successful neuroprotection in stroke. *J Neurochem* 2012; **123 Suppl 2**: 2–11.

94 Murphy TH, Corbett D. Plasticity during stroke recovery: from synapse to behaviour. *Nat Rev Neurosci* 2009; **10**: 861–872.

95 Font MA, Arboix A, Krupinski J. Angiogenesis, Neurogenesis and Neuroplasticity in Ischemic Stroke. *Curr Cardiol Rev* 2010; **6**: 238–244.

96 Kleinfeld D, Mitra PP, Helmchen F, Denk W. Fluctuations and stimulus-induced changes in blood flow observed in individual capillaries in layers 2 through 4 of rat neocortex. *Proc Natl Acad Sci* 1998; **95**: 15741–15746.

97 Kazmi SMS, Salvaggio AJ, Estrada AD, Hemati MA, Shaydyuk NK, Roussakis E *et al.* Three-dimensional mapping of oxygen tension in cortical arterioles before and after occlusion. *Biomed Opt Express* 2013; **4**: 1061–1073.

98 Rege A, Thakor NV, Rhie K, Pathak AP. In vivo laser speckle imaging reveals microvascular remodeling and hemodynamic changes during wound healing angiogenesis. *Angiogenesis* 2012; **15**: 87–98.

99 Li P, Murphy TH. Two-Photon Imaging during Prolonged Middle Cerebral Artery Occlusion in Mice Reveals Recovery of Dendritic Structure after Reperfusion. *J Neurosci* 2008; **28**: 11970–11979.

100 White SM, George SC, Choi B. Automated computation of functional vascular density using laser speckle imaging in a rodent window chamber model. *Microvasc Res* 2011; **82**: 92–95.

101 Davis MA, Kazmi SMS, Dunn AK. Imaging depth and multiple scattering in laser speckle contrast imaging. *J Biomed Opt* 2014; **19**: 086001–086001.

102 Preibisch S, Saalfeld S, Tomancak P. Globally optimal stitching of tiled 3D microscopic image acquisitions. *Bioinformatics* 2009; **25**: 1463–1465.

103 Li CH, Tam PKS. An iterative algorithm for minimum cross entropy thresholding. *Pattern Recognit Lett* 1998; **19**: 771–776.

104 Deans S. *The Radon transform and some of its applications.* Wiley and Sons: New York, 1983.

105 Drew P, Blinder P, Cauwenberghs G, Shih A, Kleinfeld D. Rapid determination of particle velocity from space-time images using the Radon transform. *J Comput Neurosci* 2010. doi:10.1007/s10827-009-0159-1.

106 Marques PM de A, Rangayyan RM. *Content-based Retrieval of Medical Images: Landmarking, Indexing, and Relevance Feedback*. Morgan & Claypool Publishers, 2013.

107 Mostany R, Chowdhury TG, Johnston DG, Portonovo SA, Carmichael ST, Portera-Cailliau C. Local Hemodynamics Dictate Long-Term Dendritic Plasticity in Peri-Infarct Cortex. *J Neurosci* 2010; **30**: 14116–14126.

108 Tennant KA, Brown CE. Diabetes Augments In Vivo Microvascular Blood Flow Dynamics after Stroke. *J Neurosci* 2013; **33**: 19194–19204.

109 Brown CE, Li P, Boyd JD, Delaney KR, Murphy TH. Extensive Turnover of Dendritic Spines and Vascular Remodeling in Cortical Tissues Recovering from Stroke. *J Neurosci* 2007; **27**: 4101–4109.

110 Zhou Y, Lekic T, Fathali N, Ostrowski RP, Martin RD, Tang J *et al.* Isoflurane Posttreatment Reduces Neonatal Hypoxic–Ischemic Brain Injury in Rats by the

Sphingosine-1-Phosphate/Phosphatidylinositol-3-Kinase/Akt Pathway. *Stroke* 2010; **41**: 1521–1527.

111 Zheng S, Zuo Z. Isoflurane Preconditioning Induces Neuroprotection against Ischemia via Activation of P38 Mitogen-Activated Protein Kinases. *Mol Pharmacol* 2004; **65**: 1172–1180.

112 Knowland D, Arac A, Sekiguchi KJ, Hsu M, Lutz SE, Perrino J *et al.* Stepwise Recruitment of Transcellular and Paracellular Pathways Underlies Blood-Brain Barrier Breakdown in Stroke. *Neuron* 2014; **82**: 603–617.

113 Lee J, Wu W, Jiang JY, Zhu B, Boas DA. Dynamic light scattering optical coherence tomography. *Opt Express* 2012; **20**: 22262–22277.

114 Lee J, Radhakrishnan H, Wu W, Daneshmand A, Climov M, Ayata C *et al.* Quantitative imaging of cerebral blood flow velocity and intracellular motility using dynamic light scattering-optical coherence tomography. *J Cereb Blood Flow Metab Off J Int Soc Cereb Blood Flow Metab* 2013; **33**: 819–825.

115 Srinivasan VJ, Mandeville ET, Can A, Blasi F, Climov M, Daneshmand A *et al.* Multiparametric, Longitudinal Optical Coherence Tomography Imaging Reveals Acute Injury and Chronic Recovery in Experimental Ischemic Stroke. *PLoS ONE* 2013; **8**: e71478.

116 Combined optical coherence tomography and electroretinography system for in vivo simultaneous morphological and functional imaging of the rodent retina. 2010.http://spiedl.aip.org/getabs/servlet/GetabsServlet?prog=normal&id=JBOPFO000015000004040506000001&idtype=cvips&gifs=Yes&type=ALERT (accessed 2 Sep2010).

117 Weber B, Burger C, Wyss MT, Von Schulthess GK, Scheffold F, Buck A. Optical imaging of the spatiotemporal dynamics of cerebral blood flow and oxidative metabolism in the rat barrel cortex. *Eur J Neurosci* 2004; **20**: 2664–2670.

118 Schaechter JD, Moore CI, Connell BD, Rosen BR, Dijkhuizen RM. Structural and functional plasticity in the somatosensory cortex of chronic stroke patients. *Brain* 2006; **129**: 2722–2733.

119 Dijkhuizen RM, Ren J, Mandeville JB, Wu O, Ozdag FM, Moskowitz MA *et al.* Functional magnetic resonance imaging of reorganization in rat brain after stroke. *Proc Natl Acad Sci* 2001; **98**: 12766–12771.

120 Dijkhuizen RM, Singhal AB, Mandeville JB, Wu O, Halpern EF, Finklestein SP *et al.* Correlation between Brain Reorganization, Ischemic Damage, and Neurologic

Status after Transient Focal Cerebral Ischemia in Rats: A Functional Magnetic Resonance Imaging Study. *J Neurosci* 2003; **23**: 510–517.

121 Chopp M, Zhang ZG, Jiang Q. Neurogenesis, Angiogenesis, and MRI Indices of Functional Recovery From. *Stroke* 2007; **38**: 827–831.

122 Heffernan ME, Huang W, Sicard KM, Bratane BT, Sikoglu EM, Zhang N *et al.* Multi-modal approach for investigating brain and behavior changes in an animal model of traumatic brain injury. *J Neurotrauma* 2013; **30**: 1007–1012.

123 Chao T-HH, Chen J-H, Yen C-T. Repeated BOLD-fMRI imaging of deep brain stimulation responses in rats. *PloS One* 2014; **9**: e97305.

124 Schallert T, Upchurch M, Lobaugh N, Farrar SB, Spirduso WW, Gilliam P *et al.* Tactile extinction: Distinguishing between sensorimotor and motor asymmetries in rats with unilateral nigrostriatal damage. *Pharmacol Biochem Behav* 1982; **16**: 455–462.

125 Li X, Blizzard KK, Zeng Z, DeVries AC, Hurn PD, McCullough LD. Chronic behavioral testing after focal ischemia in the mouse: functional recovery and the effects of gender. *Exp Neurol* 2004; **187**: 94–104.

126 Schallert T, Fleming SM, Leasure JL, Tillerson JL, Bland ST. CNS plasticity and assessment of forelimb sensorimotor outcome in unilateral rat models of stroke, cortical ablation, parkinsonism and spinal cord injury. *Neuropharmacology* 2000; **39**: 777–787.

127 Hunter AJ, Hatcher J, Virley D, Nelson P, Irving E, Hadingham SJ *et al.* Functional assessments in mice and rats after focal stroke. *Neuropharmacology* 2000; **39**: 806–816.

128 Zhang L, Schallert T, Zhang ZG, Jiang Q, Arniego P, Li Q *et al.* A test for detecting long-term sensorimotor dysfunction in the mouse after focal cerebral ischemia. *J Neurosci Methods* 2002; **117**: 207–214.

129 Zhang L, Chen J, Li Y, Zhang ZG, Chopp M. Quantitative measurement of motor and somatosensory impairments after mild (30 min) and severe (2 h) transient middle cerebral artery occlusion in rats. *J Neurol Sci* 2000; **174**: 141–146.

130 Bland ST, Schallert T, Strong R, Aronowski J, Grotta JC. Early Exclusive Use of the Affected Forelimb After Moderate Transient Focal Ischemia in Rats Functional and Anatomic Outcome. *Stroke* 2000; **31**: 1144–1152.

131 Li J, Siegel M, Yuan M, Zeng Z, Finnucan L, Persky R *et al.* Estrogen enhances neurogenesis and behavioral recovery after stroke. *J Cereb Blood Flow Metab* 2011; **31**: 413–425.

132 Castro-Alamancos MA, Borrell J. Functional recovery of forelimb response capacity after forelimb primary motor cortex damage in the rat is due to the reorganization of adjacent areas of cortex. *Neuroscience* 1995; **68**: 793–805.

133 Carmichael ST. Plasticity of Cortical Projections after Stroke. *The Neuroscientist* 2003; **9**: 64–75.

134 Winship IR, Murphy TH. Remapping the Somatosensory Cortex after Stroke: Insight from Imaging the Synapse to Network. *The Neuroscientist* 2009; **15**: 507–524.

135 Kazmi SMS, Balial S, Dunn AK. Optimization of camera exposure durations for multi-exposure speckle imaging of the microcirculation. *Biomed Opt Express* 2014; **5**: 2157.

136 Yuan S, Devor A, Boas DA, Dunn AK. Determination of optimal exposure time for imaging of blood flow changes with laser speckle contrast imaging. *Appl Opt* 2005; **44**: 1823–1830.

137 Hossmann K-A. Pathophysiology and Therapy of Experimental Stroke. *Cell Mol Neurobiol* 2006; **26**: 1055–1081.

138 Vovenko E. Distribution of oxygen tension on the surface of arterioles, capillaries and venules of brain cortex and in tissue in normoxia: an experimental study on rats. *Pflüg Arch Eur J Physiol* 1999; **437**: 617–623.

139 Devor A, Sakadžić S, Saisan PA, Yaseen MA, Roussakis E, Srinivasan VJ *et al.* 'Overshoot' of O2 Is Required to Maintain Baseline Tissue Oxygenation at Locations Distal to Blood Vessels. *J Neurosci* 2011; **31**: 13676 –13681.

140 Rumsey WL, Vanderkooi JM, Wilson DF. Imaging of phosphorescence: a novel method for measuring oxygen distribution in perfused tissue. *Science* 1988; **241**: 1649–1651.

141 Dunphy I, Vinogradov SA, Wilson DF. Oxyphor R2 and G2: phosphors for measuring oxygen by oxygen-dependent quenching of phosphorescence. *Anal Biochem* 2002; **310**: 191–198.

142 Vinogradov SA, Lo L-W, Wilson DF. Dendritic Polyglutamic Porphyrins: Probing Porphyrin Protection by Oxygen-Dependent Quenching of Phosphorescence. *Chem – Eur J* 1999; **5**: 1338–1347.

143 Shonat RD, Kight AC. Oxygen Tension Imaging in the Mouse Retina. *Ann Biomed Eng* 2003; **31**: 1084–1096.

144 Frostig RD, Lieke EE, Ts'o DY, Grinvald A. Cortical functional architecture and local coupling between neuronal activity and the microcirculation revealed by in vivo high-resolution optical imaging of intrinsic signals. *Proc Natl Acad Sci* 1990; **87**: 6082–6086.

145 Shonat RD, Wachman ES, Niu W, Koretsky AP, Farkas DL. Near-simultaneous hemoglobin saturation and oxygen tension maps in mouse brain using an AOTF microscope. *Biophys J* 1997; **73**: 1223–1231.

146 Wilson DF, Lee WMF, Makonnen S, Apreleva S, Vinogradov SA. Oxygen pressures in the interstitial space of skeletal muscle and tumors in vivo. *Adv Exp Med Biol* 2008; **614**: 53–62.

147 Adkins DL, Voorhies AC, Jones TA. Behavioral and neuroplastic effects of focal endothelin-1 induced sensorimotor cortex lesions. *Neuroscience* 2004; **128**: 473–486.

148 Gilmour G, Iversen SD, O'Neill MF, Bannerman DM. The effects of intracortical endothelin-1 injections on skilled forelimb use: implications for modelling recovery of function after stroke. *Behav Brain Res* 2004; **150**: 171–183.

149 Fuxe K, Bjelke B, Andbjer B, Grahn H, Rimondini R, Agnati LF. Endothelin-1 induced lesions of the frontoparietal cortex of the rat. A possible model of focal cortical ischemia. *Neuroreport* 1997; **8**: 2623–2629.

150 Sharkey J, Butcher SP, Kelly JS. Endothelin-1 induced middle cerebral artery occlusion: pathological consequences and neuroprotective effects of MK801. *J Auton Nerv Syst* 1994; **49 Suppl**: S177–185.

151 Windle V, Szymanska A, Granter-Button S, White C, Buist R, Peeling J *et al.* An analysis of four different methods of producing focal cerebral ischemia with endothelin-1 in the rat. *Exp Neurol* 2006; **201**: 324–334.

152 Longa EZ, Weinstein PR, Carlson S, Cummins R. Reversible middle cerebral artery occlusion without craniectomy in rats. *Stroke* 1989; **20**: 84–91.

153 Bederson JB, Pitts LH, Tsuji M, Nishimura MC, Davis RL, Bartkowski H. Rat middle cerebral artery occlusion: evaluation of the model and development of a neurologic examination. *Stroke* 1986; **17**: 472–476.

154 Tamura A, Graham DI, McCulloch J, Teasdale GM. Focal Cerebral Ischaemia in the Rat: 1. Description of Technique and Early Neuropathological Consequences

Following Middle Cerebral Artery Occlusion. *J Cereb Blood Flow Metab* 1981; **1**: 53–60.

Vita

Christian Schrandt was born in Wichita Falls, Texas in 1988 to Tom and Michele Schrandt. After graduating from Holliday High School in 2006, he attended the University of Alabama at Birmingham and received a Bachelor of Science in Biomedical Engineering. He entered graduate school at the University of Texas at Austin in July of 2010.

Permanent email: ChrisSchrandt@gmail.com

This dissertation was typed by the author.